Bulletin of the Seismological Society of America

Site-dependent amplification on topography during the 2016 Amatrice (central Italy) seismic sequence

--Manuscript Draft--

Manuscript Number:	BSSA-D-21-00234R5
Article Type:	Article
Section/Category:	Regular Issue
Full Title:	Site-dependent amplification on topography during the 2016 Amatrice (central Italy) seismic sequence
Corresponding Author:	Marta Pischiutta INGV Rome, ITALY
Corresponding Author's Institution:	INGV
Corresponding Author E-Mail:	marta.pischiutta@ingv.it
Order of Authors:	Marta Pischiutta
	Rodolfo Puglia
	Paola Bordoni
	Sara Lovati
	Giovana Cultrera
	Alessia Mercuri
	Antonio Fodarella
	Marco Massa
	Ezio D'Alema
Abstract:	Following the MW 6.0 Amatrice earthquake on August 24 2016 in Central Italy, the Emersito task force of the Istituto Nazionale di Geofisica e Vulcanologia (INGV) installed a temporary seismic network focusing on the investigation of amplification effects at municipalities located on topographic reliefs. Fourteen stations were installed at three sites: Amandola, Civitella del Tronto and Montereale. During the operational period, stations recorded about 150 earthquakes with Mw up to 4.7. Recorded signals were analyzed calculating the horizontal-to-vertical spectral ratios at single station (HVSRs), using both ambient noise and earthquake waveforms, as well as standard spectral ratios to a reference site (SSRs). To robustly estimate site amplification at each station of the site amplification effect at each station, the influence of backazimuth and epicentral distance is investigated. With the aim of reproducing the observed amplification pattern, 2D numerical simulations were performed on a section orthogonal to the topography major axis, constrained through in-situ geological investigations and geophysical surveys. While at Montereale site no clear amplification effects were observed, at Amandola site, all stations on the relief consistently detected significant peaks at about 4 Hz, and along N120-150 azimuth. At Civitella del Tronto a proper reference station is missing, implying a misleading of site response evaluation in terms of SSRs. Moreover, even if all stations show amplification in the frequency band 1-3 Hz, the direction of maximum amplification varies from NE to NW. At the three sites, observations were successfully reproduced by 2D numerical models, the latter suggesting that topography alone cannot reproduce data and the interplay with subsoil velocity structure is needed to produce a clear amplification effect. We conclude that, according to previous papers, rather than the sole topography convex shape, the geophysical structure has often a predominant role in controlling the observed amplification pattern on topography.
Author Comments:	We have followed all requests except for the following:

	+ In Figure 5, panels a3, b3, a4, b4 should all be shown with the same color-range (and a single colorbar) to highlight the differences. Currently, Fig 5 b3 has a different color range, which is not ideal We cannot modify the colorbar because the one in panel a4 would be too different from the others and would saturate the amplitude levels.
Suggested Reviewers:	Anna Kaiser A.Kaiser@gns.cri.nz Expertize in the field
	Jan Burjanek burjanekj@gmail.com Expertize in the field
Opposed Reviewers:	
Response to Reviewers:	
Additional Information:	
Question	**Response**
Key Point #1: <i>Three key points will be printed at the front of your manuscript so readers can get a quick overview. Please provide three COMPLETE sentences addressing the following: 1) state the problem you are addressing in a FULL sentence; 2) state your main conclusion(s) in a FULL sentence; and 3) state the broader implications of your findings in a FULL sentence. Each point must be 110 characters or less (including spaces).	The role of topography on seismic amplification has often been related to resonance due to convex hill shapes
Key Point #2:	Our study highlights that the geological structure plays a predominant role even on topography
Key Point #3:	Our results agree with previous studies involving a high number of not pre-selected sites on topography

Site-dependent amplification on topography during the 2016 Amatrice (central Italy) seismic sequence

M. Pischiutta[1*], R. Puglia[2], P. Bordoni[1], S. Lovati[2], G. Cultrera[1], A. Mercuri[1], A. Fodarella[3], M. Massa[2], E. D'Alema[2]

[1]Istituto Nazionale di Geofisica e Vulcanologia, Sezione Roma1, Roma, Italy

[2]Istituto Nazionale di Geofisica e Vulcanologia, Sezione di Milano, Milano, Italy

[3]Istituto Nazionale di Geofisica e Vulcanologia, Sezione Roma1, Grottaminarda (AV), Italy

[*]Corresponding Author – marta.pischiutta@ingv.it

Declaration of Competing Interests

The authors acknowledge there are no conflicts of interest recorded

Key Points:

#1 The role of topography on seismic amplification has often been related to resonance due to convex hill shapes

#2 Our study highlights that the geological structure plays a predominant role even on topography

#3 Our results agree with previous studies involving a high number of not pre-selected sites on topography

Abstract

Following the M_W 6.0 Amatrice earthquake on August 24 2016 in Central Italy, the Emersito task force of the Istituto Nazionale di Geofisica e Vulcanologia (INGV) installed a temporary seismic network focusing on the investigation of amplification effects at municipalities located on topographic reliefs. Fourteen stations were installed at three sites: Amandola, Civitella del Tronto and Montereale. During the operational period, stations recorded about 150 earthquakes with Mw up to 4.7. Recorded signals were analyzed calculating the horizontal-to-vertical spectral ratios at single station (HVSRs), using both ambient noise and earthquake waveforms, as well as standard spectral ratios to a reference site (SSRs). To robustly estimate site amplification at each station of the site amplification effect at each station, the influence of backazimuth and epicentral distance is investigated. With the aim of reproducing the observed amplification pattern, 2D numerical simulations were performed on a section orthogonal to the topography major axis, constrained through in-situ geological investigations and geophysical surveys.

While at Montereale site no clear amplification effects were observed, at Amandola site, all stations on the relief consistently detected significant peaks at about 4 Hz, and along N120-150 azimuth. At Civitella del Tronto a proper reference station is missing, implying a misleading of site response evaluation in terms of SSRs. Moreover, even if all stations show amplification in the frequency band 1-3 Hz, the direction of maximum amplification varies from NE to NW.

At the three sites, observations were successfully reproduced by 2D numerical models, the latter suggesting that topography alone cannot reproduce data and the interplay with subsoil velocity structure is needed to produce a clear amplification effect. We conclude that, according to previous papers, rather than the sole topography convex shape, the geophysical structure has often a predominant role in controlling the observed amplification pattern on topography.

1. Introduction

The role of topography on seismic amplification is a complex topic that is still under debate. Many studies in the last 5 decades approached this issue, explaining the amplification observed on the top of the reliefs in terms of constructive interference of seismic waves diffracted by the convex shape of topography, and relating the resonance frequency to the hill dimension and the mean shear-wave velocity ("topo-resonant model", as in Burjanek et al., 2014).

In earlier studies, numerical simulations assumed homogeneous subsoil in order to highlights the effect of topography; they successfully reproduced the amplified frequency band, but they generally failed in reproducing the observed amplitude levels which rarely exceeded a factor of 2 (e.g. Lee *et al.*, 2009). This inconsistency was usually attributed to several limitations, such as inappropriate reference station (e.g. Paolucci, 2002) or extremely simplified numerical models (Bouchon and Baker, 1996). Lovati *et al.* (2010) observed significant amplification on Narni hill (central Italy), but neither 2D or 3D numerical simulations adopting homogeneous models were able to reproduce observed ground motion amplitudes: they ascribed the observed amplification to the coupling of topography and stratigraphy effects. Recent works demonstrated that it is possible to attain amplitude levels comparable to observations only when considering accurate 3D velocity model (i.e. Hartzell *et al.*, 2013, 2016; Glinsky and Bertrand, 2017; Luo *et al.*, 2020; Primofiore *et al.*, 2020).

Beside significant amplification, topographic irregularities often produce directional effects, ground motion polarization being orthogonal to the topography major axis (that is the elongation in the 2-D approximation of topography shape), as firstly proposed by Spudich *et al.* (1996), due to an effect of wave field scattering from the crest (Buech *et al.* 2010; Massa *et al.* 2010; Pischiutta *et al.* 2010; Massa *et al.*, 2014).

An important issue about amplification on topography regards the site selection. In most papers, the contribution of topographic irregularities on amplification has been usually studied at single sites where significant ground-motion amplification was observed during earthquakes. However, when using a large quantity of not pre-selected topography sites, the amplification effect on topography is not systematically observed, and/or it is not consistent with the "topo-resonant models". As an example, Burjanek *et al.* (2014) used 25 Swiss (CHNet) and Japanese (KiK-net) seismological stations installed on pronounced relief, finding that many stations on rock (classified as "A" following EC8 site-class schema; EuroCode 8, CEN 2003) did not exhibit any systematic amplification even if installed in pronounced relief conditions. In a similar approach, Pischiutta *et al.* (2018) performed a systematic analysis using the Italian National Seismic Network (RSN; Margheriti et al., 2021), operated by the Istituto Nazionale di Geofisica e Vulcanologia (INGV). Despite their efforts, they did not obtain any systematic relations between seismological evidence and morphology geometry, stations often showing amplification on a broad frequency band (instead of along a single peak), as well as maximum amplification not transversal to the ridge elongation.

Therefore, rather than the sole shape of topography, other features in the subsoil can have a prevailing role in producing directional effects, as: i) large-scale open cracks (Moore *et al.*, 2011; Burjànek *et al.*, 2012); ii) microcracks in fractured rocks associated to fault activity (Martino *et al.*, 2006; Marzorati *et al.*, 2011; Pischiutta *et al.*, 2012, 2015, 2017); iii) rock instabilities (e.g. Del Gaudio et al., 2019), and, of course, iv) stratigraphic effects.

In this framework, the goal of the present study is to identify the features which mainly influenced the amplification pattern observed at the three villages Amandola, Civitella del Tronto and Montereale (Figure 1), since they are located on topographic reliefs and were affected by the 2016 Central Italy seismic sequence. The seismic sequence started on August 24, 2016, with a moment-magnitude (Mw) 6.0 earthquake localized close to the villages of Accumoli and Amatrice in the Apennines mountains, followed by a Mw 5.9 event on October 26th (nearby the village of Visso), and a Mw 6.5 earthquake on October 30th, localized in the proximity of Norcia).

The three investigated sites were instrumented with seismic stations deployed by the Emersito INGV task force (Cultrera et al., 2016; Cara et al., 2019). Data acquired at the three study areas are analyzed finding peculiar features at each site. To explain observations, 2D numerical simulations are performed by applying two different modeling approaches and tools: a linear-equivalent modeling to study the non-linear strong-motion seismic response, through the code QUAD4M (Hudson et al., 1994) together with its pre- and post-processor pro-QUAD4M (Puglia, 2020); a linear approach using a Ricker input pulse, with the package LSR2D (Stacec 2017).

This paper is organized as follows. After presenting data acquisition and analysis (section 2), as well as numerical modeling methods (section 3), the three study cases are separately approached: Amandola (section 4), Civitella del Tronto (section 5), and Montereale (section 6). For each of them we describe: the geological setting; the observed amplification effect suggested by SSR and HVSR analysis; simulation results.

We furnish several additional information in the supplementary material: a report of numerical simulations performed at the Amandola study-case using QUAD4M; tables listing selected earthquakes for the analysis; HVSR analysis results performed using seismic events and ambient noise; additional modeling results and information for LSR2D package adopted at Civitella and Montereale sites.

2. Data acquisition and analysis

After the Mw 6.0 earthquake of August 24, 2016 (01:36 UTC), which struck an extensive area in the Central Apennines (Italy), a temporary seismic network of 22 stations (Figure 1) was installed by the INGV Emersito task force, whose aim is to carry out and coordinate the monitoring of local site effects caused by geological and geomorphological settings. They chose 4 municipalities with peculiar geologic and geomorphologic settings (topographic irregularities, fault zones, alluvial plains, Cultrera et al., 2016). The temporary seismic network is identified by the international XO code and acquired continuous data which are available through the European Integrated Data Archive. The instrumental set was composed of Reftek and Quanterra digitizers (24 bit resolution), equipped with velocimetric sensors (Lennartz-3d 5s, frequency response of 0.2 to 40 Hz) and accelerometric (Episensor FBA ES-T, frequency response of DC to 200 Hz) sensors, with a sampling rate of 100hz and 200hz respectively.

Among the 22 stations, in this study we have selected the 14 of them installed on reliefs, settled in the following municipalities: Amandola (5 stations with prefix "AM"), Civitella Del Tronto (5 stations with prefix "CV") and Montereale (4 stations with prefix "MN"). For each of them, the digital elevation model and station locations are shown in Figure 1, while Table 1 reports station information. Among the very large amount of recorded data we selected several earthquakes with the constraint to be simultaneously recorded at all the stations in each site: for Amandola 151 earthquakes (Mw from 2.5 to 4.3); for Civitella and Montereale 93 earthquakes (Mw from 3 to 4.7).

The hypocentral parameters of earthquakes used for the data analysis are listed in the Supplementary material (Table S1 and S2). They were taken: from the INGV Italian Seismological Instrumental and Parametric Data-Base (ISIDe Working Group, 2007) for Amandola site; from the aftershocks catalog by Chiaraluce *et al.* (2017) for Civitella and Montereale sites.

The analysis of earthquake signals was performed following Theodoulidis *et al.* (2018), namely the standard spectral ratios (SSR) with respect to a reference station, in the assumption that recordings of the reference station contain the same source and propagation effects than records of the other stations (Borcherdt, 1970). Therefore, an improper choice of the reference site can lead to a bias on the empirical estimates of seismic response (e.g. Bordoni et al., 2010, Cadet et al., 2010, Pilz et al., 2020). Unfortunately, as pointed out by many authors, a reference site may be unavailable (Archuleta and Steidl, 1998; Steidl et al., 1996), or may not have a flat amplitude response due to geological subsurface structure, as the alteration or intensive rock fracturing (e.g. Pischiutta et al., 2012; Burjanek et al., 2010; Rovelli et al., 2002; Bindi et al., 2009; Marzorati et al., 2011; Ktenidou & Abrahamson, 2016). To overcome this problem, several alternative methods were developed that do not rely on a reference site have been developed, such as: the Nakamura technique, based on the calculation of the spectral ratio between the horizontal and vertical components of recorded ambient seismic noise (HVNSR, Nakamura, 1989); the earthquake spectral ratio between horizontal and vertical component shear-wave spectra (HVSR, Lermo and Chavez-Garcia, 1993). In addition, the generalized-inversion method proposed by Boatwright et al. (1991) requires a reference station that can be located far from the investigated site, unlike the SSR method that needs a reference in the same area. Moreover, in the Median reference Method MRM proposed by Wilson and Pavlis (2000), as a reference, the median spectrum obtained by array recordings can be employed.

For the SSR and HVSR analysis, for each earthquake recording we used a 10 s time windows starting from 1 s before S-wave arrival, and band-pass filtered in the frequency range 0.1–30 Hz. In the HVNSR analysis, we use night-time ambient noise, and apply the antitrigger algorithm (see SESAME guidelines, Bard *et al*., 2004 and 2008) furnished in the package Geopsy (Wathelet, 2005), with the aim of selecting the stationary parts and avoiding transients associated with very close disturbances. The SSR and HVSR ratios were computed in the frequency range 0.5-20 Hz for all events and for each rotated horizontal component, by using the Fourier spectra of the S-wave-window previously defined, smoothed by Konno-Ohmachi algorithm with parameters b=20 (Konno and Ohmachi, 1998). Finally, the geometrical mean was computed for each station on all the events, together with the associated standard deviation. To ensure the robustness of the results, the average was considered at frequencies where the signal-to-noise (spectral ratio between the event and the noise window) was greater than 3 and for a minimum number of 10 events.

In this work, as a further constraint, we also apply the HVNSR and the HVSR techniques. In fact, the use of HVNSR is crucial to exclude any role of the seismic source or the influence of path effects. For each rotated component, we considered a window length of 120 seconds, 5% tapered, filtered

with a 4th-order Butterworth filter in the frequency range 0.1-15 Hz and smoothed with Konno-Ohmachi (b=20). Results are shown in Figures S4, S7 and S14 of the Supplementary Material.

Finally, in order to investigate the occurrence of directional amplification effects, the calculation of SSRs, HVSRs and HVNSRs was performed by rotating the two horizontal components by steps of 10° from 0° to 180°. This further analysis is needed because, as mentioned in the introduction, following the "topo resonant model" directional effects are expected with maximum amplification and ground motion polarization orthogonal to the topography major axis (i.e. Spudich *et al.*, 1996).

3. Numerical simulations

With the aim of studying the observed amplification pattern, 2D numerical simulations were performed considering in-plane motion for a section transversal to the topography elongation, where the topographic amplification effect is maximized. We are aware about the limitations in the use of simplified models (1D/2D) to simulate geometrical effects in a complex 3D medium, and to unequivocally reproduce the observed directional amplification. But 3D approaches require more constraints, in terms of geometry and mechanical properties of subsoil than those available at these sites.

In order to discriminate the role of the sole geometric convexity with respect to the contribution of local geological structure, simulations were performed using both homogeneous and heterogeneous velocity distributions. We use a plane wave propagating vertically, the angle of incidence of the wave front potentially having an impact on the amplification observed on the relief.

Considering differences in the data set (i.e. strong motion recordings of the 30 October M6 Norcia earthquake are available only at Amandola site), we applied two different modeling approaches and tools:

- At the Amandola study case, we used a linear-equivalent approach as a proxy of non-linear strong motion seismic response, through the pre- and post-processor pro-QUAD4M (Puglia, 2020), and the software QUAD4M (Hudson et al., 1994). QUAD4M uses a finite-elements model at concentrated mass, simplifying the subsoil rheology with a visco-elastic assumption (Kevin-Voigt model) and using a linear equivalent approach, estimated following the Darendeli (2001) approach. Differential equations are solved in the time domain in terms of total stresses. The transmitting base option is used for the lower boundary, by assigning to the underlying half-space the same properties as the bedrock formation. Both vertical and horizontal components of the input motion, recorded on the ground surface, were applied to the (transmitting) base nodes after being deconvolved internally by the QUAD4M code. In fact, when the transmitting base option is used, the input motion given to QUAD4M is the

one recorded on the ground surface, while the one applied at the base nodes is the deconvolution of the input motion, depending on the material properties of the half-space below the mesh and the properties and geometries of the mesh. Further details about QUAD4M code can be found in Pagliaroli, 2018.

- At Civitella and Montereale we followed a linear approach using the package LSR2D (Stacec 2017), a time domain bi-dimensional finite element procedures code based on an equivalent-linear viscoelastic rheological model of Kelvin-Voigt, in total stress. Also this code can be used for linear analyses using G/G_0 and D constant curves. LSR2D simulations within this study are performed using such a linear approach. Moreover, the code can compute automatically the mesh size for each layer considering its S-wave velocity and a maximum frequency of 20 Hz, or alternatively a fixed mesh size can be applied in the whole model. We opted for the first option. Following the Kuhlemeyer and Lysmer (1973) criterion: h = Vs/8f the formula becomes: h=Vs/160. Therefore, in the Civitella site and in the Montereale site we are confident to correctly solve frequencies up to 20 Hz, significantly beyond our target maximum frequency. A Ricker pulse as input motion applied as one horizontal component at the base of the model.

Its theoretical approach is similar to QUAD4M (Hudson et al. 1994) but they differ in the way boundary conditions are modeled: LSR2D implemented viscous dampers also at the edges of the domain and using free-field columns in addition to the compliant base used by QUAD4M.

In both codes, viscous damping is modeled using full Rayleigh damping formulation with two control frequencies, minimum and maximum frequencies in the system response. They are automatically set to avoid significant overdamping in the frequency range of interest.

We finally stress that other calibration studies (Di Buccio *et al.*, 2017) confirmed that QUAD4M and LRS2D can give comparable results.

4. The Amandola site

The municipality of Amandola lies on a 2 km long and 300 m wide relief, mainly elongated in a SW-NE direction with average altitude of about 500 m a.s.l. (Figure 1 and Figure 2). The slope of the South and North flanks varies from 10° to 20° in the SW and NE sides, respectively, which correspond to the narrowest and steepest part of the hill and where AM03 and AM04 stations were installed.

236 **4.1 Geological setting**

237 The territory of Amandola is characterized by the Umbro-Marchigiana lithostratigraphic succession
238 (Geological Map of Italy 1:100000, sheet 132 - Norcia). In detail, the study area of Amandola falls is
239 characterized by the lithostratigraphic Flysch della Laga Formation (identified as "ALS bedrock" and
240 "LPS bedrock" in Figure 2), deposed in Messinian by turbiditic sedimentation in the foredeep during
241 the construction of the Apennine thrust belt (e.g. Bigi et al., 1999). It is formed by variations of thick
242 layered sandstone turbiditic deposits and thin layered clay, marls and calcareous marls, poorly
243 cemented sandstone and silty clay (Regione Marche 2018a).

244 Quaternary continental sediments such as the eluvium-colluvial and alluvial deposits (Holocene)
245 discontinuously cover some top areas of the hill, as for AM01 and AMO3 where colluvial silty gravel
246 deposits are present ("GM" in Figure 2a). Also silty-sandy and silty colluvial deposits outcrop in the
247 area ("SM" and "ML", respectively). They derive from ancient (middle-upper Pleistocene) and recent
248 (Holocene) alluvial processes mainly due to alteration, disintegration and subsequent sedimentation
249 of the soils that constitute the substrate.

250 The substrate is generally characterized by a monoclinal east-dipping with an inclination of the layers
251 around 70°/80°, sometimes reaching verticality. Locally there are different orientations due to the
252 presence of minor structural elements.

253 In the municipal area, no important tectonic discontinuities and active faults were found, but the
254 discontinuous presence of fractures and weak rejection faults, mainly located in correspondence of
255 incisions or transversely to the main ridges. In the Supplementary material we furnish additional
256 material to provide the subsoil geologic reconstruction at the site scale (Figures S1, S3, S3), as several
257 surveys collected in the framework of the Seismic Microzonation (Regione Marche 2018a).

258

259 **4.2 Recorded data analysis**

260 For the SSR analysis on earthquake signals recorded at the Amandola site, we consider station AM05
261 as a reference site, being installed at the topography base. Nearby this site, a stratigraphic log
262 (#109002P198, see Figure 2 panel e) provided in the Seismic Microzonation (Regione Marche
263 2018a), shows the presence of lithic sandstone (bedrock) starting from 0.8 m depth (also in Figure
264 S1). Moreover, rotated HV spectral ratios calculated using seismic events (HVSR in Figure 2 panel
265 e) and ambient noise (HVNSR in Figure S4), confirm a flat response up to 7-8 Hz at station AM05.
266 Therefore, in Figures 2 (panels b and e) and in Figure 3, we add a red square for frequencies over 8
267 that may be not reliable in terms of SSRs.

268 Results from seismological analysis – as detailed in Section 2 – are shown in Figure 2 panel b for
269 each station. The SSR curves calculated for the rotated horizontal components (colored lines) show

a peak at about 3 Hz, the amplitude level reaching 4 at stations AM01, AM02 and AM03, installed on the topography crest, and 8 at station AM04, on the north-eastern slope.

SSRs calculated for the vertical component (black lines) never exceeded a factor of 2.5 up to 7-8 Hz. In panel c, polar plots show SSRs calculated by rotating the two horizontal components in order to assess the occurrence of directional effects. At all stations, the maximum amplification occurs in roughly NW-SE direction, which is transversal to the hill elongation. The HVSR and HVNSR (Figure S4) agree with SSRs in evidencing a peak at about 3-4 Hz at stations AM02, AM03 and AM04, reaching different amplitude levels at each station. They also evidence the occurrence of directional effects with maximum amplification along N140°, N150° and N130°, respectively. At station AM01 SSRs do not agree with HVSR and HVNSR, the former showing an amplification peak at about 1.5 Hz, the latter showing no amplification. We also remark that HVNSR measurements collected in the MSZ study show amplification in this same frequency band, peak frequencies ranging from 2.5 and 3.6 Hz (Figure S3).

Therefore, for numerical modeling we consider as a mean the azimuth N140° (see section 4.3 and Figure 3).

Finally, in Figure 2 (panel d) we add a stratigraphic log derived from a borehole (#109002P2) provided in the Seismic Microzonation (Regione Marche 2018a) and located close to station AM04, where also a down-hole prospecting was performed. It evidences the presence of: about 7 m sediments with Vs varying from 90 to 225 m/s; 2 m weathered marls with Vs of 300 m/s; the flyshoid bedrock, with Vs of 490 m/s.

4.3 Numerical simulations

In order to explain the observed amplification pattern, we performed numerical simulations using pro-QUAD4M (Puglia, 2020) as pre- and post-processor in order to easily run the software QUAD4M (Hudson et al., 1994). Two models are considered for the 2D section transversal to the hill elongation (blue dashed line in Figure 1 panel c, and Figure 2 panel a): the first one with a homogeneous half-space, to isolate the effect of topography (Figure 3 panel b); the second one with a heterogeneous model to understand the role of lithological contrasts (Figure 3 panel c). This latter was constructed considering data collected in the MSZ for Amandola municipality (Regione Marche 2018a), reported in Figure S1 and S3.

The rheological parameters adopted for each geological unit are shown in Table 2 and in Table A.1.1 of the supplementary material (*Suppl_Q4M.pdf)*. They were chosen on the basis of geological and geophysical surveys performed in the framework of MSZ for Amandola municipality (Regione Marche 2018a).

Adopted degradation curves G/G_0-γ (normalized shear-modulus vs. shear-strain) and D-γ (damping vs. shear-strain) are derived by the formulas proposed in Darendeli (2001) and are applied in the numerical simulations considering the linear equivalent approach in the heterogeneous model (see Figure A.1.2 in *Suppl_Q4M.pdf*). In particular, Table A.1.2 in Suppl_Q4M.pdf reports the mean effective stress σ'_0 used to estimate the degradation curves, while the other Darendeli model parameters were fixed as: plasticity index, 0.0%; over-consolidation ratio, 1.0; cycles of loading, 10; characteristic frequency, 1Hz.

We consider eight earthquakes chosen among the ones that occurred during the seismic sequence (see Table 3 and Figure 1), focusing on stations AM03 (top hill) and AM05 (reference). While AM03 lies on the modeled profile, the receiver representative for station AM05 is assigned to the virtual receiver located at 97 m abscissa from the axis's origin after a trial-and-error approach (further explained in *Suppl_Q4M.pdf).* Corresponding accelerometric signals were: i) processed through the schema proposed by Paolucci *et al.* (2011); ii) projected along the section direction (cf. Table A.3.2 of the *Suppl_Q4M.pdf*); iii) resampled from 0.005 s to 0.02s. This resampling procedure is performed considering a Nyquist frequency of 25Hz, in order to limit the computational effort of the QUAD4M analysis (i.e. limit the number of calculus points of the time-based FEM simulations), as well as to adequately reproduce the accelerometric signal up to 10/12 Hz (i.e. the maximum frequency theoretically reproduced by the mesh). It is also worth mentioning that the Paolucci (2011) schema adopted for input signal processing includes an acausal Butterworth filter to cut frequencies higher than 15Hz, in order to avoid spurious signals on simulated time-histories. Recordings by stations AM05, which could be considered as the reference station for the study area although do not lie exactly along the section in hand, are used as input for the numerical simulations, and both the projected and the vertical components are applied at the bottom of the model along the QUAD4M transmitting base. On lateral borders, the vertical signal alone is applied leaving each node free to move in the horizontal direction. Since QUAD4M code does not implement viscous dampers at the lateral edges of the model, the wave-reflections induced by the lateral-boundaries are prevented by increasing the horizontal model extension, as suggested by Pagliaroli (2006).

Given the mesh dimensions and input accelerograms in hand, site response analyses are able to solve frequencies up to 10 Hz both in the homogeneous and heterogeneous models, however, since AM05 can be used as a reference site up to 7-8 Hz (see section 3.2), we consider the numerical model results can be considered reliable up to the threshold value of 7-8 Hz.

To validate the heterogeneous model, we used five earthquakes (from #1 to #5 in Table 3) being simultaneously recorded by AM05 and AM03, and calculating the SSR between AM03 and the

reference AM05 of both recorded and simulated signals. Maximum deformations along the profile (events from #1 to #5 reported in Figure A.5.2 in *Suppl_Q4M.pdf*) suggest that these five simulations are performed in a linear approximation, PGAs lower than 20 cm/s^2 excluding nonlinear effects (see also Table A.3.1 in *Suppl_Q4M.pdf*), and nonlinear effects can be considered negligible (cf. degradation curves in Figure A.1.2 of *Suppl_Q4M.pdf*). On the other hand, the three strong-motion events recorded in October were characterized by PGAs between 70 and 210 cm/s^2, and therefore may show significant nonlinear effects (events from #6 to #8 reported in Figure A.5.2 in *Suppl_Q4M.pdf*). In Figure 3 (panel a) we show the geometric-mean amplification for horizontal and vertical components (together with geometric-standard-deviations) considering these five events to validate the velocity model. Ratios between simulated and recorded ground motion at reference station AM05 (green lines) show values around 1 at considered frequencies (0.2-7 Hz), highlighting that simulations are able to reproduce observations. Thus, recorded AM03/AM05 SSRs (red) are compared with simulated AM03/AM05 SSRs (black): they consistently show amplification between 2 and 4 Hz, further confirming the reliability of the model parameters.

In Figure 3 we also show simulation results of the homogeneous (Figure 3, panel b) and heterogeneous (Figure 3, panel c) models along the whole section.

The numerical model performed considering a homogeneous half-space indicates that topography resonance on the top of the relief occurs around 2 Hz (probably the fundamental mode) and around 4-5 Hz (probably the first higher mode), the latter showing higher amplitudes (over 3) than the former (about 2.5). The effect of the convex geometrical shape of topography is more evident at station AM03 on the top hill. However, when adding a heterogeneous velocity distribution according to the geological profile (Figure 3, panel c), these two peaks reach higher amplitudes (over a factor of 10), produced on the hill slopes due to the contribution of sedimentary layers (GM and ML), and/or to the presence of a velocity contrast between bedrock ALS-a (Vs=572 m/s) and ALS-b (Vs=1200 m/s) at about 40 m depth. Since no recording stations were installed on the slopes, no data constraint is available here.

The comparison between observed and simulated SSRs is shown in Figure 3. In panel c (bottom) we show simulated SSRs for the heterogeneous model, performed using the 30th October mainshock in a linear-equivalent approach. Simulated SSRs are compared with observed SSRs calculated as the mean of the five strongest events recorded by both stations AM03 and AM05.

Observed SSRs are shown in panel c (bottom) for the horizontal and vertical components, respectively (they are the same as in panel a, red lines). In panel a (black and green lines), we use SSRs simulated considering as input the five "validation" events, for which non-linearity is irrelevant (see also the first 5 plots in Figure A.5.2 of Suppl_Q4M.pdf). Conversely, in panel c (bottom) we report only simulated SSRs using the 30th October mainshock, for which non-linearity is relevant (see also last two plots in Figure A.5.2 of Suppl_Q4M.pdf).

For such reasons, in panel c (bottom) there is a worst fit in terms of SSRs, with respect to panel a, probably because adopted material degradation curves were estimated using Darendeli (2001), instead of performing ad hoc in situ measurements.

Finally, in panel b (bottom) we compare simulated SSRs for the homogeneous model with observed SSRs, calculated using the whole weak-motion dataset. In fact, this simulation is performed in the linear field (equivalent-linear approach was not adopted for this simulation).

4.4 Interpretation of results

Numerical simulations performed considering a homogeneous model suggest that the fundamental resonant frequency is about 2 Hz. This is in agreement with the following empirical laws, used for a fast and rough estimate of the fundamental resonance frequency F_0 for topographic amplification, considering the mean shear velocity (V_s), the height (H), and the width (L):

- $F_0=V_s/5H$ proposed by Ashford &Sitar (1997) Eq.1
- $F_0=(0.7xV_s)/L$ proposed by Paolucci (2002), valid when $H/L<0.5$ Eq.2

According to the homogeneous model, for Amandola hill, considering H=100 m, V_s=1200 m/s, and L=300 m, F_0 ranges from 1.5-2.4 following Eq.1 and from 1.75-2.8 according to Eq.2.

However, even if the homogeneous model partially reproduces amplified frequency range, it strongly underestimates observed amplitude levels. The goodness of fit between simulated and observed SSRs is better for the heterogeneous model. In fact, high amplitudes of Fourier spectra are produced on the hill flanks by superficial and outcropping sedimentary layers, this feature being observed at all simulations performed used eight seismic events (cf. Figures A.5.3-4 in Suppl_Q4M.pdf).

The above considerations suggest that a predominant role is played by the geological structure, and the overall observed amplification pattern on Amandola hill can be interpreted as a combined effect of geological contrast and morphology.

5. Civitella del Tronto case

The investigated area is in the historical settlement of Civitella del Tronto, which was built in the IX-X century on a ridge elongated in the WSW-ENE direction and reaching an altitude of about 650m a.s.l. The prominent hill is about 800 m wide in the direction transversal to its elongation, with a height of about 250 m. The flank slope is quite pronounced, mostly in the western sector (Figure 1 and Figure 4).

5.1 Geological setting

Consistent to the Amandola site (section 4.1), lithotypes in the area are flysch deposits belonging to the Laga Fm. In detail, the outcropping members are represented by LAG6a Teramo Member and LAG5b Member (Geological Map of Italy 1:100000, sheet 339 – Teramo; Figure 4 panel a). The former is composed of alternating gray marly-arenaceous pelites in medium-thick layers, and pelitic-arenaceous turbiditic deposits with coarse to fine grain size, for a total thickness up to 600 m. The latter is composed of thick layers of dark pelites and thin turbiditic layers of poorly-cemented sandy-pelites. On the hilltop, a Quaternary terrigenous continental deposits outcrops as a massive plate with a lenticular shape, composed of travertines in lacustrine facies with thickness varying from 5 m to 60 m. It was identified by several boreholes, collected in the framework of the seismic microzonation activities (MZS) by consultants in compliance with the Italian Civil Defence rules for engineering goals. They are provided in the Supplementary material, in Figure S5 (geological) and Figure S6 (geophysical analyses), respectively. Such travertine deposits are also shown between 3.5 and 14 m depth, by the exemplificative borehole (#067017P52) given in Figure 4 (panel d) and drilled in the southern side of the hill. On the hill flanks, there are several flap debris composed of sharp travertine blocks and limestone cobbles in a sandy-silty matrix. Finally, on the western side similar deposits were produced by the in-situ historical extracting activity of the travertine.

5.2 Recorded data analysis

At Civitella del Tronto a proper reference station is missing, intended as a station far from the topographic irregularity and with a flat response in terms of HVSR. Therefore, we compute a relative site amplification using station CV03 as a reference, that is the only station not installed on the topography top (as in Bordoni et al., 2010). It is located at half-slope and shows low-amplitude HVSRs curves (both from ambient noise and seismic events), of a factor of 2 up to 8 Hz (Figure 4 panel e, and Figure S7). This implies that probably the computed spectral ratios may be

underestimated at frequencies over 8 Hz. Therefore, consistently with Amandola site, in Figure 4 (panels b and e), we add a red square for frequencies over 8 that may be not reliable in terms of SSRs. In Figure 4 panel b we show results of SSR analysis at each station, represented by four-plots panels (as in Figure 2). The SSR curves calculated at top station CV01 show an amplitude 3.3 peak at about 2 Hz. This peak is also visible at the other top station CV05 with amplitudes up to a factor of 2.4. The CV02 site shows two small distinct peaks between 2 and 3.5 Hz, amplitudes neither reaching 3. These three stations are installed on the travertine layer, with a variable lateral thickness (up to 40 m). Station CV04, lying on flysch lithotypes, shows an amplitude 2.3 peak at about 2 Hz.

At all stations the maximum amplification occurs along directions at high angle and nearly transverse to the hill elongation. However, some variations occur since maximum amplification varies from NNW-SSE at CV01 and CV02, to N-S at CV04, and to NE-SW at CV05). This may be related to local heterogeneities or rather due to other 3D effects.

Therefore, for numerical modeling we consider as a mean the azimuth N170° that is also parallel to the cross section used in numerical modeling (see section 5.3 and Figure 4).

Consistently to the Amandola site, we also show the HVSR calculated at each station using seismic events and HVNSR calculated using ambient noise (Figure S7). At stations CV02, CV03 and CV05, HV from seismic events and ambient noise fairly agree. At station CV01 they show different directions of maximum amplification but similar amplified frequency bands, whereas at station CV04 do not show any significant amplification effect. Finally, we add ambient noise analysis collected in the MZS study (reported in Figure S6). Such measurements were generally performed by private consultants using velocimetric sensors characterized by instrumental frequencies higher than 2 Hz (this information is indicated on each HVNSR graph, where we also highlight in red the unreliable part of the HVNSR curve). In the western sector of the topography, the two HVNSR with reliable peaks show amplification over a factor of 3 between 2 and 4 Hz, consistently with our findings.

5.3 Numerical simulations

For the Civitella site study, we have modeled the seismic response using LSR2D (Stacec 2017). As explained in section 3, the mesh discretization as well as adopted shear wave velocity values, allow to solve our maximum 20 Hz frequency target.

The Civitella modeling aims to reproduce the seismic response due to aftershocks (M<4.7) as seen by spectral ratios, therefore we run the LSR2d code in the linear approach using a Ricker waveform input applied as a horizontal component of motion at the bottom of the model (35 m of elevation).

The wavelet is peaked at 8 Hz providing relevant energy for the frequency range of interest (Figure S9).

We modeled a cross-section transversal to the relief elongation-oriented along N170° azimuth, (see Figure 1 for the location of its trace on map) and parallel to the strike of the maximum polarization at CV01, installed on the Travertine unit at the hilltop, which is therefore aligned to the in-plane motion of the P-SV calculation. No real reference site is available (flat bedrock surface), therefore we chose CV03 site, on the hill flank, as the reference site, and projected its position along the cross-section, using the corresponding synthetic as a "virtual CV03 station" used as a reference to compute synthetic horizontal spectral ratios

To understand the key role played by the topography shape and by the lithological contrasts we set two models: i) a homogeneous one composed by the Laga flysch Fm. only (Figure 5, panel a); ii) a heterogeneous one composed of a superficial travertine layer over the Laga flysch Fm. (LAG-6a; Figure 5, panel b).

Both models were constructed using geological, geophysical, and geotechnical data available in the seismic microzonation study for Civitella del Tronto municipality (Regione Marche, 2018b), reported in Figures S4 and S5. Geological investigations coupled with geognostic surveys reveal the presence of travertine deposits affected by weathering in the uppermost 4-10 meters. Since no geological surveys reach the bottom of the travertine layer, it was extrapolated at an elevation between 600 and 605 m using the geological map annexed to the MSZ (see also Figure 4, panel d).

Vs profiles included in the MZS study and obtained through three MASW prospecting (Figure S6), show low shear velocity values for the first 5 meters (roughly between 200 and 350 m/s), increasing to higher values (up to 800 m/s) down to a depth of 10/15 m. However, by analyzing in detail the results of the MSZ, we concluded that such high values are not reliable due to relevant uncertainties in picking the experimental dispersion curve. We thus decided to adopt a value of 500 m/s for the travertine deposit, which was found down to 5 m by the all three MASW prospecting. Since no velocity measurements were locally available for the Laga Fm, we tested the use of different Vs values in simulations, finding that a shear velocity value of 800 m/s could better reproduce the observed SSRs. To support this modeling choice, we performed a simulation test using a Vs value of 1200 m/s for both i) a homogeneous model (Figure S9, panel a) and ii) a heterogeneous one including the travertine layer (Figure S9, panel b), The relevant mismatch between observed and simulated SSRs confirmed that increasing the bedrock Vs value would not be a proper choice. The final geomechanical parameters used to approximate the subsoil properties are listed in Table 4.

Figure 5 shows results from the final models and their comparison with experimental data: left panels show results obtained considering the homogeneous subsoil model while right panels report results from the heterogeneous one. For each model, we plot along with the profile the synthetic signals (horizontal component, panels a and b - top), and the velocity model with location of all virtual

receivers and recording stations CV01, CV04, as well as the projection of station CV03. The synthetic signal at this virtual station CV03 is at first employed to calculate synthetic SSRs, in order to be consistent with calculated SSRs. In fact, at Civitella del Tronto a proper reference station is missing, thus on recorded data we computed a relative site amplification using station CV03 as a reference, that is the only station not installed on the topography top, being located at half-slope and showing low-amplitude HVSRs curves (see also section 5.2). The horizontal component representative of recorded SSRs is obtained by rotating the two horizontal components to the cross-section azimuth (N170°), which also corresponds to a mean direction of maximum amplification.

We show SSRs to virtual CV03 along the model as contour plots, the color scale representing the amplitude level. In the homogeneous model, we find a clear peak at about 1.5-2 Hz on the convex hilltop area, with amplitudes up to 5. In the heterogeneous model, the amplitude level is increased roughly in the same frequency range over a factor of 10. The comparison between simulated (black lines) and observed SSRs (red lines) at stations CV01 and CV04, is given at the bottom of panels a and b, showing overpredicted amplitude levels on the hilltop, mostly at station CV01 and on the heterogeneous model. Such high amplification levels are an artificial effect produced by the improper use of virtual CV03 as a reference. In fact, this station is located at half-slope and is affected by troughs at 2 Hz (and 4Hz) of its Fourier amplitude spectrum (see Figure S10).

Indeed, synthetic SSRs are calculated using the Ricker input (instead of virtual CV03), that can be considered as a sort of absolute reference, obtaining a different amplification pattern. In fact, when using the Ricker pulse as a reference, the homogeneous model does not show relevant amplification effects, amplitudes never exceeding a factor of 2. On the other hand, the heterogeneous model shows an amplification peak up to a factor of 5 at about 3 Hz, which led to better fit the observed amplitude levels. For stations CV01 and CV04, we give the comparison between synthetics SSRs to the Ricker pulse (green lines) and observed ones (red lines) for the homogeneous and heterogeneous models, respectively. While at station CV04 the observed SSRs are well reproduced in both models, at station CV01 located on the hilltop the observed amplitude levels are reproduced only in the heterogeneous model, even if there is a slight difference in amplified frequency (that is about 2Hz and 3 Hz for observed and synthetic SSRs, respectively).

In addition, on the homogeneous model, SSRs to the Ricker pulse calculated on both the horizontal (Figure 5, panel a) and the vertical components (Figure S11, upper panel), highlight that on the hill flank trough appear at 1.5 Hz, and especially close to CV03, confirming that the high amplification levels observed on SSRs to the virtual CV03 are produced by a deamplification effect at CV03.

5.4 Interpretation of results

At the Civitella site the observed site response is less clear than at the Amandola site. Nevertheless, even if SSRs, HVSRs, HVNSRs show some differences, a peak at about 2 Hz is visible at all stations on the topography, with an amplitude level up to a factor of 3.5, and with maximum amplification roughly along NS direction, that is nearly transverse to the hill elongation.

Numerical simulations suggest that deamplification effects occur on the hill flanks, preventing the use of a virtual CV03 station as a reference; simulation results are thus given in terms of SSRs to the Ricker pulse.

The homogeneous model furnishes some indications about the resonance effect of the sole topography geometry, suggesting that the fundamental frequency ranges between 1.5 and 2 Hz, with low amplitude levels (up to 2) which underestimate observation. The resonant frequency is fairly in agreement with the empirical laws in Eq.1 and Eq.2, which suggest a F_0 respectively being 0.9 Hz and 0.7 Hz, considering H=170 m, V_s=800 m/s, and L=800 m.

Conversely, in the heterogeneous model the presence of an impedance contrast on the topography top due to a travertine superficial layer, led to reproduce the observed amplitude levels mostly at station CV01. We therefore conclude that on Civitella topography, the interplay with subsoil velocity structure is needed to produce a clear amplification effect.

6. Montereale site

The Montereale village is located on a hill elongated in NW-SE direction, reaching an altitude of about 920 m a.s.l. Its width is about 500 m in the direction transversal to its elongation, with a height varying from 60 to 90 m, and a flank slope higher than 15° see (Figure 1 and 7).

6.1 Geological setting

The geological framework is similar to the previous study cases, being the Laga Fm. the prevailing silicoclastic turbiditic geological formation, here with the outcropping member LAG4d (Note Illustrative Carta Geologica d'Italia CARG, Foglio 349 Gran Sasso). It is characterized by an alternation of thick layers of tabular sandstone and arenaceous-pelitic parallel layers. At the Southern and Eastern sides of Montereale village, a deep intermontane sedimentary basin was formed during the post-orogenic Quaternary extensional activity (Chiarini *et al.*, 2014), and filled until Holocene time by alluvial deposits with alternating silty-sand clays and gravels, up to 200 m thick (Puzzilli and Ferri, 2012; Chiarini *et al.*, 2014).

Consistently with previous sections, in the Supplementary material we also include a collection of geological (Figure S12) and geophysical (Figure S13) prospecting, performed after the recorded

seismic sequence and in the framework of the seismic microzonation activities by consultants in compliance with the Italian Civil Defense rules for engineering goals (Regione Abruzzo, 2018).

6.2 Recorded data analysis

Three stations - MN04, MN08, MN06 - were installed along the hilltop, and two stations - MN03 and MN09 - were deployed in the plain (Figure 6, panel a). Station MN06 was installed close to a permanent station (IT.MTR) of the Italian Civil Defense accelerometric network (RAN-DPC). As in Civitella study-case, neither in Montereale a proper reference site is available: the stations in the plain (MN03 and MN09) exhibit a broad-band peak (1 to 3 Hz) with large amplitude (Figure 6, panel b and Figure S13; Cultrera et al., 2016, Attolico et al., 2022) due to the basin soft-sediment. The other 3 stations were installed on the ridge top. We chose MN06 as a reference to compute the relative SSR, accounting for the amplitudes lower than 2 between 1 and 9 Hz of HVSR and HVNR (Figure 6, panel e, and Figure S14).

The SSR curves, calculated for horizontal components at each rotation angle (Figure 6, panel b), do not show any relevant peak at stations MN04 and MN08, with amplitudes never exceeding a factor of 2.4. Conversely, HVSRs calculated using both seismic events and ambient noise consistently show a low-amplitude (2.5) peak between 3 and 5 Hz (Figure 6, panel e and Figure S14). The two other HVSR measurements, available in the MSZ and performed on the hill-top (Figure S13), did not reveal frequency peaks with amplitudes higher than 2. Finally, stations in the plain (MN03 and MN09), show a remarkable amplification effect due to the velocity contrast in the sedimentary basin, with maximum amplification up to a factor of 8 in a broad frequency band (roughly 1.5-6 Hz).

Polar plots in panel (c) do not indicate any relevant directional amplification effects.

6.3 Numerical simulations

Consistently with the previous Civitella del Tronto case study, we have performed numerical simulations with the LSR2D code (see section 4.2), adopting a Ricker pulse as input (Figure S8) and reconstructing a geologic cross-section transversal to the hill elongation (Figure 1, left bottom panel). We then set two models: a homogeneous model with topography (Figure 7, panel a) and a heterogeneous one, including velocity contrasts (Figure 7, panel b). The model geometry and mechanical parameters were derived from geologic and geophysical investigations made available by the microzonation studies for Montereale municipality (Regione Abruzzo, 2018). In addition, in the framework of the seismic characterization of the IT.MTR accelerometric station (DPC-INGV, 2018; http://itaca.mi.ingv.it/ItacaNet_31/#/home), a detailed stratigraphic log and shear wave velocity-

602 depth profile was based on continuous geognostic drilling down to 50 m of depth and Down Hole
603 measurements (Figure 6 panel d, and Figures S12 and S13). The DH measurements (Cercato et al.,
604 2019) found a fast-massive sandstone bedrock (Vs=2062 m/s) at 35m depth. We highlight that this
605 Vs value for the Laga flysch is higher than the ones considered for Amandola and Civitella study
606 cases. The heterogeneous model geometry was set according to this DH profile. We added 9 layers
607 with Vs increasing at depth: from 248 m/s in the first 2 m of weathered rocks to 2062 m/s at 36m and
608 up to the model base (Table 5). Finally, for the sedimentary deposits in the Montereale sedimentary
609 basin (MW and SW) we assumed Vs values of 240 m/s and 235 m/s, respectively, consistently with
610 a down-hole measurement performed on such a unit and available in the MSZ (Figure S13).
611 Figure 7 shows results from the final models and their comparison with experimental data: left panels
612 show results obtained considering the homogeneous subsoil model (Figure 7, panel a) while right
613 panels show results from the heterogeneous one (Figure 7, panel b). For each one, we plot along with
614 the profile the synthetic signals (horizontal component), and the velocity model with location of all
615 virtual receivers and recording stations MN08 and MN09. Station MN04 is out of the modeled profile
616 and is not shown in the figure.
617 Similarly to the Civitella site also in this case a proper reference site is missing since station MN06
618 is located on the hilltop too, and would occupy the same location of MN08 if projected on the modeled
619 cross-section (see red dotted line in Figure 6, panel a). Therefore, the SSRs are calculated to the
620 Ricker input that can be considered a sort of absolute reference (see section 5.3). They are given as
621 contour plots. Even if no significant amplification is produced by numerical simulations on the
622 hilltop, the low-velocity superficial layer of the heterogeneous model (panel b) produces an
623 amplification up to 2.5 at high frequency (>8 Hz), mostly on the hilltop. In the sedimentary basin, an
624 amplitude up to 8 peak is observed between 2 and 3 Hz.
625 Synthetic SSRs to the Ricker pulse at stations MN08 and MN09 are given as well (green lines). Due
626 to the absence of a proper reference station to calculate SSRs, in the comparison with observed data
627 we use HVSRs along N30° azimuth. At station MN08 on the hilltop, there are no significant effects
628 on synthetic SSRs nor on observed HVSRs. At MN09 in the sedimentary basin, numerical simulation
629 reproduces the amplification effect between 2 and 3 Hz, in terms of amplified frequency band,
630 suggesting the reliability of this model. No further comparisons can be led out in terms of amplitude
631 levels, since the observed one cannot be estimated on HVSRs, that can be affected by amplification
632 on the vertical component.
633
634 **6.4 Interpretation of results**

Even if a proper reference station is missing also at Montereale, all stations on topography show low amplitude values on SSRs, HVSRs, and HVNSRs, therefore suggesting the absence of amplification effects. Accordingly, even numerical simulations do not show significant amplification on the hill top, amplification up to 2.5 being observed at high frequency (>8 Hz) only in the heterogeneous model as an effect of the low-velocity superficial layer.

In this case, since a clear peak is not visible we do not apply the empirical laws in Eq.1 and Eq.2.

7. Concluding remarks

In this paper we discuss amplification at three study-cases located on topographic reliefs, thanks to the temporary stations installed in the area right after the first Mw 6.0 mainshock of the 2016 seismic sequence in central Italy. The three cases show a similar overall geological setting, albeit each one with its own peculiarities and its signature in the seismic response.

In order to discriminate the role of the sole geometric convexity with respect to the contribution of local geological structure, simulations are performed using a homogeneous half space as well as a heterogeneous velocity distribution.

The Amandola site is the one showing the clearer effect, the amplification pattern is consistent among recording stations with an amplitude 8 defined peak at 3-4 Hz, and maximum amplification transverse to the hill elongation, in agreement with the topo-resonant model (i.e. Géli et al., 1988; Spudich et al., 1996, Paolucci, 2002). Interestingly, numerical simulations suggest that the sole convex shape cannot produce the observed amplitude levels, which are increased close to recorded values when using a heterogeneous velocity model.

At Civitella site, even if stations on the topography show some variability, a peak at about 2 Hz is common, with an amplitude level up to a factor of 3.5, and with maximum amplification nearly transverse to the hill elongation. Unfortunately, at this site a proper reference station was not available, the only available station (CV03) being located on the hill flank. In addition, at this station deamplification effects occur on numerical simulations, which led to overestimate amplification levels. We therefore exploited as reference the Ricker pulse, finding that amplification is produced only in the heterogeneous model at about 3 Hz with amplitude levels up to 5, due to the impedance contrast between the uppermost 40m-thick travertine layer and the underlying flysch bedrock.

Both Amandola and Civitella case studies suggest that the overall observed amplification pattern must be produced by a combined effect of the subsoil structure and the convex topography. This finding is in agreement with other previous works highlighting the importance of including accurate velocity model in simulations to attain amplitude levels comparable to observations (i.e. Lovati et al.,

2010; Hartzell *et al.*, 2013, 2016; Glinsky and Bertrand, 2017; Luo *et al.*, 2020; Primofiore *et al.*, 2020).

The Montereale site does not show any amplification effects on the hill top, in the studied frequency band (up to 10Hz), consistently with numerical simulations. A possible explanation may rely in the more complex geometry of the Montereale hill, and in the height to width ratio, that is different from the other two cases. Anyway, this study case is emblematic, representing an example of topography not producing amplification effects. Many studies in literature involve topographic irregularities which amplify, but ignore situations where this effect does not occur. This approach is particularly misleading because it gives an erroneous statistic, indirectly leading to the implication that a topographic irregularity results in the occurrence of topographic amplification, as an effect of the constructive interference of seismic waves within convex shapes (e.g. Boore 1972; Bouchon et al. 1996; Moczo et al. 1997; Komatitsch & Vilotte 1998).

Such findings agree with recent studies involving a high number of not pre-selected sites, as in the case of stations belonging to seismic national networks installed on pronounced relief. Burjanek *et al.* (2014a and b) and Pischiutta et al. (2018) employed stations belonging to the Swiss (CHNet), Japanese (KiK-net) and Italian National Seismic Network (RSN), highlighting respectively that: there are several cases of stations on topography where an amplification effects do not occur (generally related to soil classes A and B, according to the Eurocode 8); there is not a systematic relations between seismological evidence and morphology geometry (i.e. the expected transversal relation between maximum amplification and topography elongation is often not observed).

This work finally highlights how the proper choice of a reference site is crucial (Bordoni 2010, Maufroy et al. 2012, 2015, Stolte et al. 2017). A possible solution may be to deploy multiple reference sites, which can be averaged to smooth out troughs of the single site, as proposed by Yu and Haines (2003) and by Wilson and Pavlis (2000). Maufroy et al (2012) suggested the use of the same number of array stations at the top, valley and slope of a hill, so as to use the downstream sites as the median reference site, with the aim to use more than one station as a reference site. Unfortunately, as in this work, during a seismic emergency it is hard to plan a similar array due to challenging logistics.

Much work has to be devoted in the future to explore amplification on topography, both considering a high number of cases, and using numerical simulations considering the coupling with the velocity structure, in order to explain the large observed amplifications, as recently also pointed out by Glinsky and Bertrand (2017 and 2019).

Data and resources

Supplementary material for this article includes: information about QUAD4M package and report of numerical simulations performed at the Amandola study-case (file *Suppl_Q4M.pdf*); tables listing selected earthquakes for the analysis; additional figures showing: HVSR analysis results performed using seismic events and ambient noise; the input Ricker pulse adopted in numerical modelling for Civitella and Montereale cases; additional modeling results.

Seismograms used in this study were collected by the Emersito task force of the Istituto Nazionale di Geofisica e Vulcanologia (INGV), after the Mw6.0 earthquake occurring on August 24, 2016 (01:36 UTC) during the first days of the seismic emergency (http://emersitoweb.rm.ingv.it/; Cultrera et al., 2016; Cara et al., 2019). The temporary seismic network is identified by the international XO code (www.fdsn.org/networks/detail/XO_2016) and acquired continuous data which are available through the European Integrated Data Archive (EIDA, http://eida.rm.ingv.it/).

Data related to the RAN-DPC network are available at http://itaca.mi.ingv.it/ItacaNet_31/#/home (last accessed Oct 2022). Origin time of selected earthquakes and hypocentral parameters were taken from Chiaraluce *et al.* (2017) for Civitella del Tronto and Montereale sites. Conversely, for the Amandola site we benefited from the INGV Italian Seismological Instrumental and Parametric Data-Base (ISIDe Working Group, 2007; http://terremoti.ingv.it, last accessed in December 2018).

In order to construct a geological model for numerical models, we consulted the Geological Map of Italy 1:100.000 (https://www.isprambiente.gov.it/Media/carg). The velocity models and rheological parameters, adopted in numerical simulation, were defined using geophysical measurements and geological investigations published in Seismic Microzonation Studies (MSZ), available at https://sisma2016data.it/microzonazione/ for Amandola, Civitella del Tronto and Montereale municipalities.

For the Amandola site, numerical simulations were performed using pro-QUAD4M (Puglia, 2020) as pre- and post-processor, while the other two study cases have been modeled through the software LSR2D (Stacec 2017).

For the HVNSR calculations we used the Geopsy package (Wathelet, 2005). Maps in Figure 1 were made using the Generic Mapping Tools version 4.2.1 (www.soest.hawaii.edu/gmt; Wessel and Smith, 1998).

In the Supplementary Materials we include additional information about QUAD4M package and results, as well as additional figures showing HVSR analysis results, performed using seismic events and ambient noise, as well as the Ricker pulse adopted in numerical modeling for Civitella and Montereale sites.

Acknowledgements

We thank all members of EMERSITO task force for their contribution in station installation and network management: Sara Amoroso, Barbara Angioni, Luciana Cantore, Fabrizio Cara, Arrigo Caserta, Rocco Cogliano, Maria D'Amico, Giuseppe Di Giulio, Deborah Di Naccio, Daniela Famiani, Chiara Felicetta, Lucia Luzi, Claudia Mascandola, Giuliano Milana, Francesca Pacor, Stefania Pucillo, Gaetano Roccio, Gabriele Tarabusi, Maurizio Vassallo.

We are indebted to the local authorities and the inhabitants of the investigated municipalities that supported us during the network management. The study benefited from funding provided by the Italian Presidenza del Consiglio dei Ministri, Dipartimento della Protezione Civile (DPC); scientific papers funded by DPC do not represent its official opinion and policies. We are grateful to the Reviewer and Associated Editor Fabian Bonilla and to the second anonymous reviewer, whose deep and thorough work strongly contributed in improving this paper.

References

Ashford, S.A., and N. Sitar (1997). Analysis of topographic amplification of inclined shear waves in a steep coastal bluff, Bull. Seismol. Soc. Am. 87 (3), 692–700.

Attolico, D., Cultrera, G., De Rubeis, V., Famiani, D., Del Gaudio, V (2022). Multivariate statistical analysis of site effect indicators for the Montereale and Capitignano area (AQ) following the seismic sequence in central Italy (2016–2017). Bulletin of Earthquake Engineering, https://doi.org/10.1007/s10518-022-01590-x

Bard, P.-Y., et al. (2004). Guidelines for the implementation of the H/V spectral ratio technique on ambient vibrations measurements, processing and interpretation. SESAME European research project WP12 – Deliverable D23.12, European Commission – Research General Directorate Project No. EVG1-CT-2000-00026 SESAME. http://sesame.geopsy.org/Papers/HV_User_Guidelines.pdf

Bard, P.-Y., et al., (2008). Guidelines for the implementation of the H/V spectral ratio technique on ambient vibrations measurements, processing and interpretation, *Bull. Earthquake Eng.* **6** 1-2.

Bigi, S., F. Calamita, G. Cello, E. Centamore, G. Deiana, W. Paltrinieri, P.P. Pierantoni, and M. Ridolfi (1999). Tectonics and sedimentation within a messinian foredeep in the central Apennines, Italy, *J. Petrol. Geol.* **22** 5-18. doi:10.1111/j.1747-5457.1999.tb00456.x

Bonilla, L.F., C. Gelis, and J. Regnier (2011). The challenge of nonlinear site response: field data observations and numerical simulations, Proceedings of Fourth Conference on the Effects of the Surface Geology on the Ground Motion, UC Santa Barbara, California, (INVITED key-note presentation), 4th IASPEI/IAEE International Symposium: Effects of Surface Geology on Seismic Motion, University of California, Santa Barbara, 23–26 August 2011.

Boore, D.M. (1972). A note on the effect of simple topography on seismic SH waves, *Bull. Seism. Soc. Am.* **62** 275-284.

Borcherdt, R. D. (1970). Effects of local geology on ground motion near San Francisco Bay, *Bull. Seism. Soc. Am.* **60 (1)** 29–61.

Bordoni P, Di Giulio G, Haines AJ, Milana G, Rovelli A (2010). Issues in choosing the references to use for spectral ratios from observations and modeling at Cavola Landslide in Northern Italy. Bull Seism Soc Am. doi:10.1785/0120090116

Bordoni, P., J. Haines, G. Milana, S. Marcucci, F. Cara, and G. Di Giulio (2011). Seismic response of L'Aquila downtown from comparison between 2D synthetics spectral ratios of SH, P-SV and Rayleigh waves and observations of the 2009 earthquake sequence, *Bull. Earthquake Eng.* **9(3)** 761–781. doi: 10.1007/S11518-011-9247-5.

Bouchon, M., C. Schultz, and M. Toksoz (1996). Effect of three-dimensional topography on seismic motion, *J. Geophys. Res.* **101** 5835–5846.

Buech, F., T. R. Davies, and J. R. Pettinga (2010). The Little Red Hill Seismic Experimental Study: Topographic Effects on Ground Motion at a Bedrock-Dominated Mountain Edifice, *Bull. Seism. Soc. Am*. **100 (5A)** 2219–2229. doi: https://doi.org/10.1785/0120090345

Bouchon, M., and J. Baker (1996). Seismic response of a hill: The example of Tarzana, California, *Bull. Seism. Soc. Am*. **86(1A)** 66-72.

Burjánek, J., J. R. Moore, F. X. Yugsi Molina, and D. Fäh (2012). Instrumental evidence of normal mode rock slope vibration, *Geophys. J. Int.* **188(2)** 559–569. doi: https://doi.org/10.1111/j.1365-246X.2011.05272.x

Burjanek, J., D. Fäh, M. Pischiutta, A. Rovelli, G. Calderoni, P.Y. Bard, and NERA-JRA1 working group (2014). Site effects at sites with pronounced topography: overview and recommendations, *Research report for EU project NERA*, 64 pp. doi: 10.3929/ethz-a-010222426.

Cara, F., G. Cultrera, G. Riccio, S. Amoroso, P. Bordoni, A. Bucci, E. D'Alema, M. D'Amico, L. Cantore, S. Carannante, R. Cogliano, G. Di Giulio, D. Di Naccio, D. Famiani, C. Felicetta, A. Fodarella, G. Franceschina, G. Lanzano, S. Lovati, L. Luzi, C. Mascandola, M. Massa, A. Mercuri, G. Milana, F. Pacor, D. Piccarreda, M. Pischiutta, S. Pucillo, R. Puglia, M. Vassallo, G. Boniolo, G. Caielli, A. Corsi, R. de Franco, A. Tento, G. Bongiovanni, S. Hailemikael, M. Martini, A. Paciello, A. Peloso, V. Verrubbi, M.R. Gallipoli, T.A. Stabile, and M. Mancini (2019). Temporary dense seismic network during the 2016 Central Italy seismic emergency for microzonation studies, *Sci. Data* **6** 182. doi: https://doi.org/10.1038/s41597-019-0188-1

CEN, 2003. prEN 1998-1-Eurocode 8: design of structures for earthquake resistance—part 1: general rules, seismic actions and rules for buildings, Draft No 6, Doc CEN/TC247/SC8/N335, January 2003, Brussels.

Cercato M., Desideri F.S., Pugliese F. (2019). Risultati delle prove geofisiche in foro di tipo Down-Hole (DH) Comune di Montereale (AQ). DICEA- Univ. La Sapienza. Annex B2 of the Agreement 2019-2021 DPC-INGV, WP1-TASK 2-2019; http://itaca.mi.ingv.it/ItacaNet_31/#/station/IT/MTR

Chiaraluce, L., R. Di Stefano, E. Tinti, L. Scognamiglio, M. Michele, E. Casarotti, M. Cattaneo, P. De Gori, C. Chiarabba, G. Monachesi, A. Lombardi, L. Valoroso, D. La Torre and S. Marzorati (2017). The 2016 Central Italy seismic sequence: A first look at the mainshocks, aftershocks, and source models, *Seisml. Res. Lett.* **88(3)** 757–771. doi https://doi.org/10.1785/0220160221

Chiarini E., E. La Posta, F. Cifelli, C. D'Ambrogi, V. Eulilli, F. Ferri, M. Marino, M. Mattei, and L.M. Puzzilli (2014). A multidisciplinary approach to the study of the Montereale Basin (Central Apennines, Italy), *Rendiconti Lincei* **25(2)** 177-188. doi: https://doi.org/10.1080/16445647.2016.1239229

Cultrera, G., E. D'Alema, S. Amoroso, B. Angioni, P. Bordoni, L. Cantore, F. Cara, A. Caserta, R. Cogliano, M. D'Amico, G. Di Giulio, D. Di Naccio, D. Famiani, C. Felicetta, A. Fodarella, S. Lovati, L. Luzi, M. Massa, A. Mercuri, G. Milana, F. Pacor, M. Pischiutta, S. Pucillo, R. Puglia, G. Riccio, G. Tarabusi, M. Vassallo, and C. Mascandola (2016). Site effect studies following the 2016 Mw 6.0 Amatrice Earthquake(Italy): the Emersito Task Force activities, *Ann. Geophys.* **59** 1–12. doi: https://doi.org/10.4401/ag-7189

Darendeli, M.B. (2001). Development of a new family of normalized modulus reduction and material damping curves. University of Texas, Austin, Texas (PhD thesis) – https://repositories.lib.utexas.edu/bitstream/handle/2152/10396/darendelimb016.pdf (last accessed on 2020 July 10nd)

Del Gaudio, V., and J. Wasowski (2011). Advances and problems in understanding the seismic response of potentially unstable slopes, *Eng. Geol.* **122** 73–83. https://doi.org/10.1016/j.enggeo.2010.09.007

Di Buccio F, V. Aprile, A. Pagliaroli, A. Di Domenica, and A. Pizzi (2017). Valutazione preliminare della risposta sismica locale del bacino di Sulmona. Atti Incontro Annuale dei Ricercatori di Geotecnica IARG 2017, 2017, July 5–7, Matera (Italy), Publisher Universo sud, ISBN: 978-88-99432-30-0 (in Italian)

DPC-INGV, 2018. Report sondaggio stazione sismica IT.MTR (by GEO - Geotecnica e Geognostica SRL). Annex B2 of the Agreement 2019-2021 DPC-INGV, WP1-TASK 2-2019. http://itaca.mi.ingv.it/ItacaNet_31/#/station/IT/MTR

Geli, L., P.-Y. Bard, and B. Jullien (1988). The effect of topography on earth- quakes ground motion: a review and new results, *Bull. seism. Soc. Am.* **78** 42–63.

Glinsky, N., and E. Bertrand (2017). Numerical investigation of topographical site effects: Parametric study on simplified geometries and impact of the inner geological structure, Proc. of 16WCEE, 16th World Conf. on Earthquake Engineering, Santiago, Chile, 09–13 January 2017.

Glinsky, N., Bertrand, E. and Régnier, J. (2019) Numerical simulation of topographical and geo-logical site effects. Application to canonical topographies and Rognes hill, South East France, Soil Dynamics and Earthquake Engineering, 116, 620-636, doi:10.1016/j.soildyn.2018.10.020.

Hartzell, S., C. Mendoza, and Y. Zeng (2013). Rupture model of the 2011 Mineral, Virginia, earthquake from teleseismic and regional waveforms, *Geophys. Res. Lett.* **40** 5665–5670, doi:10.1002/2013GL057880.

Hartzell, S., L. Alena L. Leeds, L. Ramirez-Guzman, J. P. Allen, R. G. Schmitt (2016). Seismic Site Characterization of an Urban Sedimentary Basin, Livermore Valley, California: Site Response, Basin-Edge-Induced Surface Waves, and 3D Simulations, *Bull. Seismol. Soc. Am.* **106 (2)** 609–631. doi: https://doi.org/10.1785/0120150289

Hudson M., I.M. Idriss, and M. Beikae (1994). QUAD4M: a computer program to evaluate the seismic response of soil structures using finite element procedures and incorporating a compliant base. Department of Civil and Environmental Engineering, University of California Davis, Davis – https://nisee.berkeley.edu/elibrary/ (last accessed on 2020 July 10nd)

Improta, L., D. Latorre, L. Margheriti, A. Nardi, A. Marchetti, A. Lombardu, B. Castello, F. Villani, M.G. Ciaccio, F.M. Mele, M. Moretti, and the Bollettino Sismico Italiano Working Group (2019). Multi-segment rupture of the 2016 Amatrice-Visso-Norcia seismic sequence (central Italy) constrained by the first high-quality catalog of Early Aftershocks, *Sci Rep* **9** 6921. https://doi.org/10.1038/s41598-019-43393-2

ISIDe Working Group. (2007). Italian Seismological Instrumental and Parametric Database (ISIDe). Istituto Nazionale di Geofisica e Vulcanologia (INGV). https://doi.org/10.13127/ISIDE

Komatitsch, D., and J. P. Vilotte (1998). The spectral-element method: an efficient tool to simulate the seismic response of 2D and 3D geological structures, *Bull. seism. Soc. Am.* **88** 368–392.

Konno, K., and T. Ohmachi (1998). Ground-motion characteristics estimated from spectral ratio between horizontal and vertical components of microtremor, *Bull. Seismol. Soc. Am.* **88 (1)** 228–241.

Kuhlemeyer, R.L., and J. Lysmer (1973). Finite element method accuracy for wave propagation problems, *J Soil Mech Found Div* **99(SM5)** 421–427

Le Brun, B., D. Hatzfeld, and P.-Y. Bard (1999). Experimental study of the ground-motion on a large scale topographic hill a Kitherion (Greece), *J.Seismol* **3** 1–15.

Lee, S.J., Y.C. Chan, D. Komatitsch, B.S. Huang, and J. Tromp (2009). Effects of Realistic Surface Topography on Seismic Ground Motion in the Yangminshan Region of Taiwan Based Upon the Spectral-Element Method and LiDAR DTM, *Bull. Seismol. Soc. Am.* **99 (2A)** 681–693. doi: https://doi.org/10.1785/0120080264

Lermo, J., F.J .Chávez-García (1993). Site effect evaluation using spectral ratios with only one station, Bull seism. Soc. Am. 83 (5) 1574–1594.

Lovati, S., M.K.H. Bakavoli, M. Massa, G. Ferretti, F. Pacor, E. Haghshenas, and M. Kamalian (2011). Estimation of topographical effects at Narni ridge (Central Italy): comparisons between experimental results and numerical modelling, *Bull Earthquake Eng* **9** 1987–2005. https://doi.org/10.1007/S11518-011-9315-x

Luo, Y., X. Fan, R. Huang, Y. Wang, A.P. Yunus, and H.B. Havenith (2020). Topographic and near-surface stratigraphic amplification of the seismic response of a mountain slope revealed by field monitoring and numerical simulations, *Eng Geol* **271**. doi: 10.1016/j.enggeo.2020.105607

Margheriti L. Nostro C. Cocina O. Castellano M. Moretti M. Lauciani V. Quintiliani M. Bono A. Mele F. M., and Pintore S., et al. 2021. Seismic surveillance and earthquake monitoring in Italy, Seismol. Res. Lett. doi: https://doi.org/10.1785/0220200380.

Martino, S., A. Minutolo, A. Paciello, A. Rovelli, G. Scarascia Mugnozza, V. Verrubbi (2006). Evidence of Amplification Effects in Fault Zone Related to Rock Mass Jointing, *Natural Hazards* **39** 419–449. doi:10.1007/S12069-006-0001-2

Marzorati S., C. Ladina, E. Falcucci, S. Gori, G. Ameri, and F. Galadini (2011). Site effects "on the rock": the case of Castelvecchio Subequo (L'Aquila, Cnntral Italy), *Bull. Earth. Eng.* **9** 841-868. doi: https://doi.org/10.1007/S11518-011-9263-5

Massa, M., S. Lovati, E. D'Alema, G. Ferretti, and M. Bakavoli (2010). An experimental approach for estimating seismic amplification effects at the top of a ridge, and the implication for ground-motion predictions: the case of Narni (central Italy), *Bull. seism. Soc. Am.* **100** 3020–3034.

Massa, M., S. Barani, and S. Lovati (2014). Overview of topographic effects based on experimental observations: meaning, causes and possible interpretations, *Geophys. J. Int*. **197/3** 1537–1550. doi: https://doi.org/10.1093/gji/ggt341

Maufroy, E., V.M. Cruz-Atienza, S. Gaffet (2012). A robust method for assessing 3-D topographic site effects: a case study at the LSBB Underground Laboratory, France. Earthquake Spectra, 28(3): 1097-1115. DOI: 10.1193/1.4000050

Maufroy, E.,V.M. Cruz-Atienza, F. Cotton, S. Gaffet (2015). Frequency-scaled curvature as a proxy for topographic site-effect amplification and ground-motion variability. Bull. Seismol. Soc. Am. 105(1): 354-367. DOI: 10.1785/0120140089

967 Moczo, P., E. Bystricky, J. Kristek, J.M.Carcione, and M. Bouchon (1997). Hybrid modelling of P-
968 SV seismic motion at inhomogeneous viscoelastic topographic structures, *Bull. seism. Soc. Am.* **87**
969 1305- 1323.
970
971 Moore, J.R., V. Gischig, J. Burjànek, S. Loew, and D. Faeh (2011). Site effects in unstable rock
972 slopes: dynamic behavior of the Randa instability (Switzerland), *Bull. seism. Soc. Am.* **101** 3110–
973 3116.
974
975 Pagliaroli, A. (2006). "Studio numerico e sperimentale dei fenomeni di amplificazione sismica locale
976 di rilievi isolati." Ph.D. thesis, University of Rome "La Sapienza" (in Italian).
977
978 Pagliaroli, A. (2018). Key issues in Seismic Microzonation studies: lessons from recent experiences
979 in Italy, *Italian Geotechnical Journal* **1** 5–48. doi:10.19199/2018.1.0557-1405.05
980
981 Paolucci, R. (2002). Amplification of earthquake ground motion by steep topographic irregularities,
982 *Earthquake Eng. Struct. Dyn*. **31** 1831–1853. doi:10.1002/eqe.192.
983
984 Paolucci R., F. Pacor, R. Puglia, G. Ameri. C. Cauzzi, and M. Massa (2011). Record Processing in
985 ITACA, the New Italian Strong-Motion Database. It appears as chapter 8 of the book "Earthquake
986 Data in Engineering Seismology - Predictive Models, Data Management and Networks" by Sinan
987 Akkar, Polat Gülkan, Torild van Eck (Editors) – ISBN: 978-94-007-0151-9 (Printed version) 978-
988 94-007-0152-6 (E-book version)
989
990 Pergalani, F., A. Pagliaroli, C. Bourdeau, M. Compagnoni, L. Lenti, M. Lualdi, C. Madiai, S. Martino,
991 R. Razzano, C. Varone, and V. Verrubbi (2019). Seismic microzoning map: approaches, results and
992 applications after the 2016–2017 Central Italy seismic sequence, *Bull. Earthquake Eng.* **18** 5595–
993 5629. doi:0.1007/S11518-019-00640-1.
994
995 Pischiutta, M., G. Cultrera, A. Caserta, L. Luzi, and A. Rovelli (2010). Topographic effects on the
996 hill of Nocera Umbra, central Italy, *Geophys. J. Int.* **182/2** 977–987, doi:
997 https://doi.org/10.1111/j.1365-246X.2010.04654.x
998
999 Pischiutta, M., M. Fondriest, M. Demurtas, G. Di Toro, F. Magnoni, and A. Rovelli (2017). Structural
1000 control on the directional amplification of seismic noise (Campo Imperatore, central Italy), *Earth*
1001 *Planet. Sci. Lett.* **471** 10–18. doi:http://dx.doi.org/10.1016/j.epsl.2017.04.017
1002
1003 Pischiutta, M., P. Cianfarra, F. Salvini, F. Cara, and P. Vannoli (2018). A systematic analysis of
1004 directional site effects at stations of the Italian seismic network to test the role of local topography,
1005 *Geophys. J. Int.* **214(1)** 635–650. https://doi.org/10.1093/gji/ggy133
1006
1007 Primofiore, I., M.P.J. Baron, G. Laurenzano, P. Klin, C. Muraro, and G. Vessia (2020). Evaluation
1008 of the seismic response at the Arquata Del Tronto hamlet through 3D numerical analyses. 22nd EGU
1009 General Assembly, held online 4-8 May, 2020, id.22163. Bibliocode: 2020EGUGA..2222163P
1010
1011 Puglia, R. (2020) – https://gitlab.rm.ingv.it/rodolfo.puglia/pro-quad4m (last accessed on 2020 July
1012 10nd)
1013
1014 Puzzilli, L. M., and F. Ferri (2012). Passive and active seismic methods applied to the study of an
1015 intramountain basin: Preliminary results. In Proceedings of 31 Convegno Nazionale del GNGTS

(Gruppo Nazionale Geofisica della Terra Solida) (Vol. 2, pp. 20–22). Potenza: OGS (Istituto Nazionale di Oceanografia e di Geofisica Sperimentale).

Regione Marche (2018a). Microzonazione Sismica del Livello 3 del Comune di Amandola ai sensi dell'ordinanza del commissario straordinario n. 24 (15/5/2017 n. 1065) http://www.comune.amandola.fm.it/c044004/zf/index.php/trasparenza/index/index/categoria/390 (last accessed September 2020)

Regione Marche (2018b), Microzonazione Sismica del Livello 3 del Comune di Civitella del Tronto ai sensi dell'ordinanza del commissario straordinario n. 24 (15/5/2017 n. 1065) https://www.comune.civitelladeltronto.te.it/images/schede/798allegato.pdf (last accessed September 2020)

Regione Abruzzo (2018). Microzonazione Sismica del Livello 3 del Comune di Montereale ai sensi dell'ordinanza del commissario straordinario n. 24 (15/5/2017 n. 1065) https://sisma2016data.it/microzonazione/ (last accessed September 2020)

Sànchez-Sesma, F.J. (1990). Elementary solutions for response of a wedge- shaped medium to incident SH and SV waves. *Bull. seism. Soc. Am.* **80** 737–742.

Spudich, P., M. Hellweg, and W. H. K. Lee (1996). Directional topographic site response at Tarzana observed in aftershocks of the 1994 Northridge, California, earthquake: Implications for mainshock motions, *Bull. Seismol. Soc. Am.* **86 (1B)** S193–S208.

STACEC srl (2017). LSR 2d (local seismic response 2d). http://www.stacec.com

Stolte, A.C., B.R. Cox, R.C. Lee (2017). An experimental topographic amplification study at Los Alamos National Laboratory using ambient vibrations. Bull. Seismol. Soc. Am. 107(3): 1386-1401.

Theodoulidis, N., G. Cultrera, C. Cornou, P-Y. Bard, T. Boxberger, G. DiGiulio, A. Imtiaz, D. Kementzetzidou, K. Makra, and Argostoli NERA Team (2018). "Basin effects on ground motion: the case of a high-resolution experiment in Cephalonia (Greece), *Bull. Earthquake Eng.* **16/2** 529-560. doi: 10.1007/S11518-017-0225-4

Yu, J. and J. Haines (2003). The Choice of Reference Sites for Seismic Ground Amplification Analyses: Case Study at Parkway, New Zealand. Bulletin of the Seismological Society of America, 93(2), 713–723. https://doi.org/10.1785/0120010289

Wathelet, M. (2005). Array recordings of ambient vibrations: surface-wave inversion. Ph.D. thesis, Univ. de Liège, Liège, Belgium.

Wilson, D. C., and G. L. Pavlis (2000). Near-surface site effects in crystalline bedrock: A comprehensive analysis of spectral amplitudes determined from a dense, three-component seismic array, Earth Interact. 4, 1–31

Authors' affiliations

Marta Pischiutta
Marta.pischiutta@ingv.it
Istituto Nazionale di Geofisica e Vulcanologia, Sezione Roma2, Roma, Italy
Via di Vigna Murata 605, 00143 Rome Italy

Rodolfo Puglia
Rodolfo.puglia@ingv.it
Istituto Nazionale di Geofisica e Vulcanologia, Sezione di Milano, Milano, Italy
via Alfonso Corti, 12 - 20133 Milano Italy

Paola Bordoni
Paola.bordoni@ingv.it
Istituto Nazionale di Geofisica e Vulcanologia, Sezione Roma1, Roma, Italy
Via di Vigna Murata 605, 00143 Rome Italy

Sara Lovati
Sara.lovati@ingv.it
Istituto Nazionale di Geofisica e Vulcanologia, Sezione di Milano, Milano, Italy
via Alfonso Corti, 12 - 20133 Milano Italy

Giovanna Cultrera
Giovanna.cultrera@ingv.it
Istituto Nazionale di Geofisica e Vulcanologia, Sezione Roma1, Roma, Italy
Via di Vigna Murata 605, 00143 Rome Italy

Alessia Mercuri
Alessia.mercuri@ingv.it
Istituto Nazionale di Geofisica e Vulcanologia, Sezione Roma1, Roma, Italy
Via di Vigna Murata 605, 00143 Rome Italy

Antonio Fodarella
Antonio.fodarella@ingv.it
Istituto Nazionale di Geofisica e Vulcanologia, Sezione Roma1, Grottaminarda (AV), Italy
Contrada Ciavolone, 83035 Grottaminarda (AV) Italy

Marco Massa
Marco.massa@ingv.it
Istituto Nazionale di Geofisica e Vulcanologia, Sezione di Milano, Milano, Italy
via Alfonso Corti, 12 - 20133 Milano Italy

Ezio D'Alema
ezio.dalema@ingv.it
Istituto Nazionale di Geofisica e Vulcanologia, Sezione di Milano, Milano, Italy
via Alfonso Corti, 12 - 20133 Milano Italy

Table captions

Table 1: Seismic stations installed by the EMERSITO-INGV task force at the beginning of the 2016 Amatrice seismic sequence (network code XO).

Station code	Municipality	Lat. [°]	Lon. [°]	Elev. [m]	Digitizer	Vel. Sensor	Acc. Sensor	Acquisition	Installation period
AM01	Amandola	42.980556	13.358708	549	REFTEK130	LE3D-5S	EPISENSOR	Real-time	29/08-10/10/2016
AM02	Amandola	42.979597	13.353573	516	REFTEK130	LE3D-5S	EPISENSOR	Real-time	30/08-10/10/2016
AM03	Amandola	42.981622	13.362768	511	REFTEK130	LE3D-5S	EPISENSOR	Real-time	29/08-10/10/2016
AM04	Amandola	42.983345	13.365007	455	REFTEK130	LE3D-5S	EPISENSOR	Real-time	30/08-10/10/2016
AM05	Amandola	42.977404	13.352786	464	REFTEK130	LE3D-5S	EPISENSOR	Real-time	from 30/08/2016
CV01	Civitella del Tronto	42.772736	13.666229	642	Q330	LE3D-5S	EPISENSOR	Stand-alone	31/08-26/09/2016
CV02	Civitella del Tronto	42.773104	13.669496	600	Q330	LE3D-5S	EPISENSOR	Stand-alone	30/08-26/09/2016
CV03	Civitella del Tronto	42.772644	13.672969	540	Q330	LE3D-5S	EPISENSOR	Stand-alone	30/08-26/09/2016
CV04	Civitella del Tronto	42.772273	13.66669	585	Q330	LE3D-5S	EPISENSOR	Stand-alone	31/08-26/09/2016
CV05	Civitella del Tronto	42.771551	13.663721	605	Q330	LE3D-5S	EPISENSOR	Stand-alone	31/08-26/09/2016
MN04	Montereale	42.52906	13.23519	977	REFTEK130	LE3D-5S	EPISENSOR	Stand-alone	27/08-16/09/2016
MN06	Montereale	42.5240	13.24480	923	REFTEK130	LE3D-5S	EPISENSOR	Stand-alone	26/08-16/09/2016
MN08	Montereale	42.52624	13.24125	916	REFTEK130	LE3D-5S	EPISENSOR	Stand-alone	27/08-16/09/2016
MN09	Montereale	42.52987	13.24546	827	REFTEK130	LE3D-5S	EPISENSOR	Stand-alone	27/08-16/09/2016

Table 2: Rheological parameters adopted in numerical modeling for the Amandola site.

Lithology	Description	Thickness (m)	Density (g/cm^3)	Vs (m/s)	ν (Poisson)
ML-1-2-3	Colluvial silty deposit	< 15	2.0	152	0.33
GM-a	Silty gravel	< 5	1.9	295	0.34
GM-b	Gravel in a sandy matrix	< 4	2.2	446	0.36
ALS-a	Bedrock (Flysch della Laga Fm.)	< 40	2.0	572	0.30
ALS-b	Bedrock (Flysch della Laga Fm.)	inf.	2.2	1200	0.27

Table 3: Seismic events modeled at the Amandola site; recordings at AM05 are used as input for finite-elements analyses; recordings at AM03 are used to validate the numerical model.

ID	Date-time	Mw	Latitude [deg]	Longitude [deg]	Acceleration time-histories	
					AM03	AM05
#1	01/09/16 03:53	3.6	42.6207	13.3122	Y	Y
#2	03/09/16 01:34	4.2	42.7698	13.1323	Y	Y
#3	03/09/16 10:18	4.3	42.8607	13.2173	Y	Y
#4	15/09/16 14:40	3.7	42.7680	13.1335	Y	Y
#5	19/09/16 23:34	3.7	42.6737	13.2773	Y	Y
#6	26/10/16 17:10	5.4	42.8747	13.1243		Y
#7	26/10/16 19:18	5.9	42.9087	13.1288		Y
#8	30/10/16 06:40	6.5	42.8322	13.1107		Y

Table 4: Geophysical and geotechnical parameters chosen to approximate the subsoil properties in Civitella site.

Lithology	Description	Max thickness (m)	Density (g/cm^3)	Vs (m/s)	ν (Poisson)	D (%)
TRA-a	Travertine	40	1.6	500	0.3	Linear D=3%
Lag-6a	Bedrock (Flysch della Laga Fm.)	165	2.5	1200	0.35	Linear D=1%
half-space	Bedrock (Flysch della Laga Fm.)	165	2.5	1200	0.35	Linear D=1%

Table 5: Geophysical and geotechnical parameters chosen to approximate the subsoil properties in the Montereale site.

Lithology	Description	Thickness (m)	Density (g/cm^3)	Vs (m/s)	ν (Poisson)	D (%)
MH	Sand, sandy gravels	31	2.0	240	0.40	Darendeli and Stokoe, 2001
SW	Silty gravels	23	2.0	325	0.38	Rollins et al., 1998
SFALS	Superficial fractured Bedrock	50	1.8÷2.6	248÷1700	0.27÷0.32	Linear D=1%
ALS	Bedrock (Flysch della Laga Fm.)	--	3.5	2062	0.30	Linear D=0,5%

Figure captions

Figure 1: Location of the three study-cases (Amandola, Civitella Del Tronto and Montereale), as well as aftershock epicenters recorded during the operating period of installed stations and epicenters of main events of the 2016 seismic sequence in central Italy. The detailed digital elevation model and station locations of the selected study-cases is also reported in the three subplots.

Figure 2: Geological and topographical map of the Amandola site (panel a). For each station we plot: in panel (b) average SSR computed for rotated horizontal components every 10° (colored curves) and for the vertical component (black curve); in panel (c) polar plots showing the spectral ratio amplitude along different azimuthal directions from 0.5 Hz (center of polar plot) to 15 Hz, white circles indicating 5, 10 and 15 Hz. We also mark the maximum direction of amplification using a diamond. In panel (d) we also show a representative borehole stratigraphy and a down-hole measurement (#109002P198) provided in the Seismic Microzonation (Regione Marche 2018a). In panel (e) we add the HVSR calculated for the reference station AM05, as well as a borehole stratigraphy (#109002P198) close to the reference station AM05. Both borehole locations are depicted in panel (a) through red circles.

Figure 3: Results of numerical modeling for Amandola site. Panel a) Geometric-mean amplification for horizontal and vertical components considering five validation events in table 3 (from #1 to #5): thin lines represent geometric-standard-deviations. Heterogeneous (panel b) and homogeneous (panel c) models produced using as input the Mw6.5 Norcia earthquake (event #8 in Table 3). For each model we plot along the profile from the top to the bottom: the contour plot of experimental SSRs calculated with respect to the projected location of reference station AM05; the model where the location of virtual receivers (black reverse triangles) as well as stations AM03 and projected AM05 (red reverse triangles) are depicted; the SSRs calculated as AM03/AM05 for the horizontal component (red lines) and for the vertical components (blue lines). We remark that we compare: i) simulated SSRs for the homogeneous model with observed SSRs, calculated using the whole weak-motion dataset; ii) simulated SSRs for the heterogeneous model (continuous lines), performed using the 30th October mainshock in a linear-equivalent approach, which are compared with observed SSRs calculated as the mean of the five strongest events recorded by both stations AM03 and AM05 (dotted lines). Finally, we specify that for the observed SSR calculated on the horizontal component, we chose the rotation angle corresponding to the azimuth N140°.

Figure 4: Geological and topographical map of the Civitella site (panel a). For each station we plot: in panel (b) average SSR computed for rotated horizontal components every 10° (colored curves) and for the vertical component (black curve); in panel (c) polar plots showing the spectral ratio amplitude along different azimuthal directions from 0.5 Hz (center of polar plot) to 15 Hz, white circles indicating 5, 10 and 15 Hz. We also mark the maximum direction of amplification using a diamond. In panel (d) we also show a representative stratigraphic log (#067017P51), provided in the Seismic Microzonation (Regione Marche 2018a) whose location is also shown in panel (a) through a red circle. In panel (e) we add the HVSR calculated for the reference station CV03.

Figure 5: Results of numerical modeling for Civitella site. Panel a) Homogeneous velocity model (only bedrock LAG-6a). Panel b) Heterogeneous velocity distribution. For each model we plot along the profile from the top to the bottom: the horizontal component of synthetic signals; the model where the location of virtual receivers (black reverse triangles) as well as the location of stations CV01 and CV04 (red reverse triangles) are depicted; contour plot of SSRs calculated using as a reference the projection of station CV03; contour plot of SSRs calculated using as a reference the Ricker pulse; at

station CV01 and CV04, synthetic SSRs to station CV03 (black line), synthetic SSRs to the Ricker input (green line) and observed SSRs (red lines), considering the azimuth of N170.

Figure 6: Geological and topographical map of the Montereale site (panel a). The red dotted line represents the trace of the cross section adopted in numerical modeling. For each station we plot: in panel (b) average SSR computed for rotated horizontal components every 10° (colored curves) and for the vertical component (black curve); in panel (c) polar plots showing the spectral ratio amplitude along different azimuthal directions from 0.5 Hz (center of polar plot) to 15 Hz, white circles indicating 5, 10 and 15 Hz. We also mark the maximum direction of amplification using a diamond. In panel (d) we also add the stratigraphic log and down-hole measurements (Cercato et al., 2019) obtained in the framework of the seismic characterization of the IT.MTR accelerometric station (DPC-INGV, 2018; http://itaca.mi.ingv.it/). In panel (e) we add the HVSR calculated for the reference station MN06.

Figure 7: Results of numerical modeling for Montereale site. Panel a) Homogeneous model (only bedrock). Panel b) Heterogeneous model with a superficial fractured and altered layer with lower velocity values. For each model we plot along the profile from the top to the bottom: the horizontal component of synthetic signals; the model where the location of virtual receivers (black reverse triangles) as well as the location of stations MN08 and MN09 (red reverse triangles) are depicted; contour plot of SSRs calculated using as a reference the Ricker pulse; at station MN08 and MN09, synthetic SSRs to the Ricker input (green line) and observed SSRs (red lines), considering the azimuth of N30.

Table1

Station code	Municipality	Lat. [°]	Lon. [°]	Elev. [m]	Digitizer	Vel. Sensor	Acc. Sensor	Acquisition	Installation period
AM01	Amandola	42,980556	13,358708	549	REFTEK130	LE3D-5S	EPISENSOR	Real-time	29/08-10/10/2016
AM02	Amandola	42,979597	13,353573	516	REFTEK130	LE3D-5S	EPISENSOR	Real-time	30/08-10/10/2016
AM03	Amandola	42,981622	13,362768	511	REFTEK130	LE3D-5S	EPISENSOR	Real-time	29/08-10/10/2016
AM04	Amandola	42,983345	13,365007	455	REFTEK130	LE3D-5S	EPISENSOR	Real-time	30/08-10/10/2016
AM05	Amandola	42,977404	13,352786	464	REFTEK130	LE3D-5S	EPISENSOR	Real-time	from 30/08/2016
CV01	Civitella del Tronto	42,772736	13,666229	642	Q330	LE3D-5S	EPISENSOR	Stand-alone	31/08-26/09/2016
CV02	Civitella del Tronto	42,773104	13,669496	600	Q330	LE3D-5S	EPISENSOR	Stand-alone	30/08-26/09/2016
CV03	Civitella del Tronto	42,772644	13,672969	540	Q330	LE3D-5S	EPISENSOR	Stand-alone	30/08-26/09/2016
CV04	Civitella del Tronto	42,772273	13,66669	585	Q330	LE3D-5S	EPISENSOR	Stand-alone	31/08-26/09/2016
CV05	Civitella del Tronto	42,771551	13,663721	605	Q330	LE3D-5S	EPISENSOR	Stand-alone	31/08-26/09/2016
MN04	Montereale	42,52906	13,23519	977	REFTEK130	LE3D-5S	EPISENSOR	Stand-alone	27/08-16/09/2016
MN06	Montereale	42,524	13,2448	923	REFTEK130	LE3D-5S	EPISENSOR	Stand-alone	26/08-16/09/2016
MN08	Montereale	42,52624	13,24125	916	REFTEK130	LE3D-5S	EPISENSOR	Stand-alone	27/08-16/09/2016
MN09	Montereale	42,52987	13,24546	827	REFTEK130	LE3D-5S	EPISENSOR	Stand-alone	27/08-16/09/2016

Table2

Lithology	Description	Thickness (m)	Density (g/cm^3)	Vs (m/s)	ν (Poisson)
ML-1-2-3	Colluvial silty deposit	< 15	2,0	152	0,33
GM-a	Silty gravek	< 5	1,9	295	0,34
GM-b	Gravel in a sandy matrix	< 4	2,2	446	0,36
ALS-a	Bedrock (Flysch della Laga Fm.)	< 40	2,0	572	0,30
ALS-b	Bedrock (Flysch della Laga Fm.)	inf.	2,2	1200	0,27

Table3

ID	Date-time	Mw	Latitude [deg]	Longitude [deg]	Acceleration time-histories	
					AM03	AM05
#1	01/09/16 03:53	3.6	42,6207	13,3122	Y	Y
#2	03/09/16 01:34	4.2	42,7698	13,1323	Y	Y
#3	03/09/16 10:18	4.3	42,8607	13,2173	Y	Y
#4	15/09/16 14:40	3.7	42,7680	13,1335	Y	Y
#5	19/09/16 23:34	3.7	42,6737	13,2773	Y	Y
#6	26/10/16 17:10	5.4	42,8747	13,1243		Y
#7	26/10/16 19:18	5.9	42,9087	13,1288		Y
#8	30/10/16 06:40	6.5	42,8322	13,1107		Y

Table4

Lithology	Description	Max thickness (m)	Density (g/cm^3)	Vs (m/s)	ν (Poisson)	D (%)
TRA-a	Travertine	40	1,6	500	0,3	Linear D=3%
Lag-6a	Bedrock (Flysch della Laga Fm.)	165	2,5	1200	0,35	Linear D=1%
half-space	Bedrock (Flysch della Laga Fm.)	165	2,5	1200	0,35	Linear D=1%

Table5

Lithology	Description	Thickness (m)	Density (g/cm^3)	Vs (m/s)	ν (Poisson)	D (%)
MH	Sand, sandy gravels	31	2,0	240	0,40	Darendeli & Stokoe, 2001
SW	Silty gravels	23	2,0	325	0,38	Rollins et al., 1998
SFALS	Superficial fractured Bedrock	50	1,8÷2,6	248÷1700	0,27÷0,32	Linear D=1%
ALS	Bedrock (Flysch della Laga Fm.)	--	3,5	2062	0,30	Linear D=0,5%

Figure1

Click here to access/download;Figure;Figure1_RED.jpg

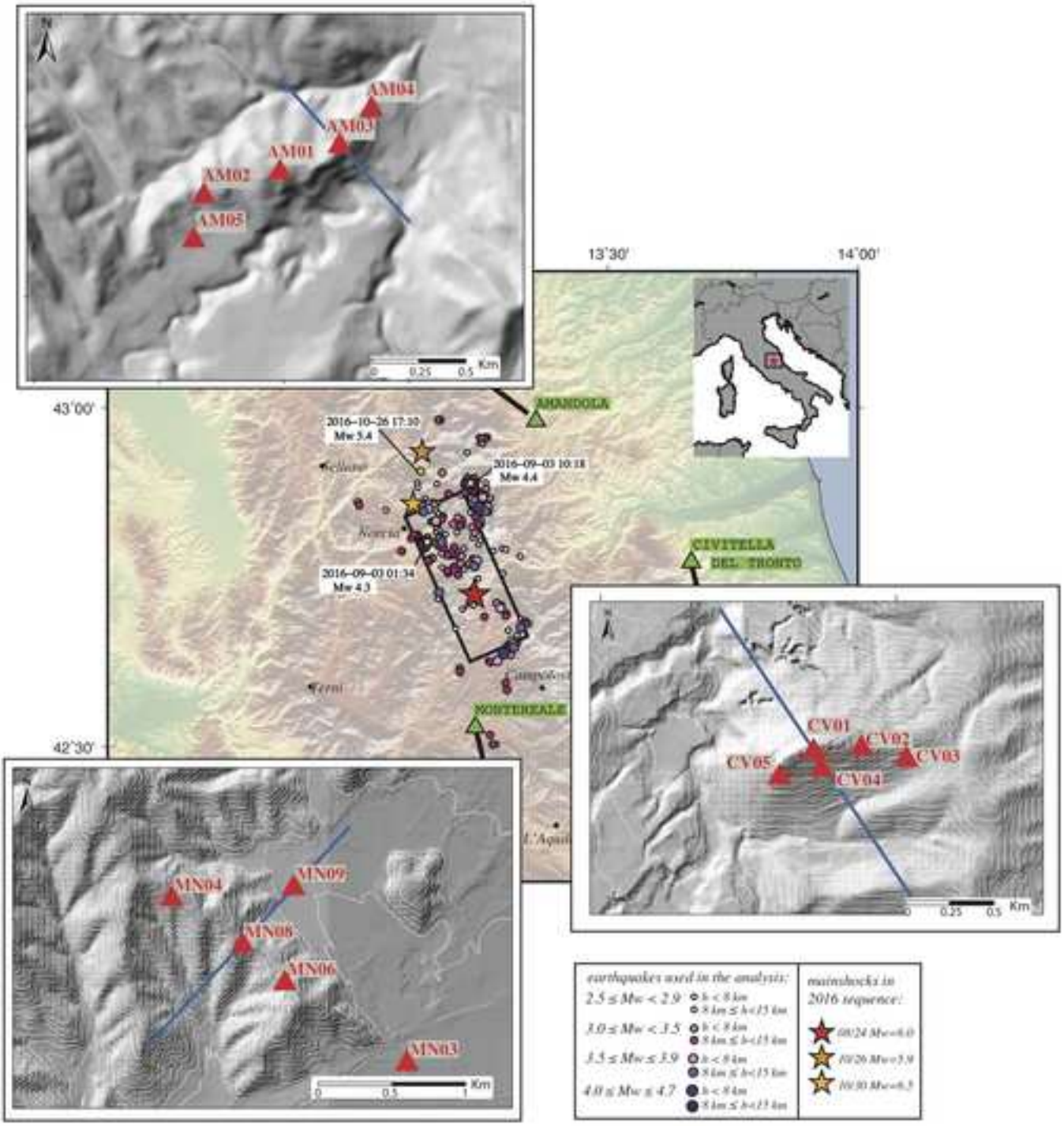

Figure2

Click here to access/download;Figure;Figure2REV.jpg

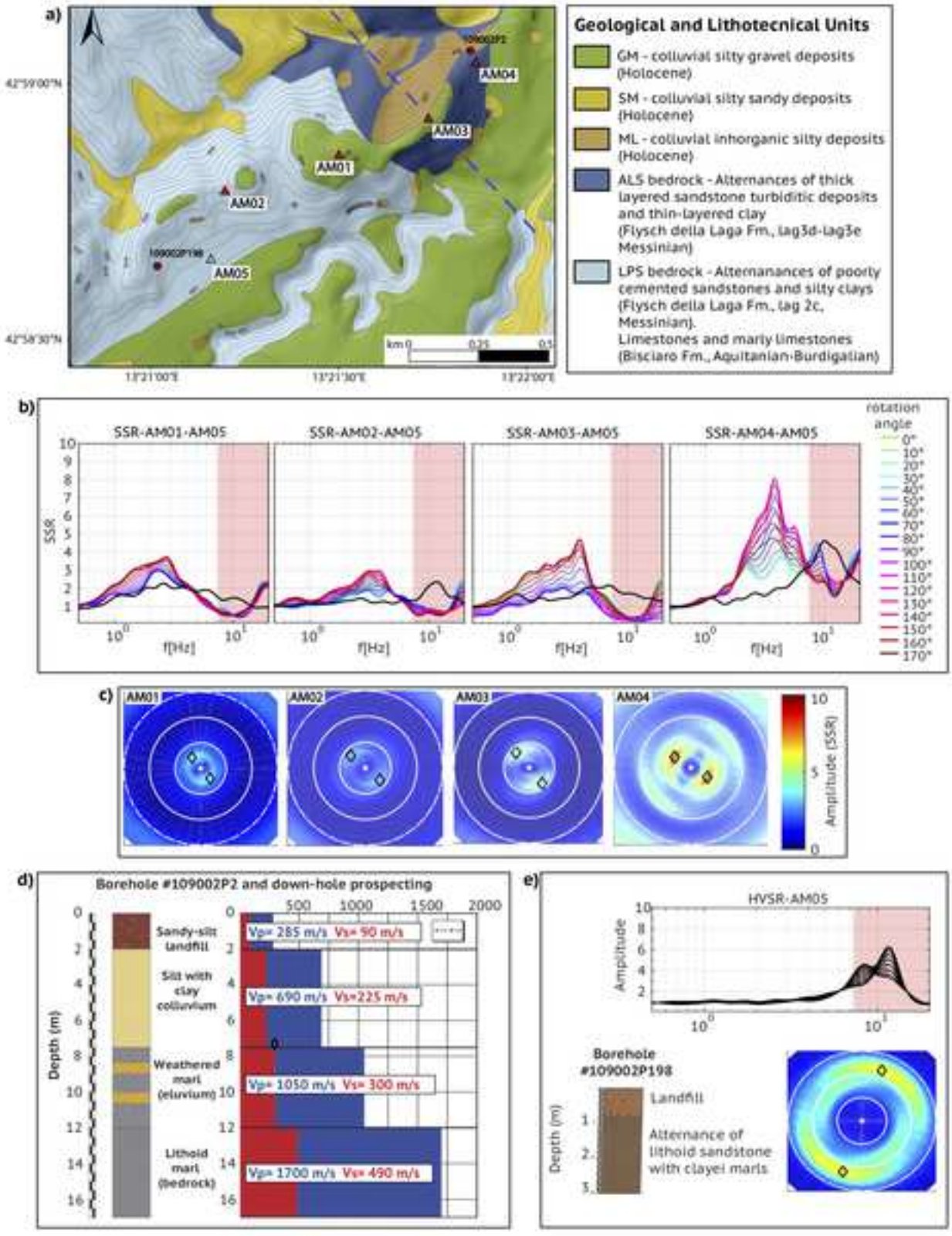

Figure3

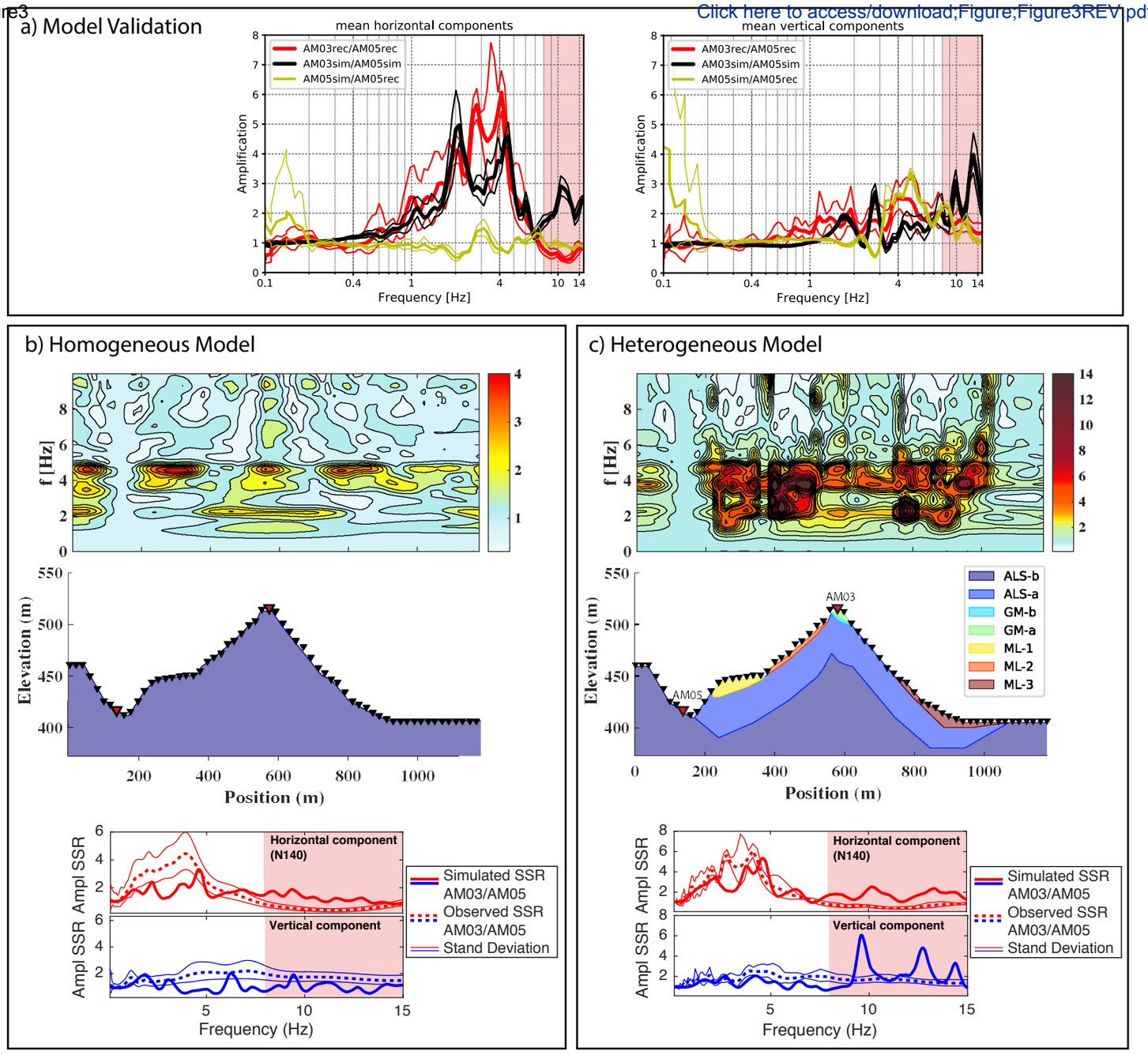

Figure5

Click here to access/download;Figure;Figure5REV.jpg

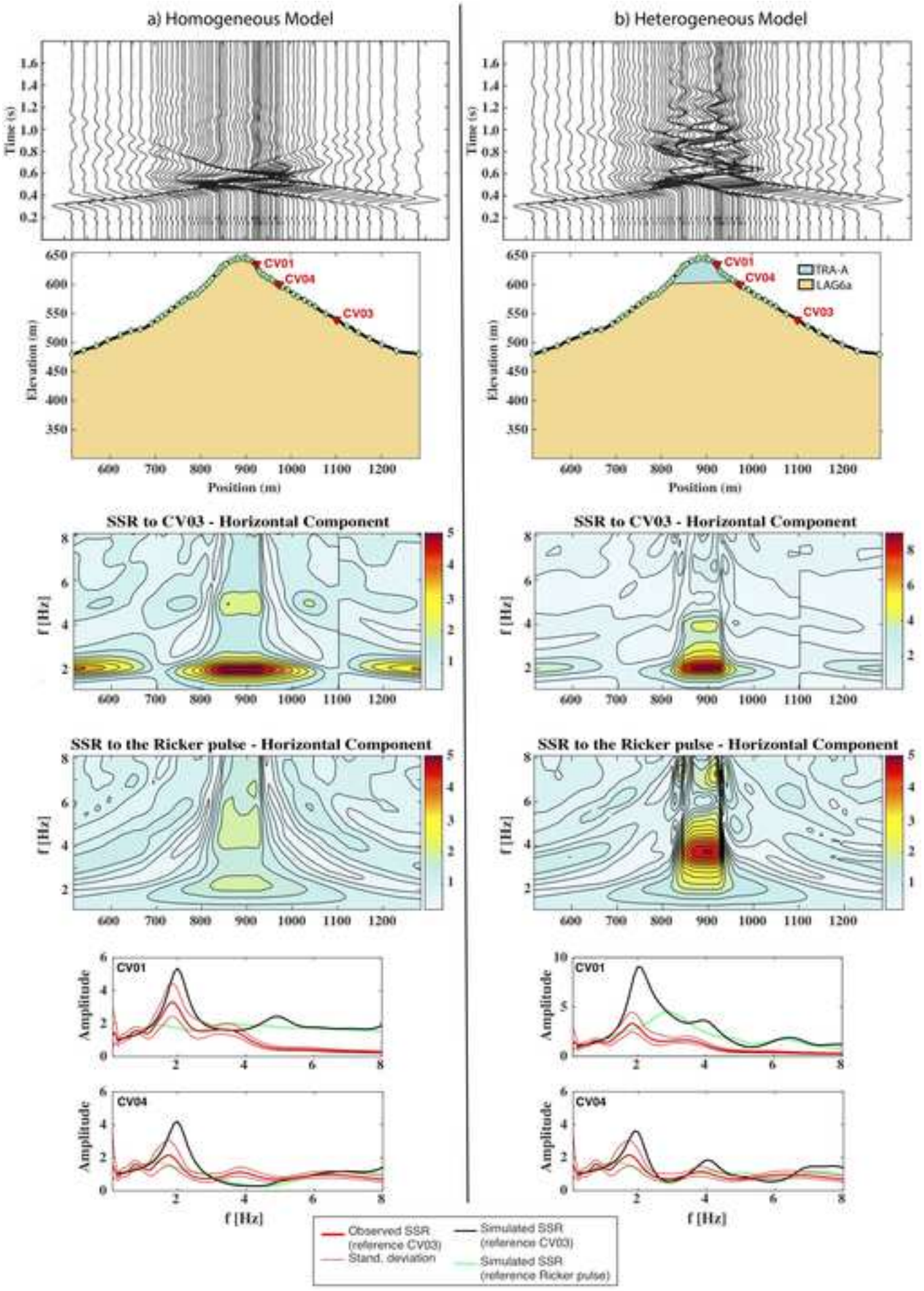

Figure6

Click here to access/download;Figure;Figure6REV.jpg

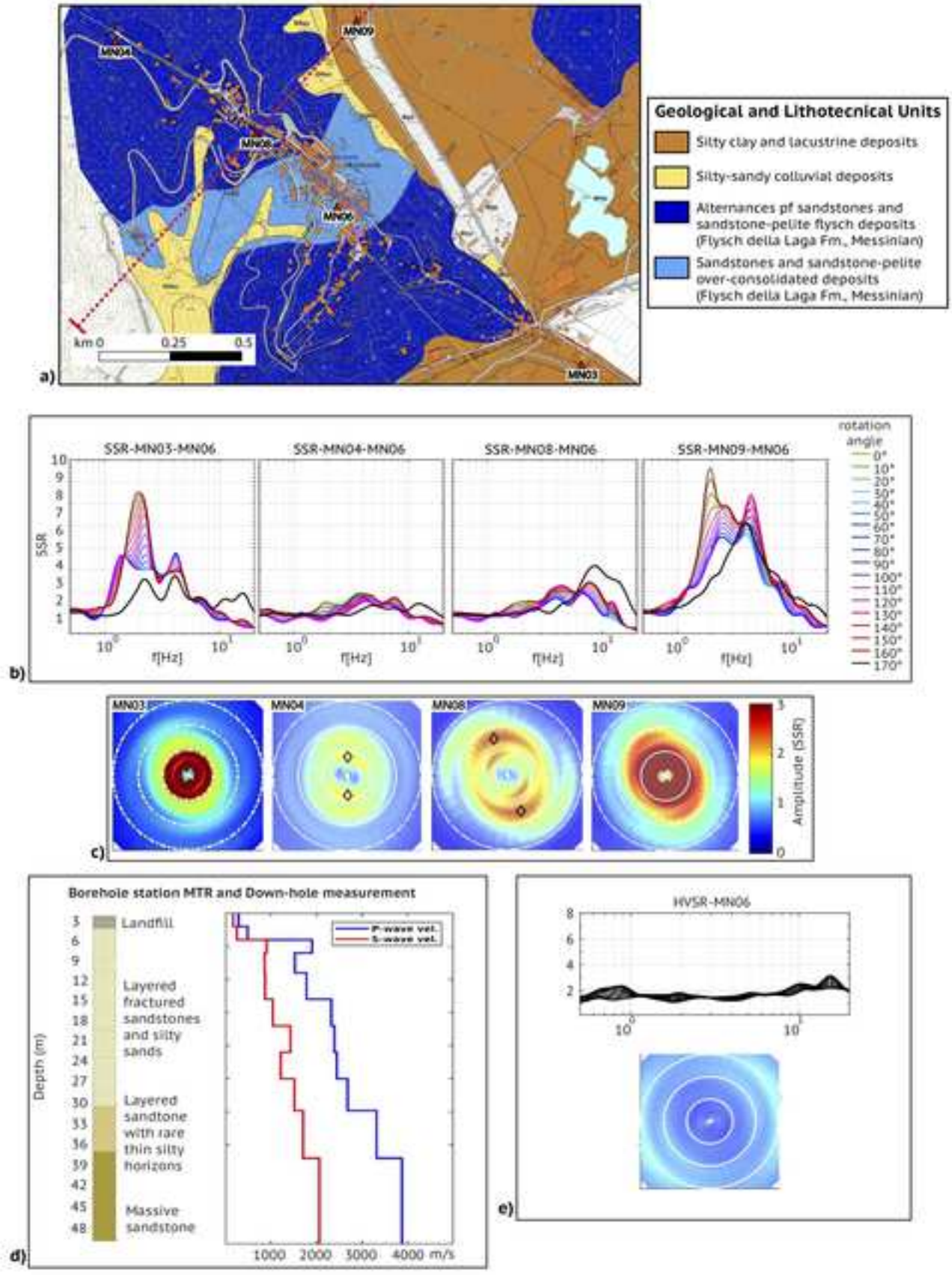

Figure7

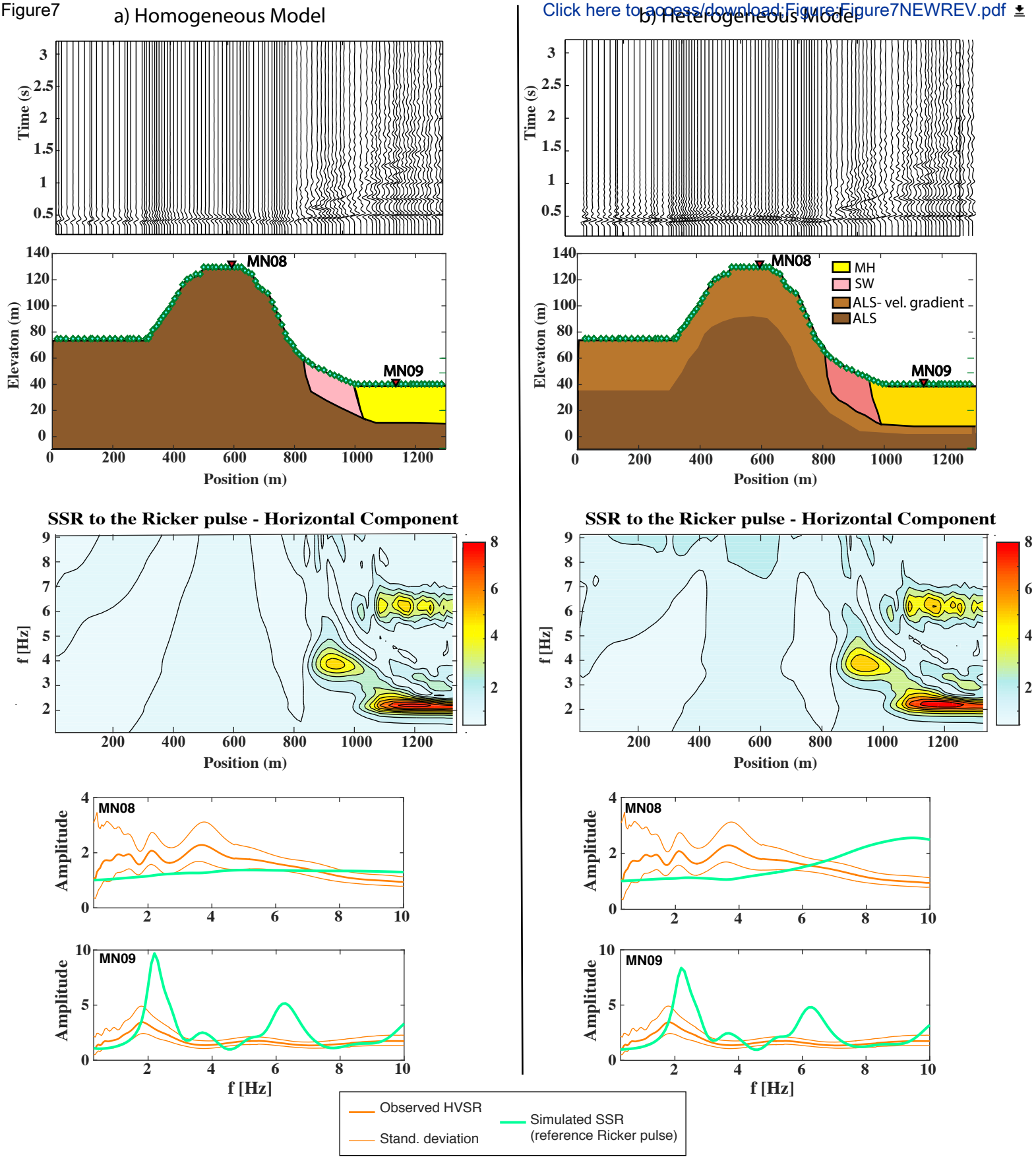

Figure4

Click here to access/download;Figure;Figure4REV_R.jpg

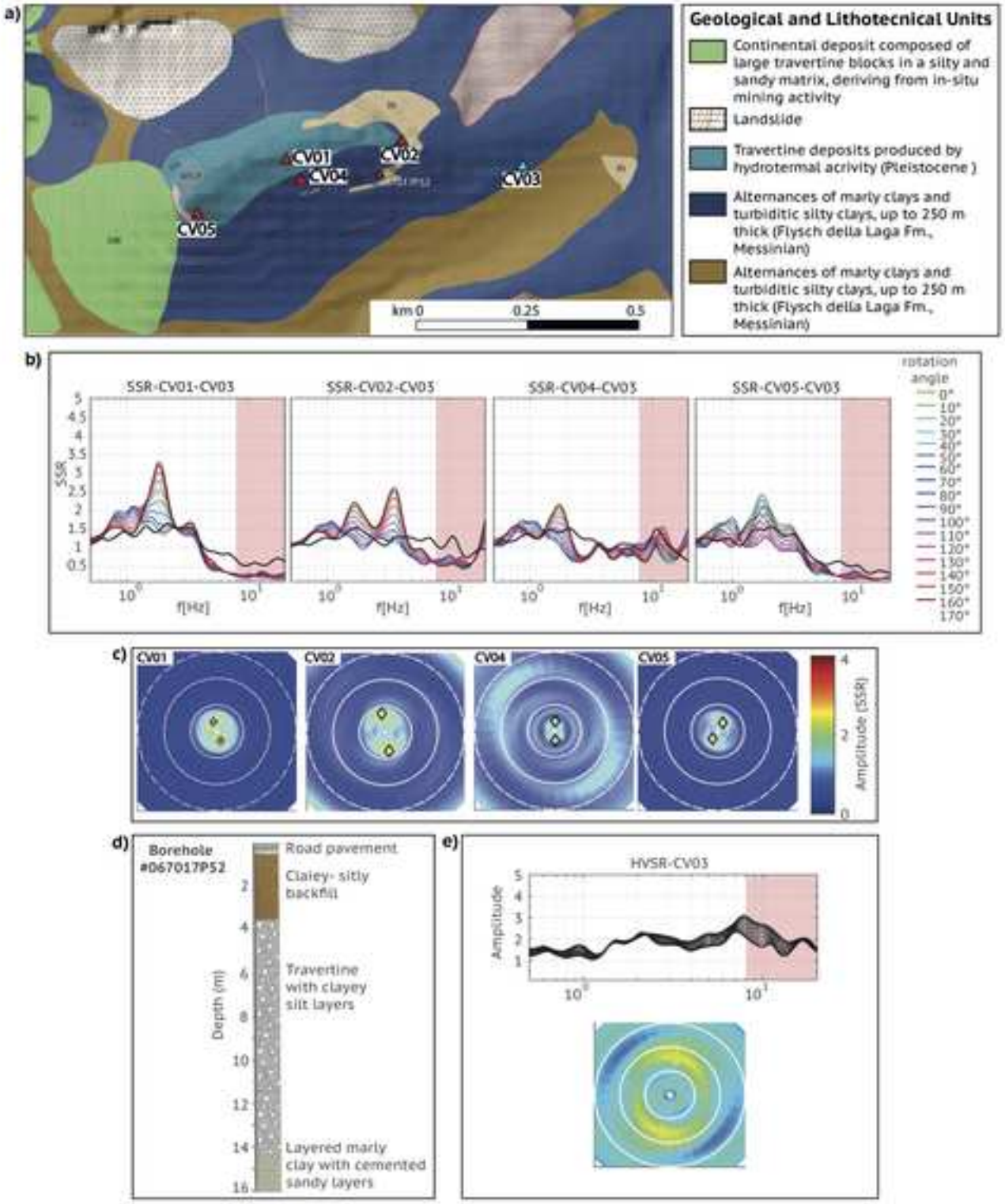

QUAD4M finite-elements analyses at the Amandola site

Amandola finite-elements analyses have been performed using pro-QUAD4M (Puglia, 2020) as pre- and post-processor, and the QUAD4M computer program (Hudson et al., 1994) in order to execute finite-elements analyses.

This report is divided in two main sections: “A. Heterogeneous model” and “B. Homogeneous model”. Section “A” focuses on linear-equivalent numerical-simulations about the heterogeneous model using, as seismic inputs, eight events - with magnitude greater than 3.5 - recorded by station XO.AM05. While section “B” regards linear numerical-simulations about the homogeneous model (since it is a linear simulation, the seismic input used in this section is not relevant).

Section “A” is composed by 5 sub-sections: “A.1 Parameters”, “A.2 Mesh”, “A.3 input time-histories”, “A.4 model validation” and “A.5 numerical modeling”.

- “A.1” shows the subdivision in strata of the heterogeneous model in Figure A.1.1, while in Table A.1.1 are reported the most significant geotechnic parameters used in numerical modeling and, in Figure A.1.2, the degradation curves for each stratum of the model are shown (these curves are needed to apply the linear-equivalent approach). Finally, Table A.1.2 reports some parameters used to estimate the above mentioned degradation curves through the Darendeli (2001) approach.

- “A.2” pictures in Figure A.2.1 the discretization in triangular and quadrilateral elements of the heterogeneous model (i.e. the mesh), while in Table A.2.1 the two selected surface-receivers – associated to Amandola stations AM03 and AM05 – are identified within the 2D model. To identify the receiver representative for station AM05, we calculate the ratio between spectra recorded at station AM05 and the simulated ones at each virtual receiver of the model: the one which corresponds to values closest to 1.0 in the considered frequency band 0.1-15 Hz is selected. The selected receiver well approximates the behavior of station AM05, and can be further used to be compared with the SSRs.

- “A.3” contains: Table A.3.1, reporting the eight selected three-components time-histories recorded by the station AM05 of the Amandola network used as seismic inputs in finite-elements analyses, among which the five three-components time-histories recorded as well by the station AM03 that are used to validate the model response (see sub-section A.4); in fact, these earthquakes are selected with the following criteria: i) the five with the highest magnitude recorded during the operational period of the whole Amandola array, ii) the three largest events with magnitude greater than 5 which have been recorded by station AM05 alone. Table A.3.2, showing the parameters used to processing each time-history with the schema proposed by Paolucci et al. (2011) and the projection angle of the horizontal component used in finite-elements analyses (the used horizontal component is projected in the same direction of the model section).

- “A.4” concerns the results of the model validation, carried out comparing real and simulated time-histories at stations AM05 and AM03 in terms of Fourier amplitudes smoothed by Konno and Ohmachi (1998) operator (with parameter “b” equal to 40): Figure A.4.1 regards horizontal component, while Figure A.4.2 the vertical one, for each validation event (i.e., those occurred in September in Table A.3.1); Figure A.4.3 depicts the mean amplifications (considering a geometric distribution) observed and simulated for the five validation events.

- “A.5” reports a series of results of finite-elements analyses for each of the eight events of Table A.3.1.

Section “B” is meant to give an idea of the geometric contribution on the model response. To accomplish this target, a finite-elements analysis on the homogeneous model shown in Figure B.1.1 is performed, with geotechnical parameters and the discretization of the model respectively pictured in Figure B.1.1, Table B.1.1 and Figure B.2.1. The analysis is conducted using the linear approach (i.e.: no degradation on soil properties is taken into account), so just the amplification functions (obtained, again, from Fourier amplitude smoothed through the Konno and Ohmachi operator) for selected surface-receivers (roughly at the same x-coordinates as in Table A.2.1) is reported in Figure B.3.1 to give an idea of the homogeneous model behavior at the top of the hill (station AM03).

The heterogeneous mesh is composed of about 20k elements/nodes with the element thickness increasing with shear-wave velocity, while the homogeneous one is of about 2.5k elements/nodes (cf., respectively, Figures A.2.1 and B.2.1). Maximum thickness of mesh elements is defined according to the condition by Kuhlemeyer and Lysmer (1973). On the other hand, in order to stabilize resolution of differential equations, the ratio between height/width is set to be lower than 2, while the maximum allowed value for the ratio between width/height cell is 3.5. In this way, both models are able to solve frequencies up to 15 Hz.

A. Heterogeneous model (linear-equivalent modeling)

A.1 Parameters

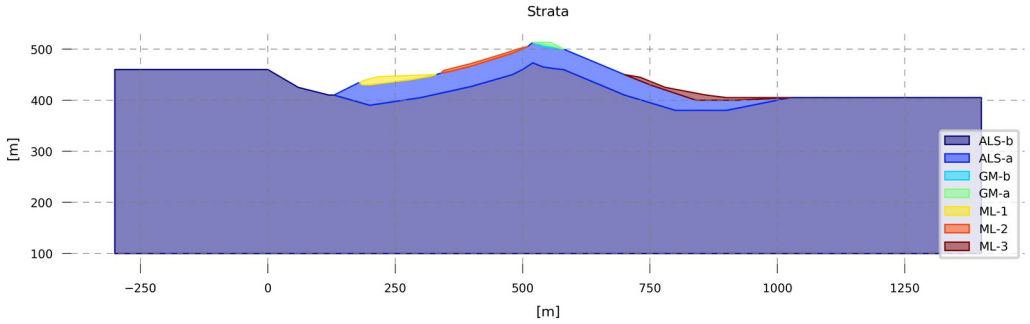

Figure A.1.1 – soil identifiers

	γ [g/cm³]	V_S [m/s]	ν (Poisson)	D_0 [%]
ML-1-2-3	2.0	152	0.33	1.15
GM-a	1.9	295	0.34	1.46
GM-b	2.2	446	0.36	1.19
ALS-a	2.0	572	0.30	0.73
ALS-b	2.2	1200	0.27	0.38

Table A.1.1 – Soil density, γ, shear-wave velocity, V_S, Poisson’s ratio, ν, and damping at low strains, D_0, obtained following the Darendeli (2001) approach

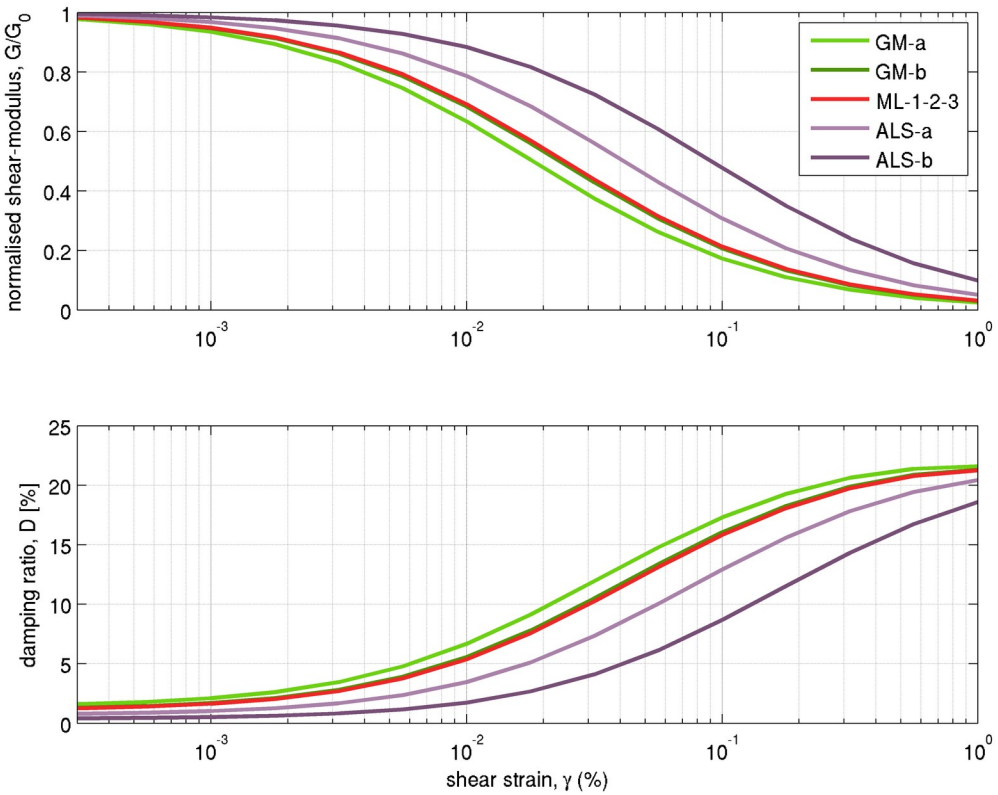

Figure A.1.2 – for each formation, soil degradation curves G/G_0-γ (normalized shear-modulus vs. shear-strain) and D-γ (damping vs. shear-strain) obtained following the Darendeli (2001) approach; it shall be noted that the curves for "GM-b" are almost equivalent to those for "ML-1-2-3", since the differences between the mean effective stresses σ'_0 used to derive them are negligible (cfr. Table A.1.2)

	H_{MAX} [m]	H_{MED} [m]	σ'_{0V} [kPa]	σ'_0 [atm]
ML-1-2-3	10.6	5.3	52	0.34
GM-a	5.0	2.5	22	0.15
GM-b	4.0	2.0	46	0.30
ALS-a	40	20	242	1.59
ALS-b	350	175	2300	15.14

Table A.1.2 – for each formation, table reports representative vertical effective stress σ'_{0V} (considering water table at the ground surface) and mean effective stress σ'_0 (which is computed from σ'_{0V} considering the coefficient of lateral earth pressure fixed to 0.50), together with the reference thickness H_{MED}, used to estimate the above mentioned stresses (considering that GM-b is below GM-a and ALS-b is below ALS-a), and the maximum thickness H_{MAX}; σ'_0 is required for the estimation of Darendeli (2001) degradation curves in Figure A.1.5; the others Darendeli model parameters have been fixed to: plasticity index, 0.0%; over-consolidation ratio, 1.0; cycles of loading, 10; characteristic frequency, 1Hz

A.2 Mesh

a)

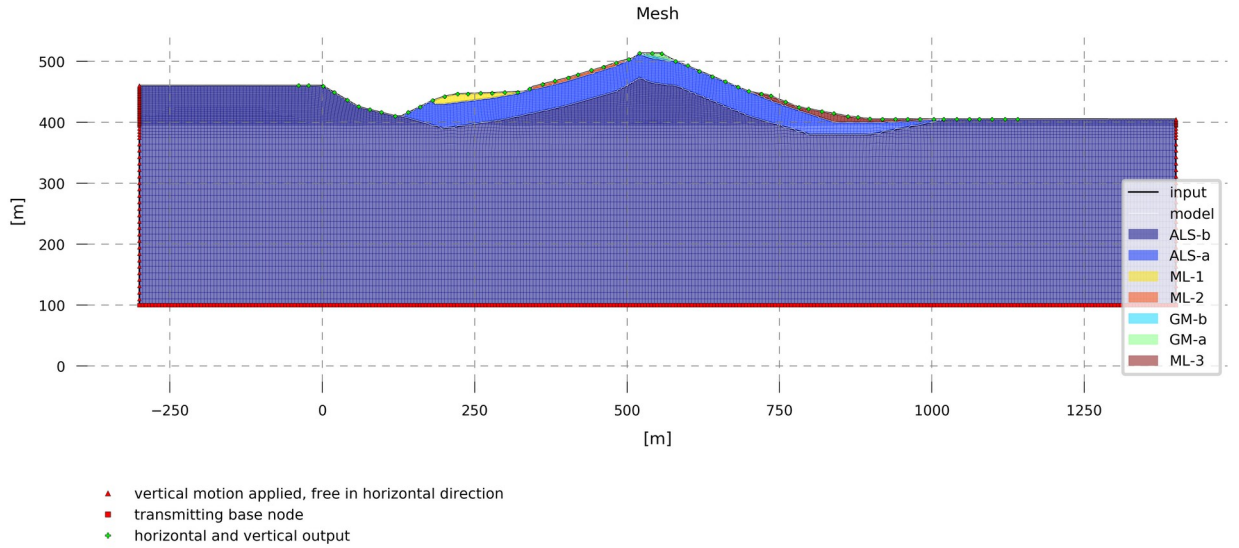

b)

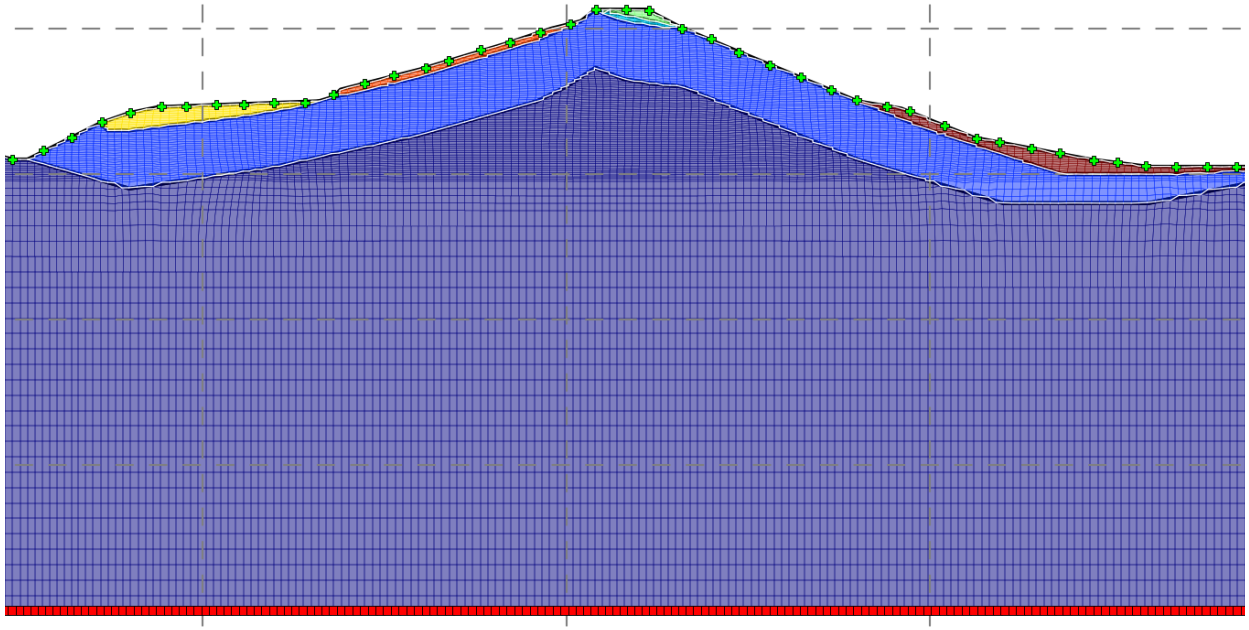

Figure A.2.1 – a) mesh adopted for heterogeneous model numerical modeling and b) closer view of the mesh

	x-coordinate [m]	mesh-node-ID
XO.AM03	541	11562
XO.AM05	97	5292

Table A.2.1 – model receivers x-coordinates for stations AM03 and AM05 (horizontal and vertical acceleration time-histories are requested as outputs at these two nodes – cf. Figure A.2.1)

A.3 input time-histories

ID	Date-time	M_W	Latitude [deg]	Longitude [deg]	Acc. time-hist. (PGA [cm/s^2])	
					XO.AM03	XO.AM05
#1	2016-09-01 03:53:03	3.6	42.6207	13.3122	Y (0.9)	Y (0.8)
#2	2016-09-03 01:34:12	4.2	42.7698	13.1323	Y (8.1)	Y (5.8)
#3	2016-09-03 10:18:51	4.3	42.8607	13.2173	Y (27)	Y (20)
#4	2016-09-15 14:40:56	3.7	42.7680	13.1335	Y (1.8)	Y (0.9)
#5	2016-09-19 23:34:29	3.7	42.6737	13.2773	Y (2.2)	Y (1.8)
#6	2016-10-26 17:10:36	5.4	42.8747	13.1243		Y (69)
#7	2016-10-26 19:18:06	5.9	42.9087	13.1288		Y (143)
#8	2016-10-30 06:40:18	6.5	42.8322	13.1107		Y (207)

Table A.3.1 – events that have been modeled using heterogeneous mesh; recordings at XO.AM05 are used as input for finite-elements analyses, XO.AM03 to validate the numerical model (so, validation events are the five occurred in September, when the whole Amandola array was in place, i.e. #1, #2, #3, #4 and #5)

low cut frequency [Hz]	0.100
high cut frequency [Hz]	15.000
sampling interval [s]	0.0200
horizontal time-histories projection angle (with respect to N) [deg]	140.0

Table A.3.2 – XO.AM03 and XO.AM05 time-histories parameters for the adopted processing schema (Paolucci et al., 2011) and projection angle for horizontal components

A.4 model validation (5 earthquakes)

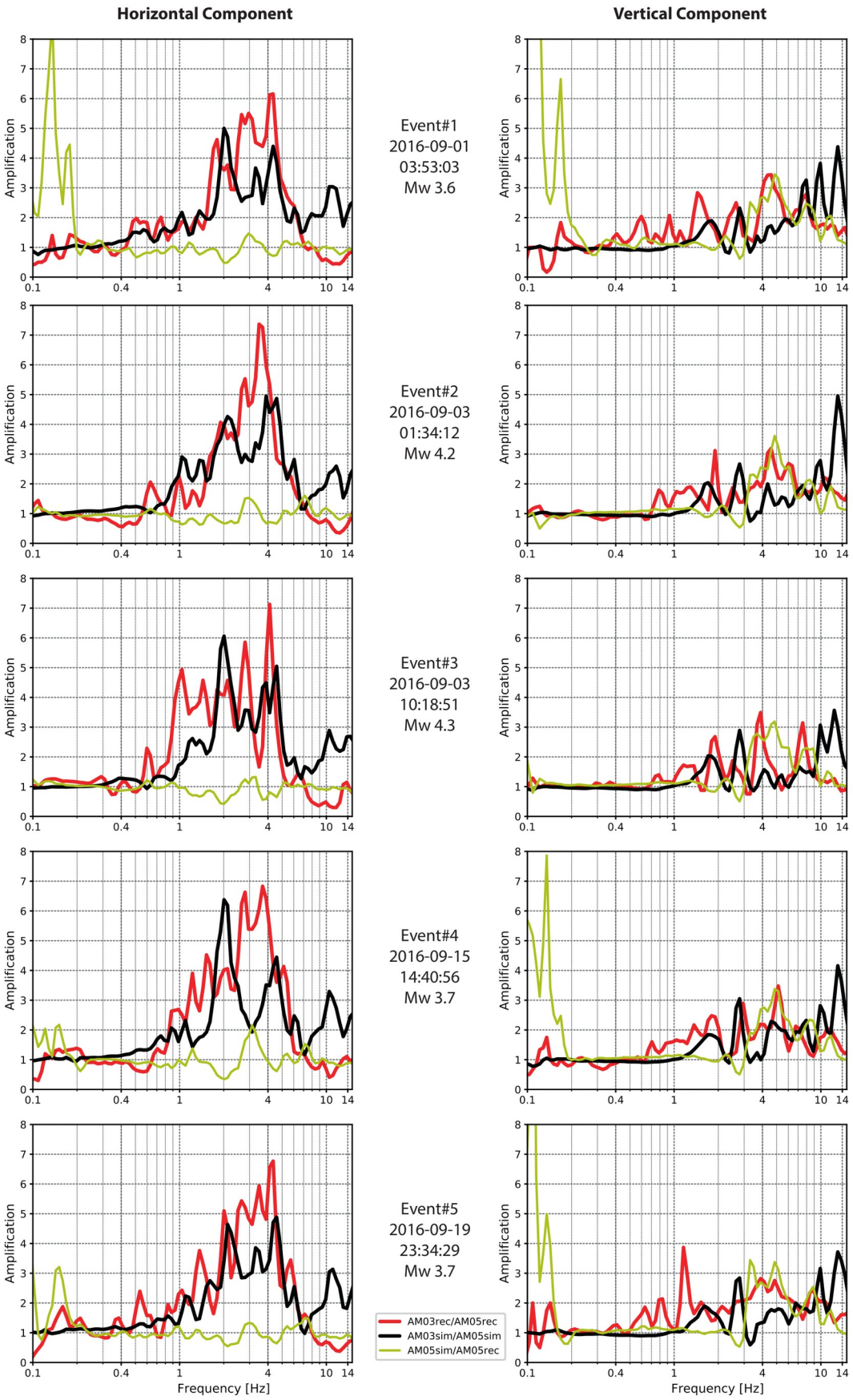

Figure A.4.1 – Spectral-Standard-Ratios (SSR) AM03/AM05 simulated (sim) and recorded (rec) for both horizontal and vertical components about the events #1, #2, #3, #4 and #5, respectively (cf. Table A.3.1); the ratio AM05sim/AM05rec evidences the representativeness of XO.AM05 receiver position (cf. Table A.2.

A.5 numerical modeling (8 earthquakes)

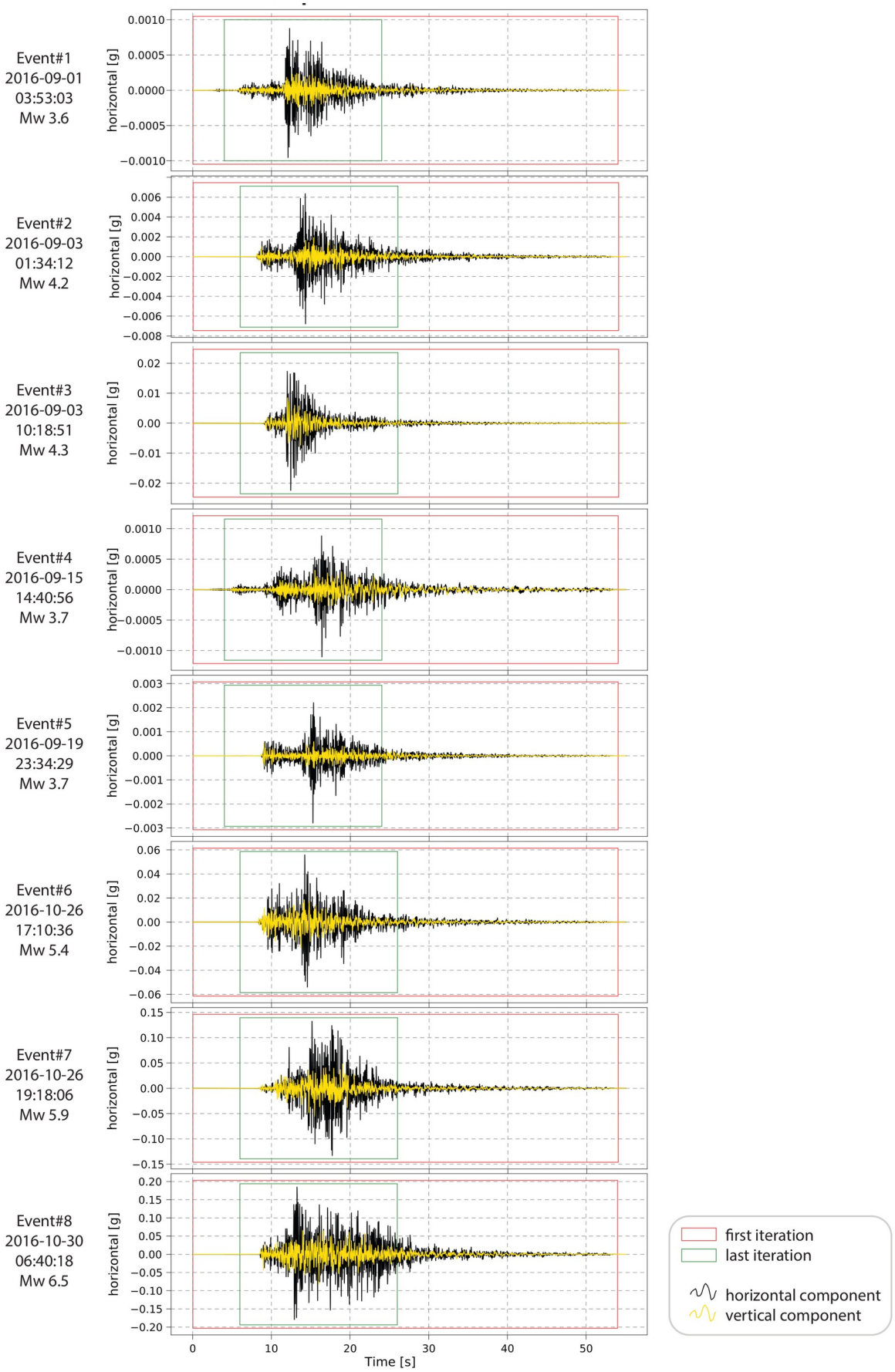

Figure A.5.1 – acceleration input time-histories (cf. Table A.3.2)

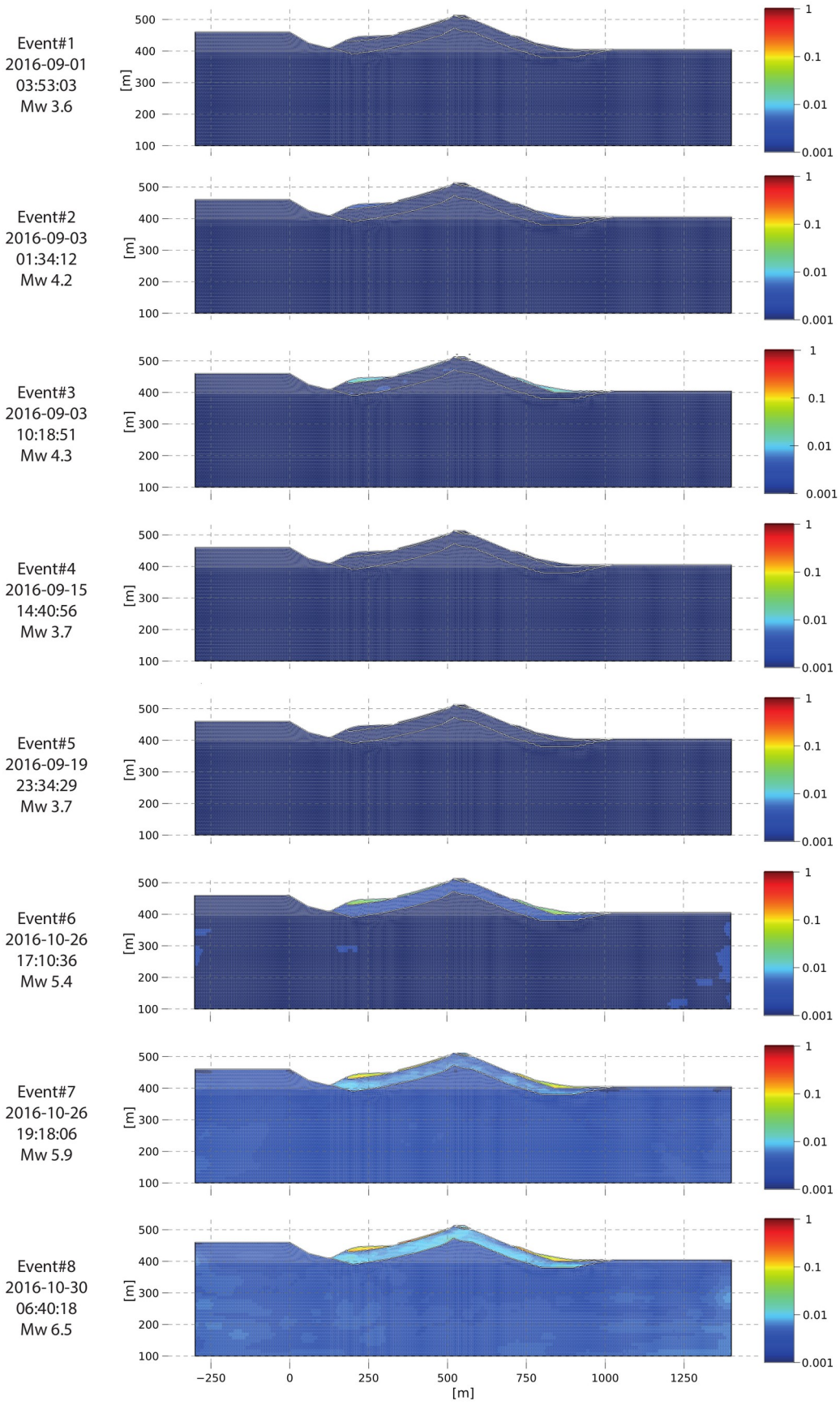

Figure A.5.2 – peak elements strains [%]

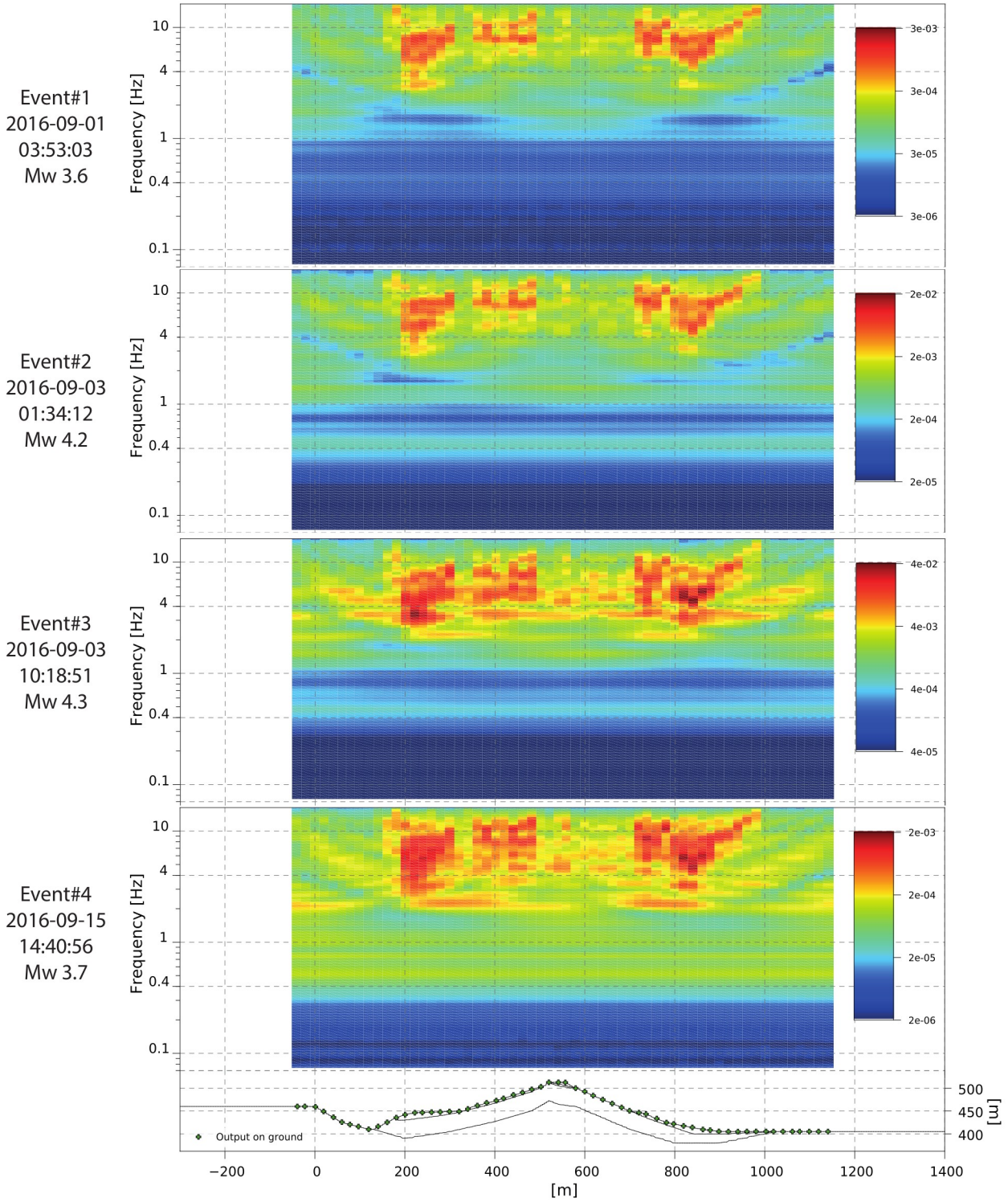

*Figure A.5.3 – Fourier spectra (horizontal component) [g*s] for events #1, #2, #3 and #4*

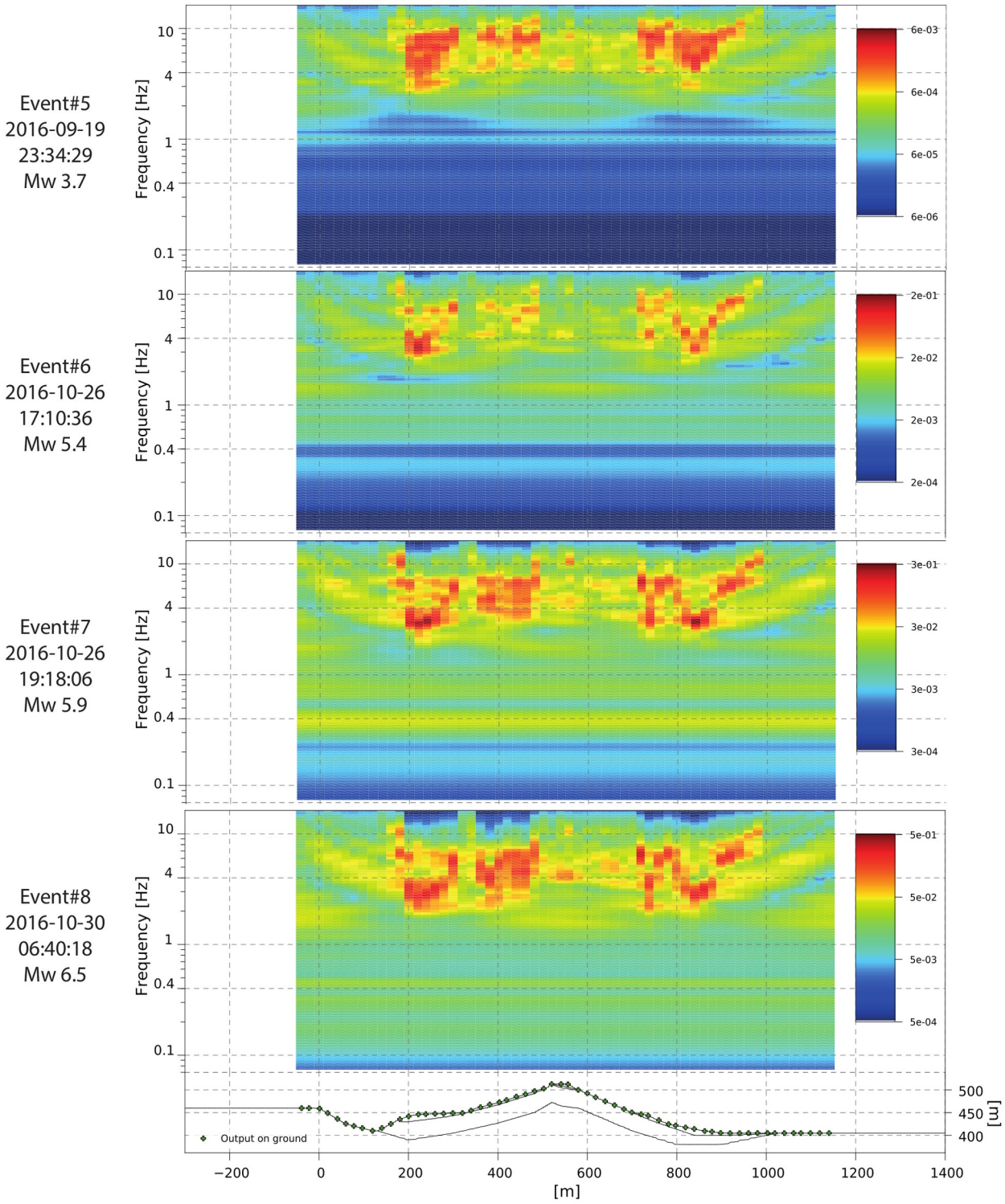

*Figure A.5.4 – Fourier spectra (horizontal component) [g*s] for events #5, #6, #7 and #8*

B. Homogeneous model (linear modeling)

B.1. Parameters

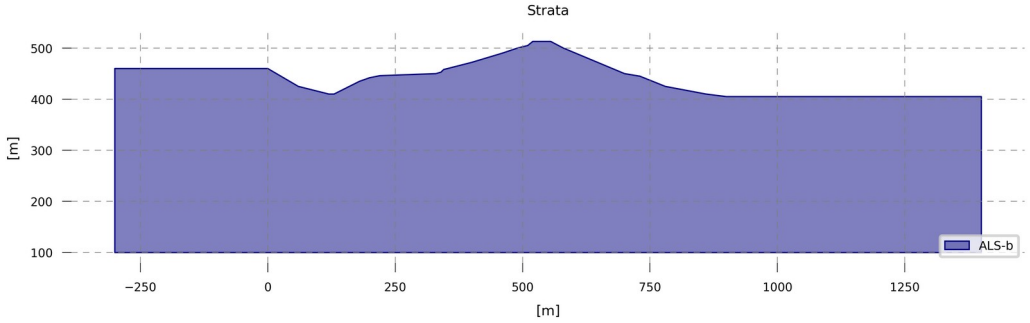

Figure B.1.1 – soil identifier

	γ [g/cm³]	V_S [m/s]	ν (Poisson)	D_0 [%]
ALS-b	2.2	1200	0.27	0.38

Table B.1.1 – Soil density, γ, shear-wave velocity, V_S, Poisson's ratio, ν, and damping at low strains, D_0, obtained following the Darendeli (2001) approach

B.2. Mesh

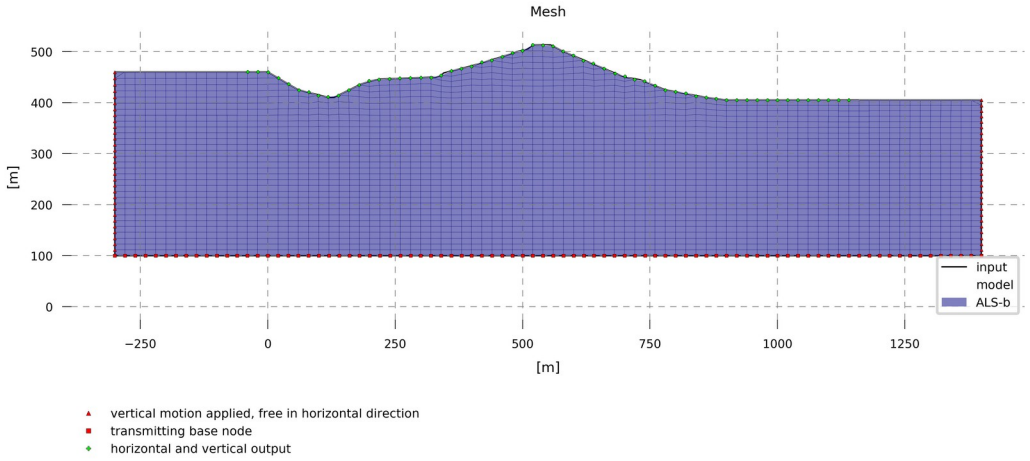

Figure B.2.1 – mesh adopted for homogeneous model numerical modeling

B.3. finite-elements linear-analysis

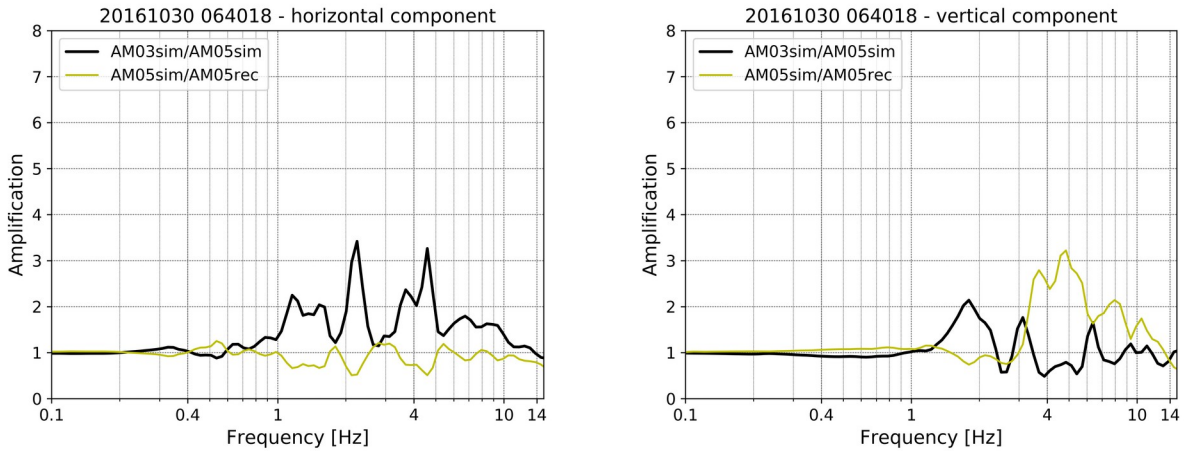

Figure B.3.1 – simulated (sim) Spectral-Standard-Ratios (SSR) AM03/AM05 for horizontal and vertical components; the ratio AM05sim/AM05rec evidences the representativeness of XO.AM05 receiver position (cf. Table A.2.1)

References

Darendeli M.B. (2001) – Development of a new family of normalized modulus reduction and material damping curves – University of Texas, Austin, Texas (PhD thesis) – https://repositories.lib.utexas.edu/bitstream/handle/2152/10396/darendelimb016.pdf (last accessed on 2020 July 10nd)

Hudson M., Idriss I. M., Beikae M. (1994) – User's manual for QUAD4M - A computer program to evaluate the seismic response of soil structures using finite element procedures and incorporating a compliant base – University of California, Davis, California – https://nisee.berkeley.edu/elibrary/ (last accessed on 2020 July 10nd)

Konno K., and Ohmachi T. (1998). Ground-motion characteristic estimated from spectral ratio between horizontal and vertical components of microtremor. Bulletin of the Seismological Society of America 88, 228–241.

Paolucci R., Pacor F., Puglia R., Ameri G., Cauzzi C., Massa M. (2011) – Record Processing in ITACA, the New Italian Strong-Motion Database – It appears as chapter 8 of the book “Earthquake Data in Engineering Seismology - Predictive Models, Data Management and Networks” by Sinan Akkar, Polat Gülkan, Torild van Eck (Editors) – ISBN: 978-94-007-0151-9 (Printed version) 978-94-007-0152-6 (E-book version)

Puglia R. (2020) – https://gitlab.rm.ingv.it/rodolfo.puglia/pro-quad4m (last accessed on 2020 July 10nd)

Table S1

Click here to access/download;Supplemental Material (Main Page, Tables, Figures);Table1_S.xlsx

Origin Time yyyy-mm-d	Latitude (N)	Longitude (E)	Depth(km)	Magnitude	Type
2016/08/30 175143	42.47730	13.27700	15.0	2.7	ML
2016/08/30 175200	42.47730	13.27020	15.9	3.1	ML
2016/08/30 195117	42.83070	13.25930	9.6	2.7	ML
2016/08/30 221115	42.82120	13.26130	9.6	3.1	ML
2016/08/30 223741	42.86620	13.21400	8.9	2.8	ML
2016/08/30 230409	42.82620	13.24950	9.6	2.5	ML
2016/08/30 230528	42.79420	13.16320	11.0	2.5	ML
2016/08/31 014148	42.80600	13.15870	10.7	3.1	ML
2016/08/31 032941	42.90820	13.21880	9.9	2.5	ML
2016/08/31 044204	42.73570	13.21280	10.5	2.7	ML
2016/08/31 063230	42.80620	13.14520	10.4	2.6	ML
2016/08/31 094616	42.75680	13.17920	10.6	3.3	ML
2016/08/31 104331	42.75730	13.18680	11.0	2.6	ML
2016/08/31 112601	42.83150	13.12630	9.6	3.9	Mw
2016/08/31 115231	42.85300	13.22130	8.3	3.4	Mw
2016/08/31 123053	42.86170	13.22670	8.8	2.7	ML
2016/08/31 132304	42.75070	13.23050	11.2	3.3	Mw
2016/08/31 151906	42.75820	13.18730	10.8	2.7	ML
2016/08/31 180724	42.75500	13.32470	16.3	2.6	ML
2016/08/31 181252	42.82180	13.25530	8.6	3.5	Mw
2016/08/31 200507	42.81770	13.16180	10.6	2.6	ML
2016/08/31 200802	42.82130	13.13120	9.5	3.5	ML
2016/08/31 214252	42.77600	13.16800	9.8	3.5	ML
2016/08/31 221409	42.74080	13.23350	9.2	3.5	ML
2016/08/31 225422	42.75230	13.22870	11.0	2.8	ML
2016/08/31 234638	42.76720	13.21280	14.1	2.6	ML
2016/09/01 015552	42.84700	13.18130	15.1	3.1	ML
2016/09/01 034322	42.77470	13.16270	10.4	2.9	ML
2016/09/01 035304	42.62070	13.31220	8.9	3.6	Mw
2016/09/01 064934	42.85830	13.23420	10.4	3.1	ML
2016/09/01 094029	42.81300	13.23580	9.7	3.1	ML
2016/09/01 101604	42.64580	13.30080	13.5	2.5	ML
2016/09/01 110243	42.81000	13.16850	10.6	3.1	ML
2016/09/01 113557	42.55780	13.29880	10.8	3.3	Mw
2016/09/01 142549	42.69230	13.16080	12.8	2.6	ML
2016/09/01 144303	42.81020	13.23580	7.2	2.5	ML
2016/09/01 220502	42.82320	13.05730	8.1	2.5	ML
2016/09/01 233021	42.84180	13.23650	9.9	2.9	ML
2016/09/02 023524	42.92080	13.24980	8.9	2.6	ML
2016/09/02 025503	42.84520	13.20650	8.8	2.9	ML
2016/09/02 092649	42.86630	13.23850	9.2	2.8	ML

2016/09/02 092813	42.86280	13.23130	8.6	2.5 ML
2016/09/02 093559	42.85930	13.23170	8.8	2.5 ML
2016/09/02 123547	42.75520	13.18480	11.3	2.9 ML
2016/09/02 130625	42.75180	13.20350	11.6	2.7 ML
2016/09/02 130723	42.85680	13.12050	8.3	2.6 ML
2016/09/02 131106	43.28630	12.65620	8.5	2.6 ML
2016/09/02 132039	42.93080	13.24250	9.6	2.7 ML
2016/09/02 143818	42.86270	13.11930	6.1	2.9 ML
2016/09/02 152327	42.75070	13.14220	9.4	3.0 ML
2016/09/02 153607	42.85650	13.22200	8.4	2.5 ML
2016/09/02 160015	42.81430	13.24300	9.1	2.5 ML
2016/09/02 190150	42.81750	13.23670	9.3	2.7 ML
2016/09/02 192617	42.82370	13.15520	10.7	2.9 ML
2016/09/02 210015	42.62580	13.31970	8.1	2.9 ML
2016/09/02 223437	42.85730	13.22330	8.8	2.5 ML
2016/09/03 013412	42.76980	13.13230	8.9	4.2 Mw
2016/09/03 014233	42.78230	13.13680	10.2	2.7 ML
2016/09/03 031914	42.81170	13.19970	7.7	3.0 ML
2016/09/03 042627	42.92150	13.24880	9.9	2.8 ML
2016/09/03 045836	42.75730	13.17930	10.7	2.7 ML
2016/09/03 054139	42.83350	13.15930	10.9	2.9 ML
2016/09/03 061043	42.92870	13.24820	10.1	3.0 ML
2016/09/03 063744	42.73000	13.29020	14.0	2.7 ML
2016/09/03 070135	42.74380	13.23550	12.8	2.5 ML
2016/09/03 081648	42.73480	13.18830	10.0	2.5 ML
2016/09/03 091635	42.92920	13.25480	9.7	3.0 ML
2016/09/03 094351	42.73620	13.19020	10.4	2.7 ML
2016/09/03 101851	42.86070	13.21730	8.3	4.3 Mw
2016/09/03 102939	42.86420	13.21820	9.4	2.5 ML
2016/09/03 103110	42.86270	13.21420	8.7	3.0 ML
2016/09/03 103209	42.75930	13.16720	11.0	2.6 ML
2016/09/03 121941	42.86580	13.22130	8.6	2.7 ML
2016/09/03 122032	42.73530	13.18930	10.5	2.6 ML
2016/09/03 132704	42.79050	13.19770	10.2	2.5 ML
2016/09/03 141622	42.78280	13.13720	8.6	2.6 ML
2016/09/03 152626	42.86770	13.21670	8.6	3.0 ML
2016/09/03 153324	42.86880	13.22220	8.6	2.6 ML
2016/09/03 163222	42.85920	13.22530	9.3	3.2 ML
2016/09/03 211908	42.78720	13.12170	9.0	2.5 ML
2016/09/03 212016	42.78750	13.11180	9.8	3.2 ML
2016/09/04 042643	42.76320	13.27170	14.2	2.8 ML
2016/09/04 053135	42.85130	13.23030	9.1	2.9 ML
2016/09/04 070645	42.78300	13.23030	6.9	2.6 ML

2016/09/04 082508	42.76500	13.29630	15.2	2.8 ML
2016/09/04 083349	42.81980	13.22530	9.5	2.7 ML
2016/09/04 103855	42.76600	13.28930	14.7	2.5 ML
2016/09/04 144024	42.85630	13.22830	9.3	2.9 ML
2016/09/04 161020	42.78830	13.11900	9.8	2.7 ML
2016/09/04 163823	42.64830	13.19620	10.5	2.5 ML
2016/09/04 210508	42.87250	13.22080	9.5	2.7 ML
2016/09/04 221121	42.92270	13.24370	8.4	2.5 ML
2016/09/04 231310	42.84150	13.22630	6.1	2.7 ML
2016/09/05 024756	42.79150	13.15680	10.0	2.5 ML
2016/09/05 042220	42.84870	13.21530	8.6	3.2 ML
2016/09/05 090723	42.84620	13.20930	7.6	2.8 ML
2016/09/05 114828	42.85370	13.25530	8.3	2.5 ML
2016/09/05 144905	42.63280	13.30670	11.0	2.8 ML
2016/09/05 184251	42.76880	13.17080	12.7	3.0 ML
2016/09/05 195937	42.85570	13.23620	9.4	3.2 ML
2016/09/05 213611	42.65020	13.32620	9.6	3.5 ML
2016/09/05 224946	42.83000	13.00300	9.5	3.0 ML
2016/09/05 232752	42.77250	13.24200	13.3	2.5 ML
2016/09/05 233409	42.77870	13.24520	14.8	2.6 ML
2016/09/05 234049	42.65570	13.34380	9.8	2.5 ML
2016/09/06 001811	42.65570	13.33580	10.0	3.2 ML
2016/09/06 073821	42.60100	13.26050	11.3	2.5 ML
2016/09/06 095626	42.76020	13.18850	9.9	3.2 ML
2016/09/06 095736	42.75480	13.19820	9.9	2.5 ML
2016/09/06 112355	42.73680	13.19900	10.0	2.6 ML
2016/09/06 205239	42.86430	13.22320	9.5	3.2 ML
2016/09/07 000410	42.73480	13.19180	12.8	3.3 ML
2016/09/07 012249	42.67880	13.28770	9.2	2.5 ML
2016/09/07 021459	42.68330	13.23170	12.4	2.5 ML
2016/09/07 044823	42.80020	13.20920	10.3	2.6 ML
2016/09/07 050847	42.80020	13.20430	10.2	3.4 ML
2016/09/07 094947	42.77830	13.13370	10.2	2.5 ML
2016/09/07 121845	42.68320	13.28520	8.8	2.5 ML
2016/09/07 135519	42.66270	13.32620	9.6	2.5 ML
2016/09/07 143911	42.66720	13.29630	12.4	3.0 ML
2016/09/07 181326	42.80280	13.24280	9.7	3.3 Mw
2016/09/07 181945	42.80870	13.24720	10.1	2.5 ML
2016/09/07 192231	42.83970	13.13580	10.9	2.9 ML
2016/09/08 125623	42.83680	13.24980	9.2	2.6 ML
2016/09/08 145643	42.86170	13.15850	9.5	2.6 ML
2016/09/08 225626	42.84720	13.24230	8.7	2.7 ML
2016/09/09 025922	42.85650	13.21470	9.7	2.6 ML

2016/09/09 053935	42.81480	13.24170	7.1	2.6	ML
2016/09/09 090707	42.67980	13.28150	9.5	2.5	ML
2016/09/09 103712	42.81920	13.25450	6.0	2.5	ML
2016/09/09 153130	42.63880	13.31900	10.0	2.5	ML
2016/09/09 164842	42.73920	13.16820	8.6	2.5	ML
2016/09/12 125755	42.86370	13.25600	9.6	2.5	ML
2016/09/12 185858	42.78780	13.17580	10.5	2.5	ML
2016/09/12 202114	42.86600	13.23980	9.7	2.5	ML
2016/09/13 052608	42.78470	13.16920	9.6	2.9	ML
2016/09/13 110420	42.58380	13.20450	15.9	3.4	ML
2016/09/14 021849	42.72220	13.24100	10.2	2.7	ML
2016/09/14 030744	42.73370	13.17870	13.8	3.1	ML
2016/09/15 135129	42.77920	13.12780	10.2	3.1	ML
2016/09/15 144047	42.77580	13.13280	8.5	3.1	ML
2016/09/15 144052	42.76800	13.13350	9.2	3.7	Mw
2016/09/15 144351	42.77470	13.13030	10.0	3.7	ML
2016/09/15 144424	42.77620	13.13420	8.3	3.7	ML
2016/09/15 144700	42.77450	13.14230	6.0	2.6	ML
2016/09/15 165144	42.74830	13.14030	10.2	3.0	ML
2016/09/15 172754	42.76320	13.08680	10.5	3.1	ML
2016/09/17 132525	42.66600	13.25320	11.2	3.3	ML
2016/09/17 153518	42.78450	13.13980	10.6	2.6	ML
2016/09/17 163245	42.67720	13.20950	11.6	2.6	ML
2016/09/17 214544	42.83530	13.15070	9.9	2.6	ML

Table S2

Click here to access/download;Supplemental Material (Main Page, Tables, Figures);Table2_S.xlsx

Origin Time yyyy-mm-dd hh:mm:ss.sss)	Latitude (N)	Longitude (E)	Depth(km)	(Ml or Mw)
2016-08-26 04:08:03.680	42.7043	13.2284	10,865	3.0
2016-08-26 04:21:10.714	42.61166	13.29918	6,490	3.0
2016-08-26 04:28:26.695	42.6122	13.29173	7,174	4.7
2016-08-26 05:08:31.598	42.78168	13.16302	4,385	3.2
2016-08-26 05:08:55.531	42.62038	13.30602	7,010	3.3
2016-08-26 05:17:06.294	42.75497	13.20786	5,396	3.2
2016-08-26 05:32:53.110	42.77609	13.15727	4,651	3.3
2016-08-26 05:50:35.159	42.62365	13.29919	2,389	3.1
2016-08-26 11:06:45.572	42.6182	13.30167	7,420	3.0
2016-08-26 14:32:51.339	42.6009	13.27945	7,386	3.7
2016-08-26 16:05:29.786	42.70198	13.16263	9,245	3.5
2016-08-26 20:49:13.267	42.79979	13.15787	5,444	3.2
2016-08-26 23:13:37.714	42.84271	13.25335	1	3.2
2016-08-27 01:26:40.549	42.84203	13.25039	2,013	3.7
2016-08-27 02:50:59.957	42.84434	13.24836	1,104	3.9
2016-08-27 02:52:24.726	42.62392	13.30385	2,730	3.0
2016-08-27 03:00:55.378	42.84652	13.25148	1,814	3.1
2016-08-27 09:41:39.336	42.80293	13.19041	5,123	3.2
2016-08-27 21:31:43.255	42.59885	13.26532	9,457	3.4
2016-08-28 05:16:34.931	42.60921	13.3057	7,898	3.1
2016-08-28 06:37:20.396	42.72759	13.20087	9,710	3.3
2016-08-28 07:59:54.604	42.79802	13.22841	2,115	3.0
2016-08-28 10:25:33.393	42.78168	13.10698	9,252	3.0
2016-08-28 15:55:36.188	42.82813	13.24134	3,694	4.4
2016-08-28 16:42:02.561	42.82459	13.14102	5,431	3.7
2016-08-28 20:22:31.568	42.74408	13.20538	6,463	3.1
2016-08-29 01:44:26.376	42.76819	13.19339	8,630	3.4
2016-08-29 16:43:53.391	42.83113	13.15285	4,364	3.0
2016-08-29 17:52:23.308	42.85974	13.2214	1,302	3.3
2016-08-30 00:35:56.646	42.80674	13.15179	5,561	3.3
2016-08-30 14:05:32.895	42.73073	13.1808	9,020	3.0
2016-08-30 17:52:01.396	42.49123	13.26494	12,287	3.1
2016-08-30 22:11:16.603	42.82704	13.26004	3,134	3.1
2016-08-31 01:41:49.917	42.8047	13.15973	6,060	3.1
2016-08-31 09:46:16.834	42.75988	13.18483	9,061	3.3
2016-08-31 11:52:32.050	42.85783	13.22608	2,149	3.4
2016-08-31 18:12:52.995	42.82758	13.26004	2,628	3.5
2016-08-31 21:42:53.004	42.7799	13.16474	5,294	3.5
2016-08-31 22:14:10.510	42.74857	13.23852	5,978	3.5
2016-09-01 01:55:52.959	42.84598	13.18229	12,588	3.1
2016-09-01 03:53:04.922	42.62528	13.311	4,057	3.6
2016-09-01 06:49:35.361	42.85197	13.23216	4,139	3.1
2016-09-01 09:40:30.321	42.8171	13.23838	2,881	3.1
2016-09-01 11:02:44.507	42.81383	13.17047	8,158	3.1

2016-09-01 11:35:57.953	42.5682	13.29555	9,122	3.3
2016-09-02 15:23:28.794	42.75279	13.14936	1,732	3.0
2016-09-03 01:34:13.081	42.77609	13.1389	3,216	4.3
2016-09-03 03:19:14.808	42.80838	13.20785	1,623	3.0
2016-09-03 06:10:44.474	42.92908	13.25059	3,223	3.0
2016-09-03 09:16:36.172	42.93017	13.25808	2,730	3.0
2016-09-03 10:18:51.819	42.86246	13.22795	2,286	4.4
2016-09-03 10:31:11.845	42.86655	13.22359	1,274	3.0
2016-09-03 16:32:23.550	42.86287	13.23278	2,143	3.2
2016-09-03 21:20:17.319	42.78644	13.11647	2,382	3.2
2016-09-05 04:22:21.126	42.85265	13.22577	1,657	3.2
2016-09-05 18:42:52.420	42.77064	13.16194	9,642	3.0
2016-09-05 19:59:38.568	42.85224	13.23746	2,266	3.2
2016-09-05 22:49:47.178	42.83453	13.00093	7,393	3.0
2016-09-06 00:18:12.077	42.6592	13.3342	5,458	3.2
2016-09-06 09:56:27.370	42.7626	13.19603	7,174	3.2
2016-09-06 20:52:40.309	42.8705	13.23216	11,166	3.2
2016-09-07 00:04:11.351	42.73958	13.19278	8,985	3.3
2016-09-07 05:08:48.571	42.80306	13.2077	5,171	3.4
2016-09-07 14:39:12.610	42.67038	13.29692	9,628	3.0
2016-09-07 18:13:27.322	42.80238	13.24585		3.3
2016-09-08 06:25:54.547	42.95591	13.16146		3.2
2016-09-10 02:29:40.553	42.84039	13.26379	3,366	3.0
2016-09-10 14:23:37.522	42.95551	13.16536	1,377	3.2
2016-09-10 17:00:03.790	42.78971	13.23355	3,134	3.3
2016-09-11 18:39:03.621	42.68604	13.27782	3,824	3.3
2016-09-13 11:04:21.638	42.58932	13.20417	13,326	3.4
2016-09-14 03:07:45.092	42.7325	13.17971	9,860	3.1
2016-09-14 16:06:50.738	42.85429	13.25663	1,589	3.0
2016-09-15 13:51:30.805	42.77732	13.13065	1,623	3.1
2016-09-15 14:40:47.831	42.77718	13.13018	2,491	3.1
2016-09-15 14:43:52.617	42.77446	13.13268	3,175	3.7
2016-09-15 14:44:25.095	42.77895	13.13376	1,787	3.9
2016-09-15 16:51:45.739	42.74789	13.14189	2,553	3.0
2016-09-15 17:27:54.985	42.7626	13.08834	6,053	3.1
2016-09-16 21:57:03.158	42.82336	13.24306	1,965	3.1
2016-09-17 07:35:22.918	42.8378	13.23402	4,713	3.4
2016-09-18 01:55:36.895	42.68073	13.28574	4,146	3.2
2016-09-18 03:51:50.586	42.82268	13.24446	2,081	3.1
2016-09-19 16:49:56.579	42.68264	13.28668	3,585	3.0
2016-09-19 23:34:26.004	42.67869	13.28497	5,396	3.7
2016-09-20 01:20:54.253	42.67828	13.28388	3,257	3.2
2016-09-20 03:30:03.508	42.80497	13.15537	5,362	3.1
2016-09-20 03:30:20.651	42.80511	13.1574	4,549	3.4
2016-09-21 07:07:24.863	42.80742	13.15661	5,116	3.5
2016-09-22 20:03:55.826	42.75933	13.1867	6,436	3.4

2016-09-22 20:04:56.038	42.75879	13.18919	6,791	3.3
2016-09-25 06:46:30.128	42.74408	13.22342	5,998	3.0
2016-09-28 10:04:10.865	42.87813	13.16917	2,443	3.0

Figure S1

Click here to access/download;Supplemental Material (Main Page, Tables, Figures);Figure S1.jpg

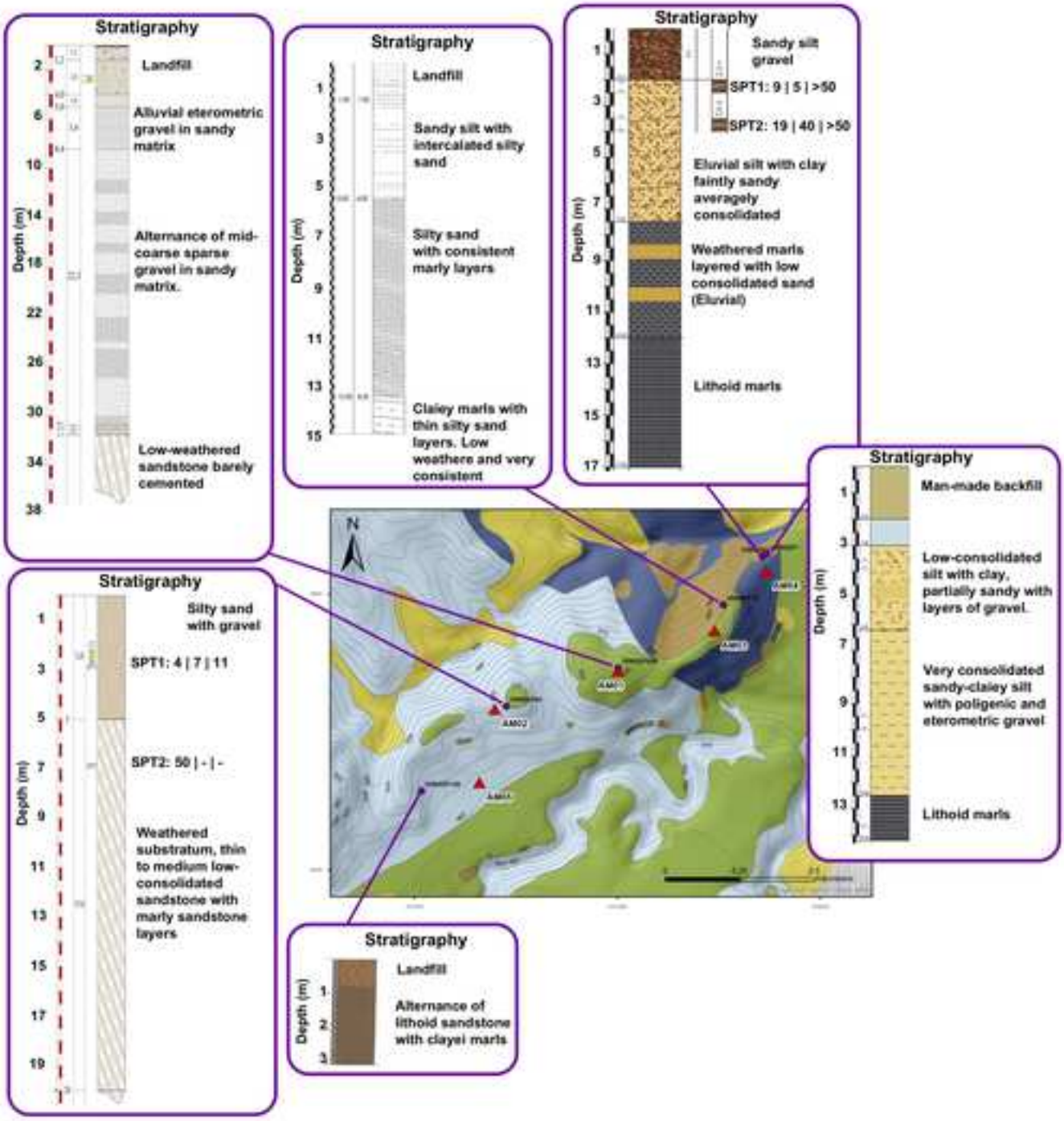

Figure S1 - Geological investigations collected in the Seismic Microzonation for Amandola municipality (Regione Marche, 2018): stratigraphies from geognostic surveys.

Figure S2

Click here to access/download;Supplemental Material (Main Page, Tables, Figures);Figure S2.jpg

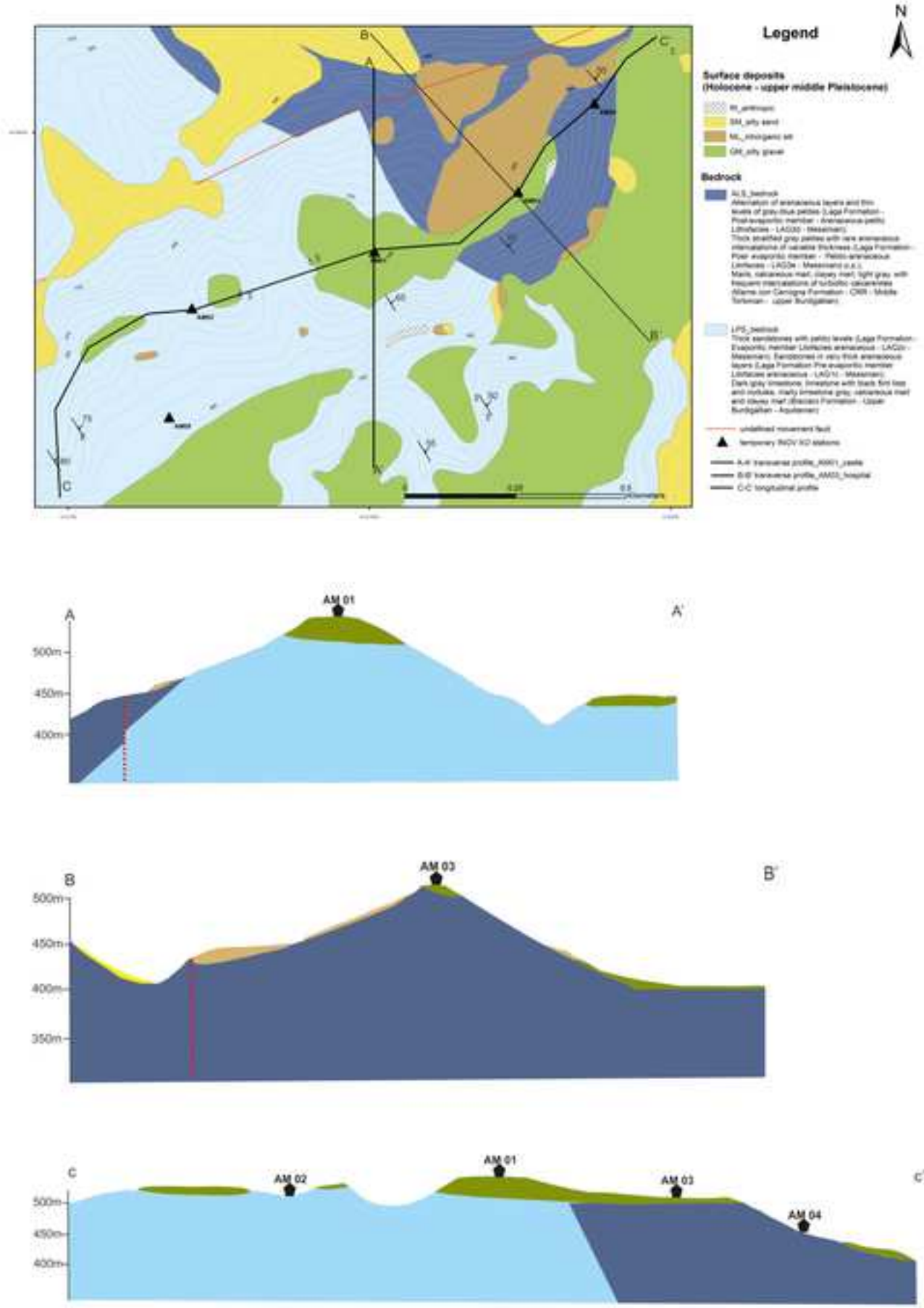

Figure S2 - Geological sections deduced from in-situ surveys and geophysical analyses (mainly coming from the regional Microzonation studies) reported in Figures S1 and S3.

Figure S3

Click here to access/download;Supplemental Material (Main Page, Tables, Figures);Figure S3.jpg

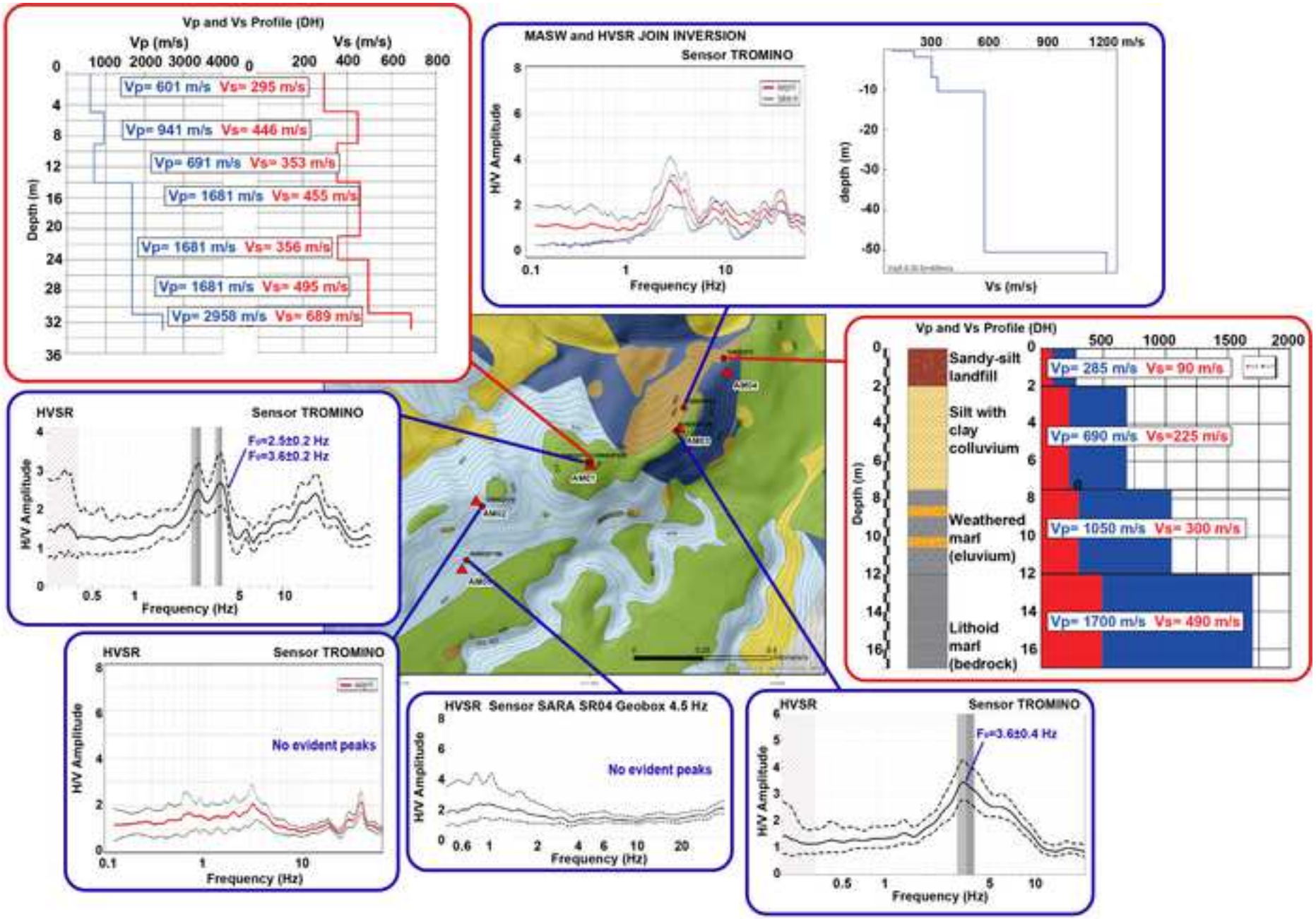

Figure S3 - Geophysical investigations collected in the Seismic Microzonation study (Regione Marche, 2018) and performed by Geologists Consultants for private and civil engineering goals. They consist of Vs profiles attained through Dowh-hole (DH) measurements (red frames) and HVSRs calculated from ambient noise measurements (blue frames).

Figure S4

Click here to access/download;Supplemental Material (Main Page, Tables, Figures);Figure S4.jpg

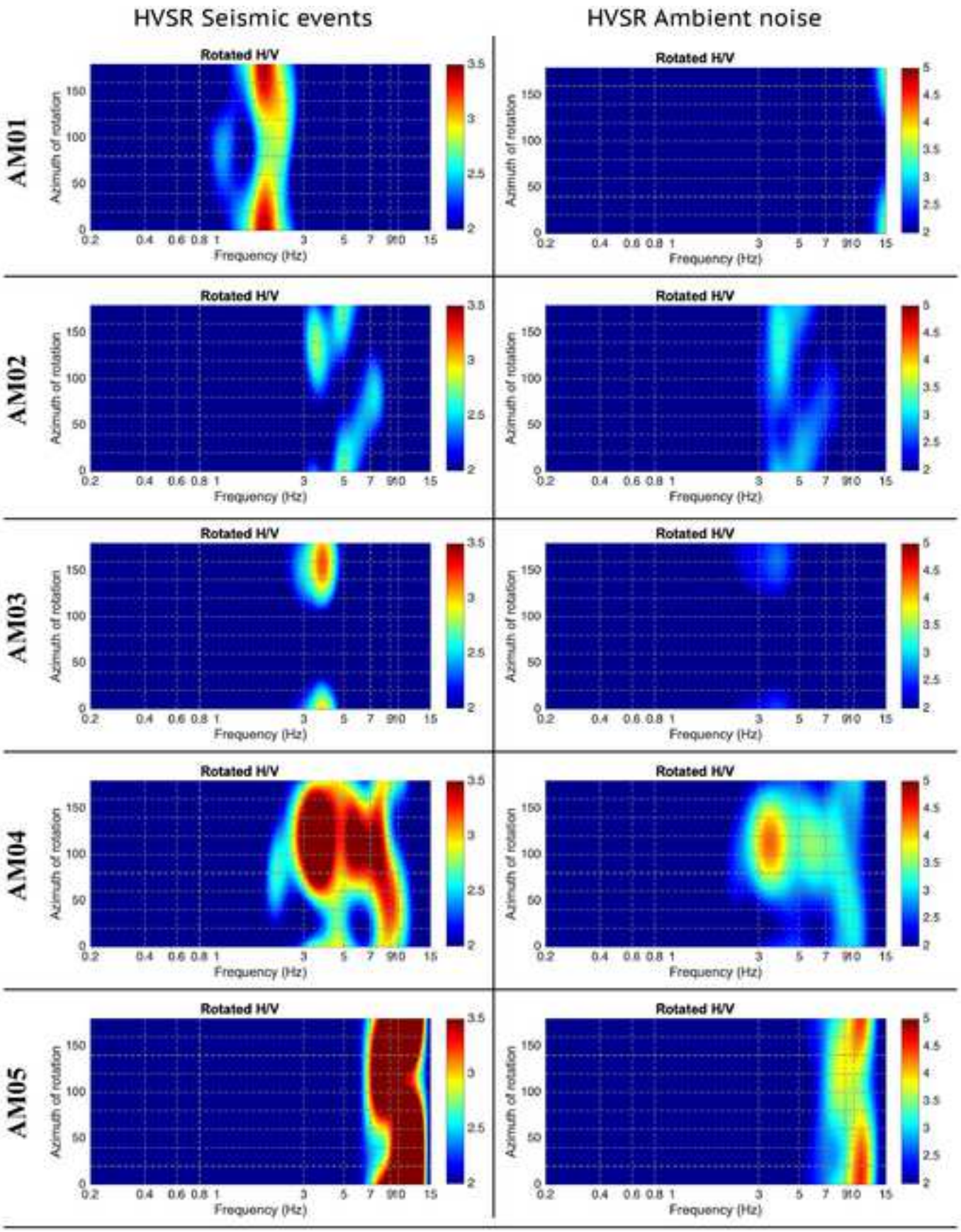

Figure S4: H/V spectral ratios calculated for Amandola case. In the left column we show HVSRs calculated on seismic events, in the right column HVSRs calculated on ambient noise. They are given using a contour plot representation, the x-axis representing frequency, the y-axis the rotation angle, the color scale being related to H/V amplitudes.

Figure S5

Click here to access/download;Supplemental Material (Main Page, Tables, Figures);Figure S5.jpg

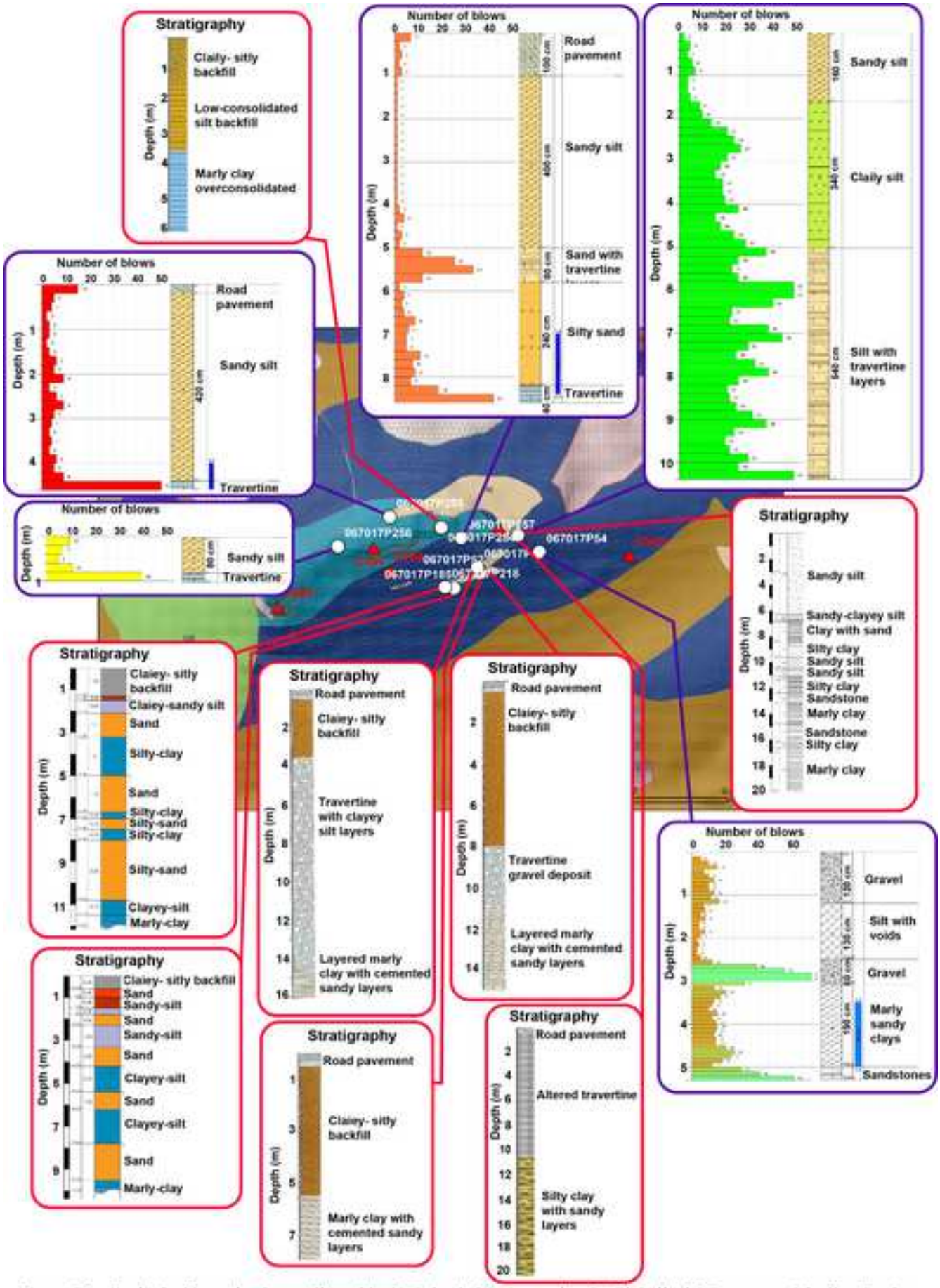

Figure S5 - Geological investigations collected in the Seismic Microzonation for Civitella del Tronto municipality (Regione Marche, 2018): stratigraphy from geognostic surveys (red frames) and dynamic probing super heavy drilling (DPSH) results (violet frames).

Figure S6

Click here to access/download;Supplemental Material (Main Page, Tables, Figures);Figure S6.jpg

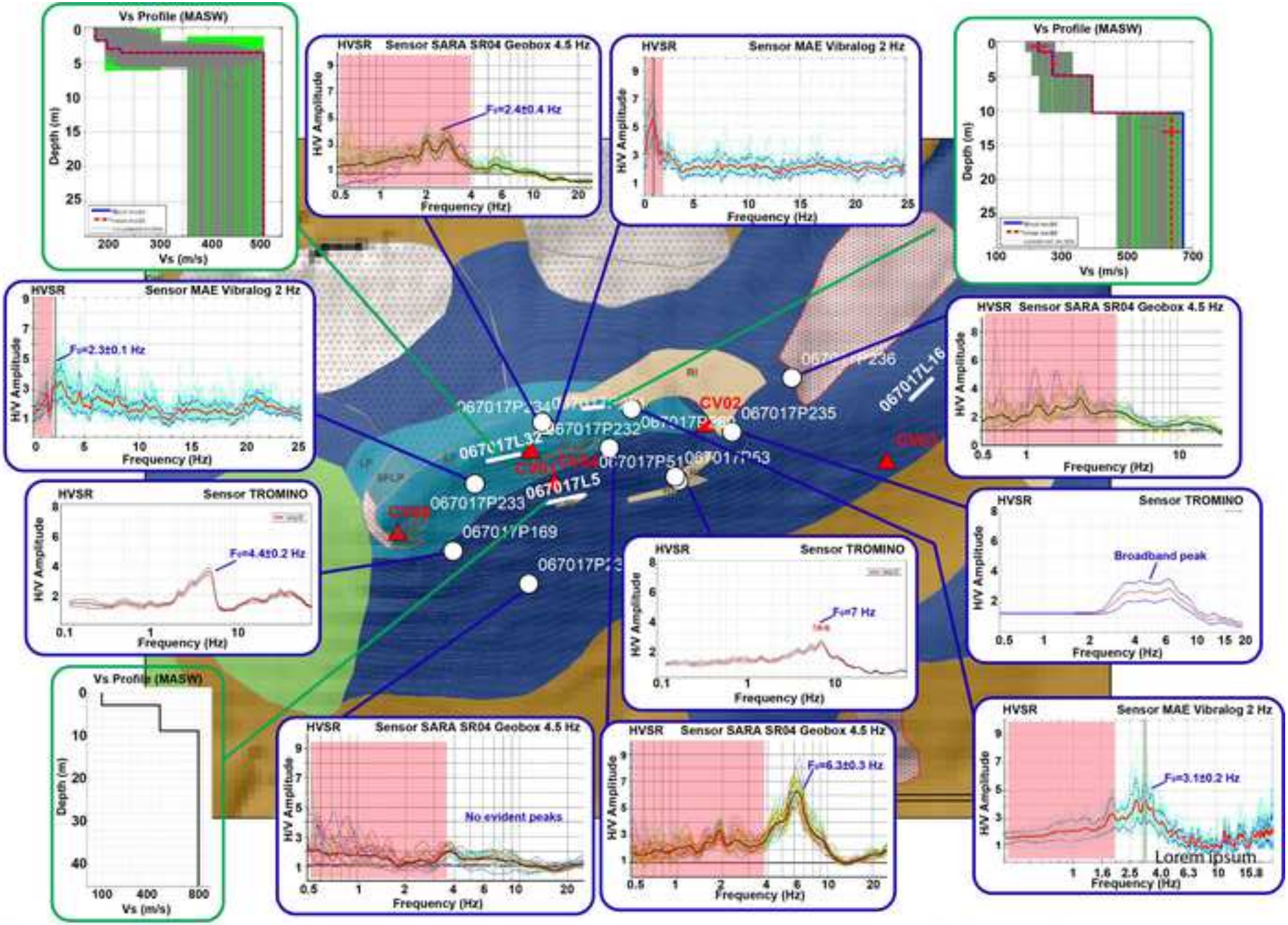

Figure S6 - Geophysical investigations collected in the Seismic Microzonation study (Regione Marche, 2018) and performed by Geologists Consultants for private and civil engineering goals. They consist of Vs profiles attained through MASW (Multichannel-Analysis of Surface Waves) measurements (green frames) and HVSRs calculated from ambient noise measurements (blue frames).

Figure S7

Click here to access/download;Supplemental Material (Main Page, Tables, Figures);Figure S7.jpg

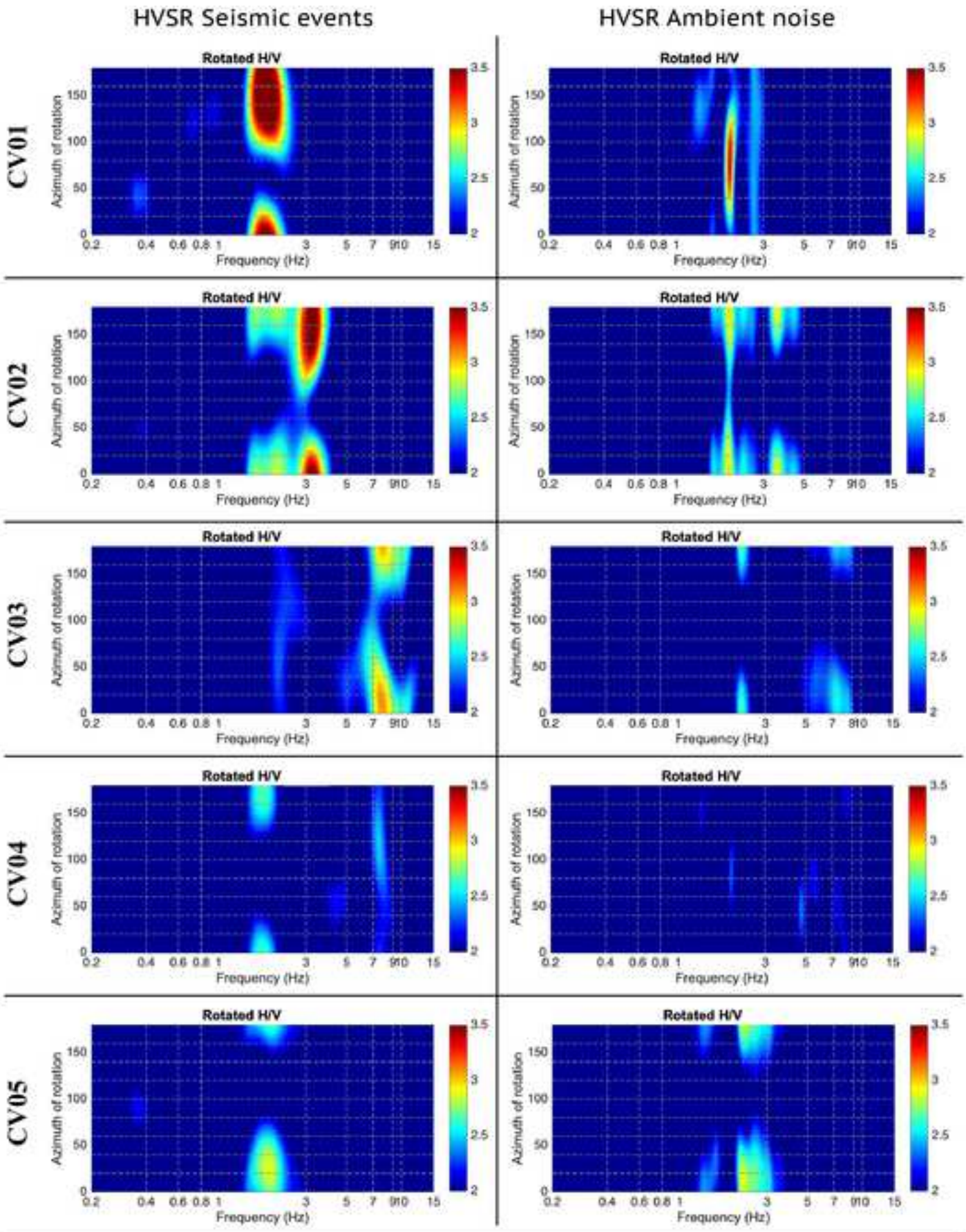

Figure S7: HV spectral ratios calculated for Civitella case plotted as in FigureS4.

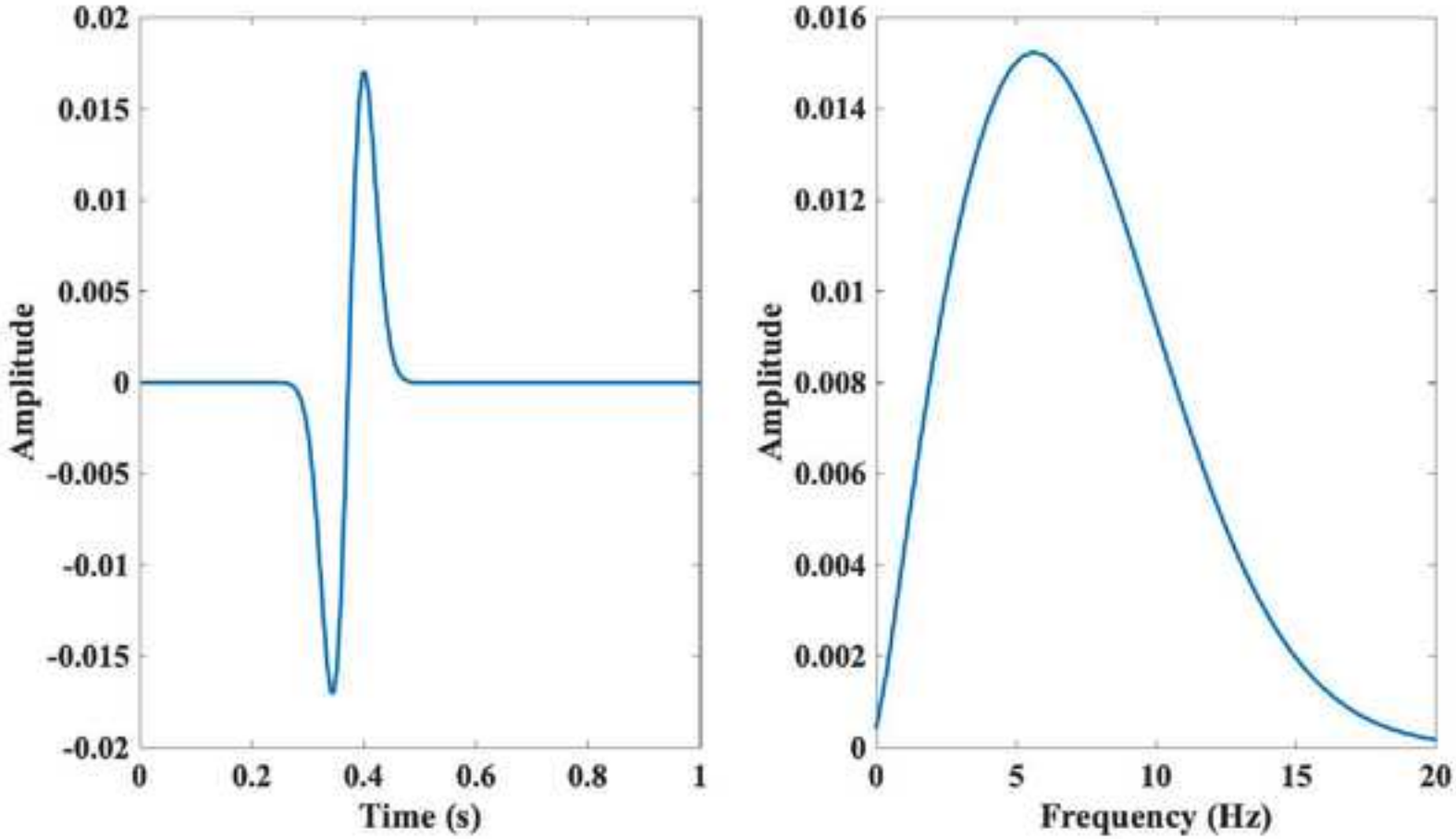

Figure S8: Ricker pulse adopted in numerical modelling for Civitella and Montereale cases. This excitation pulse ensured energy until up to 10 Hz.

Figure S9

Click here to access/download;Supplemental Material (Main Page, Tables, Figures);Figure S9.jpg

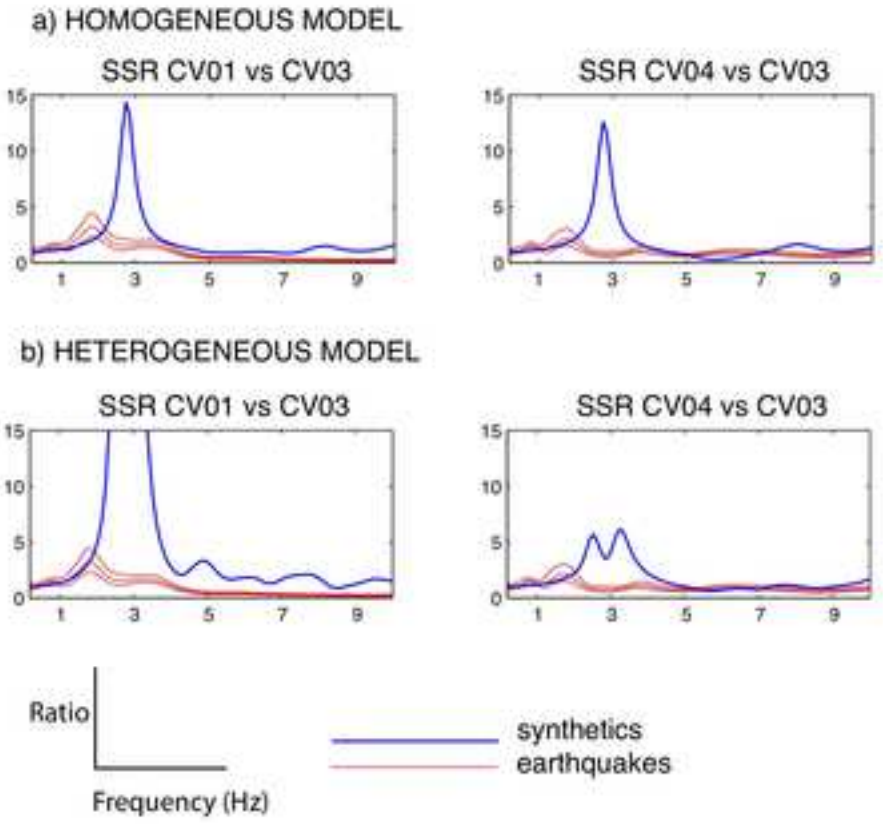

Figure S9: Comparison of results at CV01 and CV04 from former modeling exercises run using Vs value of 1200 m/s for (a) the homogeneous and (b) the heterogeneous model.

Figure S10

Click here to access/download;Supplemental Material (Main Page, Tables, Figures);Figure S10.jpg

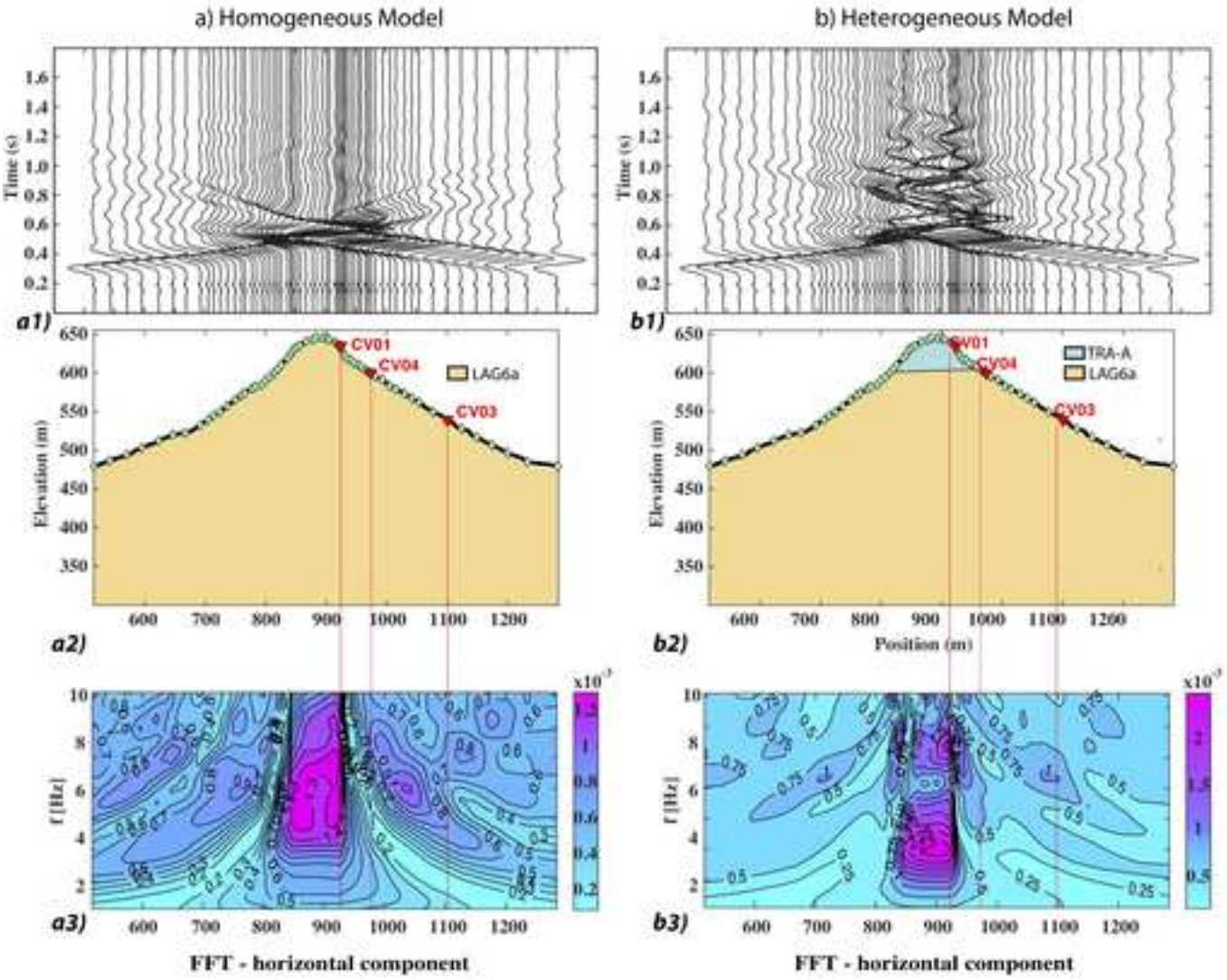

Figure S10: Contour plots of Fast Fourier Transforms of horizontal synthetic motion, for both the homogeneous (a) and the heterogeneous (b) models. Please note that in both models the half-slopes are affected by deamplification. This is the reason for the high amplification levels obtained by calculating the SSRs using as a reference a virtual CV03.

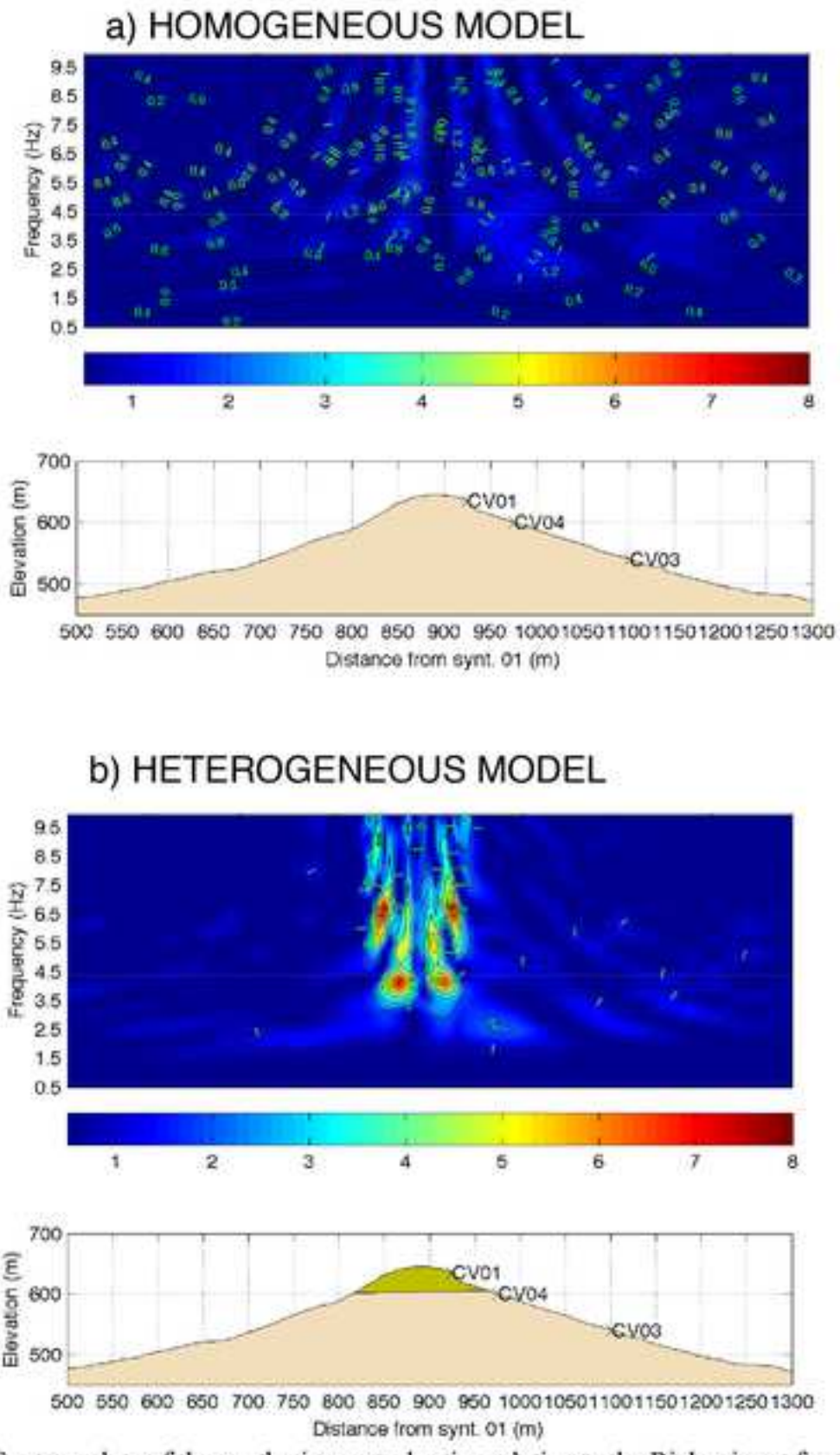

Figure S11: Contour plots of the synthetic spectral ratios relative to the Ricker input for the vertical components of the homogeneous model (a) and the heterogeneous model (b); in this latter amplification of the vertical component appear over 3 Hz.

Figure S12

Click here to access/download;Supplemental Material (Main Page, Tables, Figures);Figure S12.jpg

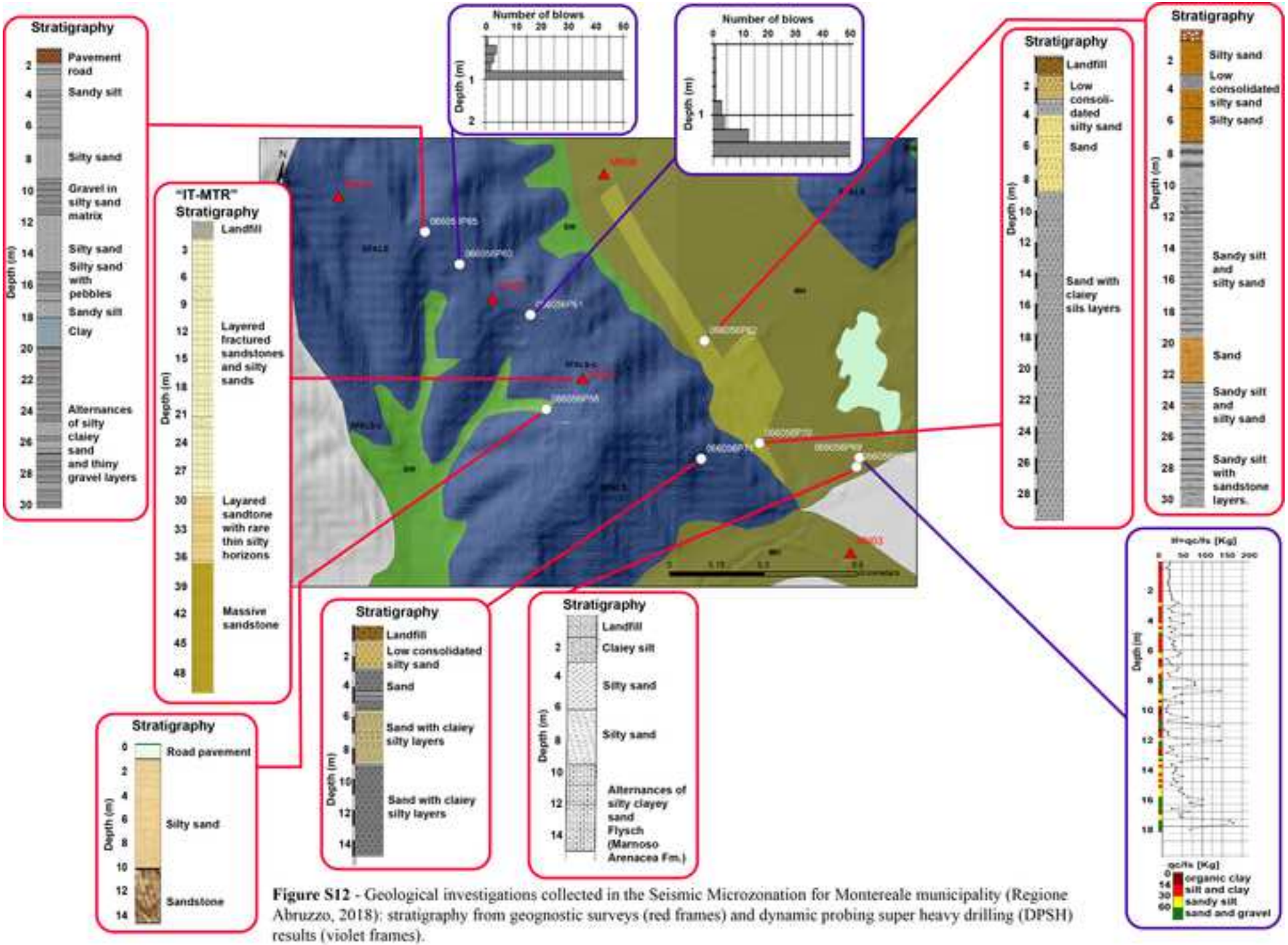

Figure S12 - Geological investigations collected in the Seismic Microzonation for Montereale municipality (Regione Abruzzo, 2018): stratigraphy from geognostic surveys (red frames) and dynamic probing super heavy drilling (DPSH) results (violet frames).

Figure S13

Click here to access/download;Supplemental Material (Main Page, Tables, Figures);Figure S13.jpg

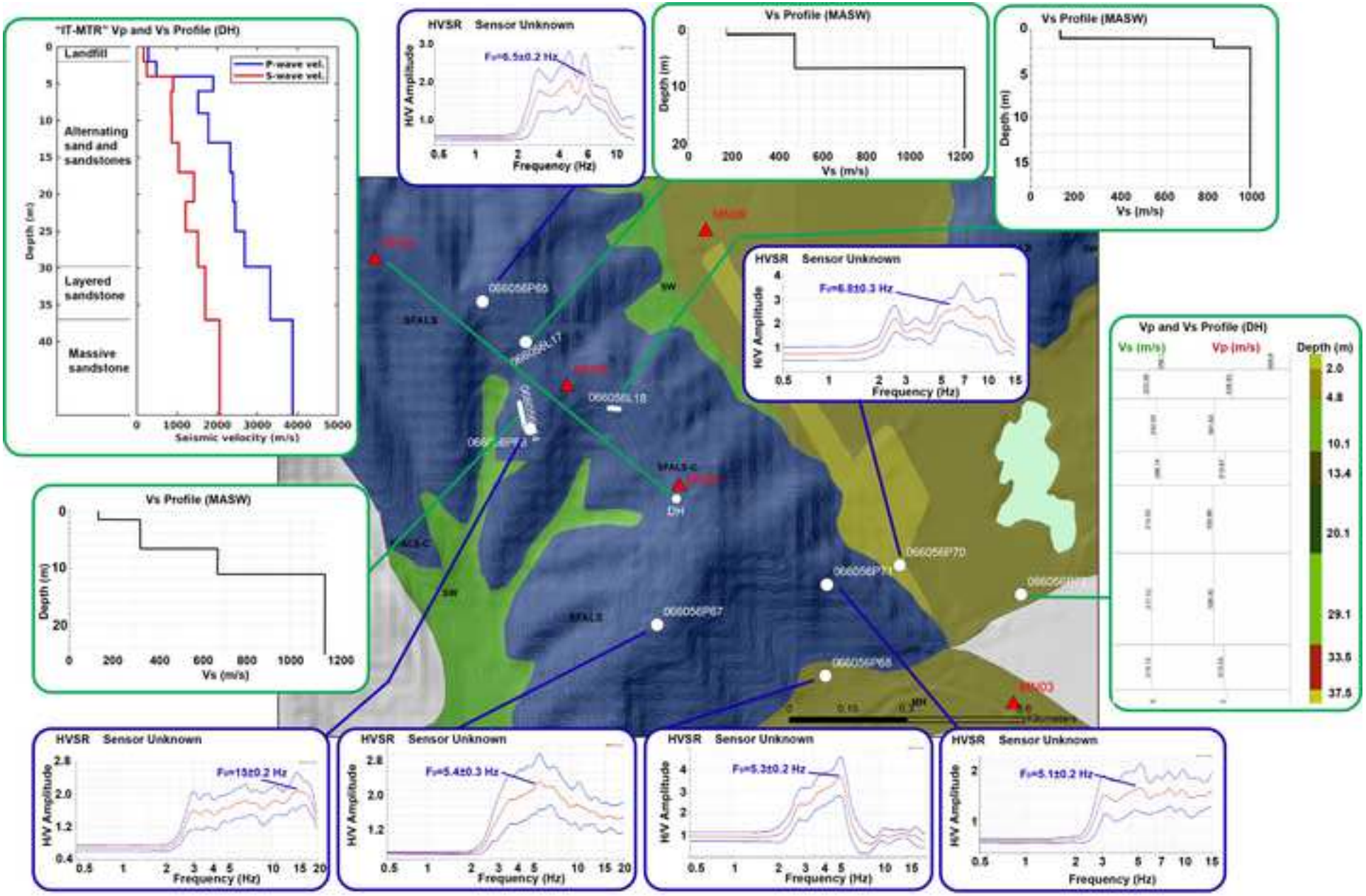

Figure S13 - Geophysical investigations collected in the Seismic Microzonation study (Regione Abruzzo, 2018). They consist of down-hole measurements of seismic wave velocities (Vp and Vs) and Vs profiles attained through MASW (Multichannel-Analysis of Surface Waves) measurements (green frames); HVSRs calculated from ambient noise measurements (blue frames).

Figure S14

Click here to access/download;Supplemental Material (Main Page, Tables, Figures);Figure S14.jpg

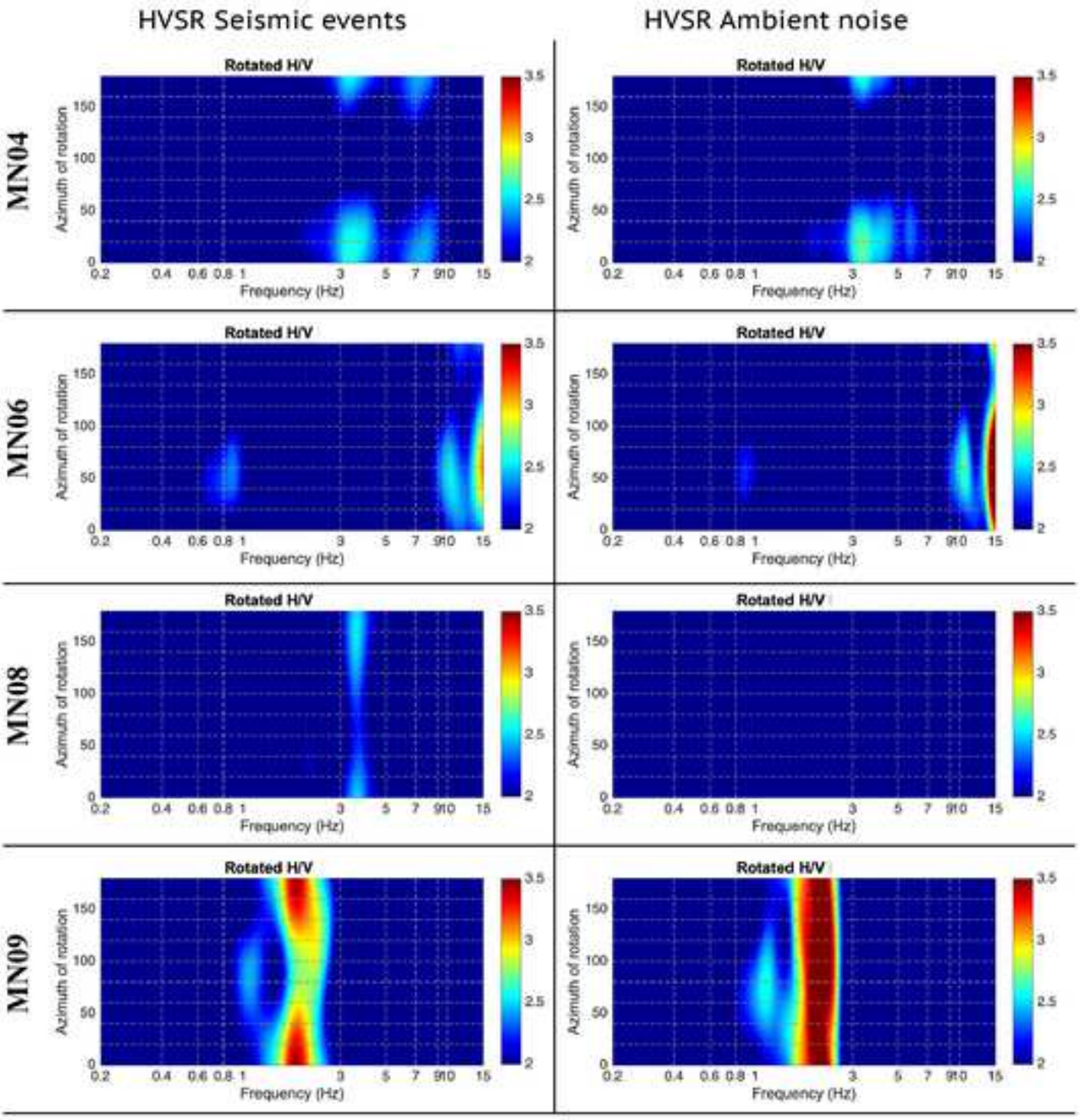

Figure S14: HV spectral ratios calculated for Montereale case plotted as in FigureS4.

Site-dependent amplification on topography during the 2016 Amatrice (central Italy) seismic sequence

Authors:

M. Pischiutta[1], R. Puglia[2], P. Bordoni[1], S. Lovati[2], G. Cultrera[1], A. Mercuri[1], A. Fodarella[3], M. Massa[2], E. D'Alema[2]

Description of the Supplemental Material:

Additional information about QUAD4M package and report of numerical simulations performed at the Amandola study-case (file *Suppl_Q4M.pdf*).

Tables listing selected earthquakes for the analysis.

Additional figures showing: HVSR analysis results performed using seismic events and ambient noise; the input Ricker pulse adopted in numerical modelling for Civitella and Montereale cases; additional modeling results.

List of Supplemental Table Captions:

Table1S: Hypocentral parameters of selected earthquakes used in the data analysis for the Amandola case: origin time, hypocentral localization and magnitude.

Table2S: Hypocentral parameters of selected earthquakes used in the data analysis for Civitella and Montereale case: origin time, hypocentral localization and magnitude.

List of Supplemental Figure Captions:

Figure S1: Geological investigations collected in the Seismic Microzonation for Amandola municipality (Regione Marche, 2018a): stratigraphy from geognostic surveys.

Figure S2: Geological sections deduced from in-situ surveys and geophysical analyses coming from the regional Microzonation studies reported in Figures S1 and S3.

Figure S3: Geophysical investigations collected in the Seismic Microzonation study (Regione Marche, 2018a) and performed by Geologists Consultants for private and civil engineering goals. They consist of Vs profiles attained through Dowh-hole (DH) measurements (red frames) and HVSRs calculated from ambient noise measurements (blue frames).

Figure S4: H/V spectral ratios calculated for Amandola case. In the left column we show HVSRs calculated on seismic events, in the right column HVSRs calculated on ambient noise. They are given using a contour plot representation, the x-axis representing frequency, the y-axis the rotation angle, the color scale being related to H/V amplitudes.

Figure S5: Geological investigations collected in the Seismic Microzonation for Civitella del Tronto municipality (Regione Marche, 2018b): stratigraphy from geognostic surveys (red frames) and dynamic probing super heavy drilling (DPSH) results (violet frames).

Figure S6: Geophysical investigations collected in the Seismic Microzonation study (Regione Marche, 2018b) and performed by Geologists Consultants for private and civil engineering goals. They consist of Vs profiles attained through MASW (Multichannel-Analysis of Surface Waves) measurements (green frames) and HVSRs calculated from ambient noise measurements (blue frames).

Figure S7: HV spectral ratios calculated for Civitella case plotted as in FigureS1.

Figure S8: Ricker pulse adopted in numerical modelling for Civitella and Montereale cases. This excitation pulse ensured energy until up to 10 Hz.

Figure S9: Comparison of results at CV01 and CV04 from former modeling exercises run using Vs value of 1200 m/s for (a) the homogeneous and (b) the heterogeneous model.

Figure S10: Contour plots of Fast Fourier Transforms of horizontal synthetic motion, for both the homogeneous (a) and the heterogeneous (b) models. Please note that in both models the half-slopes are affected by deamplification. This is the reason for the high amplification levels obtained by calculating the SSRs using as a reference a virtual CV03.

Figure S11: Contour plots of the synthetic spectral ratios relative to the Ricker input for the vertical components of the homogeneous model (a) and the heterogeneous model (b); in this latter amplification of the vertical component appear over 3 Hz.

Figure S12: Geological investigations collected in the Seismic Microzonation for Montereale municipality (Regione Abruzzo, 2018): stratigraphy from geognostic surveys (red frames) and dynamic probing super heavy drilling (DPSH) results (violet frames).

Figure S13: Geophysical investigations collected in the Seismic Microzonation study (Regione Abruzzo, 2018). They consist of down-hole measurements of seismic wave
velocities (Vp and Vs) and Vs profiles attained through MASW (Multichannel-Analysis of Surface Waves) measurements (green frames); HVSRs calculated from ambient noise measurements (blue frames).

Figure S14: H/V spectral ratios calculated for Montereale case. In the left column we show HVSRs calculated on seismic events, in the right column HVSRs calculated on ambient noise. They are given using a contour plot representation, the x-axis representing frequency, the y-axis the rotation angle, the colour scale being related to H/V amplitudes.